NORTHWESTERN UNIVERSITY

Crack Response to Weather Effects, Blasting, and Construction Vibrations

A Thesis

Submitted to the Graduate School In Partial Fulfillment of the Requirements

For the Degree

MASTER OF SCIENCE

Field of Civil Engineering

By

Mickey L. Snider

EVANSTON, IL

May 2003

Table of Contents

Acknowledgements	iii
Abstract	iv
List of Figures	v
List of Tables	xi
Chapter 1- Introduction	**1**
Chapter 2- Blast Vibration Response, Southbury, Connecticut	**5**
Structural Description	
Instrumentation	
Blast Response	
Crack Response to Environmental Effects	
Comparison of Computed and Measured Crack Displacements	
Chapter 3- Effect of Blast Design on Crack Displacement	**39**
Introduction	
Shot 1 (Narrow V, single face) vs. Shot 9 (Wide V, double face)	
Shot 8 (Shallow stemming) vs. Shot 15 (Normal stemming)	
Shot 14 (19 Hz long. direction) vs. Shot 22 (27 Hz long. direction)	
Shot 18 (Total shot time, 436ms) vs. Shot 19 (Total shot time, 215ms)	
Chapter 4- Construction Vibrations, Las Vegas, Nevada	**59**
Introduction	
Ann Road Soil Profile	
Construction Equipment	
Structural Details	
Instrumentation	
Ground Attenuation Study	
Chapter 5- Construction Vibration Response Analysis and Recording	**70**
Introduction	
Long-term Triggering and Crack Response to Environmental Effects	

Table of Contents (cont.)

Individual Event Triggering and Transient Response

Miscellaneous Activities

Trenching Activities

Vibratory Compaction

Comparisons of Traditional Motion Controls with Measured Crack Displacements

Chapter 6- Comparison of Crack Displacements resulting from Connecticut Blasting Vibrations and Las Vegas Construction Vibrations 123

Introduction

Time Histories

Single Degree of Freedom Response Spectra

Homogenous Excitation

Structural Sensitivity

Chapter 7- Conclusions 142

References 146

Appendix A- Conversion Factors for Connecticut and Las Vegas Instruments 147

Appendix B- Specifications for Construction Equipment in Las Vegas 148

Acknowledgements

This thesis was a collaboration amongst several individuals who deserve much more than simple acknowledgement. Thank you first, and foremost, to my advisor Professor Charles Dowding for guidance, expertise, and motivation, without which this thesis would certainly not have been possible. Thank you also to Dr. Catherine Aimone-Martin of the New Mexico Institute of Mining and Technology for not only collecting data from Connecticut, but for the extraordinary consultation and patience she showed throughout the entire scope of this project.

Thank you to Dr.'s Dowding, Richard J. Finno, Raymond J. Krizek, Catherine Aimone-Martin, and Gustavious P. Williams for their teaching and educational support over the last two years. Thank you to Darren Pleiman and Marco Furlan at Kleinfelder, Inc., Las Vegas, for an effort of gargantuan proportions in logistical support and data collection. Thank you to Jill Roboski, Tanner Blackburn, Terry Holman, and all the geotechnical graduate students at Northwestern University who have helped me get through many hours every day.

The long term financial support of the Infrastructure Technology Institute, which is funded by a block grant from the U.S. Department of Transportation, is gratefully acknowledged. A special thanks to Laureen McKenna who left me the Autonomous Crack Monitoring project in excellent shape after an intensive and priceless training period. Thank you to everyone at the Infrastructure Technology Institute, in particular to Daniel Marron and David Kosnik who dropped everything for the sake of technical and logistical support of this project on more than their fair share of occasions.

Thank you more than any other to Mom, Dad, Marc, and Matt for being the best family in the world and understanding everything I do, as ridiculous as it might sound at first. Thank you to my dearest Beth and my closest friends, Paul, Pete, and Liz, for proving every day that I live in the greatest place on earth. And finally, to my special little guy, the Mighty Touba, thank you for being my best buddy in the whole world.

Abstract

Autonomous Crack Measurement (ACM) facilitates simultaneous measurement of crack response to environmental changes and vibrations produced by various construction activities. Dual-purpose crack displacement sensors measure crack response, while the vibration environment is defined by standard seismological transducers and the weather environment is defined as changes in temperature and humidity.

This investigation involved an ACM study to examine the effects of rock blasting at the Stiles Road Quarry site in Southbury, Connecticut and vibrations produced by heavy construction equipment at the West Ann Road site in Las Vegas, Nevada. The study also allowed for the examination of blast design effects on crack displacement and a comparison of crack response from typical blasting and construction activities with that produced by weather changes.

Measurements and analysis show that (i) long-term weather-induced crack displacement is 30 to 150 times greater than the crack displacement produced by the largest blasting event (≈0.35 ips) at the Connecticut site and the largest construction event (≈0.45 ips) at the Las Vegas site, (ii) ground vibration frequency and stemming length have the largest effect on crack displacement of the four blast design controls studied, (iii) appropriate triggering mechanisms and on-site observation greatly facilitate vibration monitoring, and (iv) rock blasting at distances of approximately 2500 feet produced homogenous crack response, while localized construction activity in soils at distances less than 50 feet produced time varying, localized crack response.

List of Figures

2.1 Single-Story Connecticut House with Apartment Addition 5

2.2 Plan View of Connecticut House with Crack and Sensor Locations 8

2.3 Elevation View of Connecticut House with Crack and Sensor Locations 8

2.4 Photos of Connecticut house (a) from the rear of the structure, and (b) outside the apartment/garage addition 9

2.5 Photos of ceiling joist systems (a) garage ceiling/apartment floor system, (b) apartment addition ceiling truss system 10

2.6 Schematic of apartment/garage addition joist systems 10

2.7 Wall view and detail photographs of Cracks 1 (top) and 3 (bottom) with sensors 12

2.8 Time histories of Crack 1 and 3 displacements from blast event 15 on July 22nd, 2002 at 11:49 AM compared to longitudinal, transverse, and vertical velocity ground excitation, S_2 response velocity, S_1 response velocity, and air blast 14

2.9 Time histories of Crack 1 and 3 displacements from blast event 15 on July 22nd, 2002 at 11:49 AM compared to longitudinal, transverse, and vertical ground displacements, S_2 displacement response, S_1 displacement response, (S_2-S_1) relative displacement, and air blast 15

2.10 Free response of an S_2 velocity time history in the Connecticut house 16

2.11 Spectra of S_2 velocity FFT with ground velocity FFT ratio (top), S_2 velocity FFT (middle) and ground velocity FFT (bottom) for (a) longitudinal response, Blast 15 and (b) transverse response, Blast 8 17

2.12 Single degree of freedom response spectrum of longitudinal ground motion produced by Blast 15 on July 22nd, 2002 at 11:49 AM, showing the estimated relative displacement of an 11 Hz structure 18

2.13 Time history of Crack 1 displacement from Blast event 8 on June 10th, 2002 at 11:49 AM compared to longitudinal, transverse, and vertical ground excitation, longitudinal, transverse, and vertical S_2 response, and air blast 20

2.14 Single degree of freedom response spectrum of longitudinal, transverse, and vertical ground motion produced by Blast 8 on June 10th, 2002 at 11:49 AM 21

2.15 Long-term Crack 1, Crack 3, and null gage displacement, temperature, and humidity versus time 23

2.16 Long-term Crack 1 displacement magnified to show 48-hours of response data surrounding blast event 8 26

2.17 Correlations between measured Crack 3 displacement and longitudinal ground motions, relative structural displacements, and airblast 33

2.18 Correlations between measured Crack 1 displacement and longitudinal ground motions and relative structural displacements 34

List of Figures (cont.)

2.19 Correlations between measured Crack 1 displacement and transverse ground motions, relative structural displacements, and Crack 1 airblast response versus airblast induced upper structure response 35
2.20 Correlations between measured Crack 1 displacement and vertical ground motions, relative structural displacements, and airblast 36
2.21 Correlations between measured Crack 1 displacement and vertical structural and midceiling velocity and displacements 37
2.22 Time histories of Crack 1 and 3 displacements from blast event 20 on August 23rd, 2002 at 11:49 AM compared to longitudinal, transverse, and vertical ground velocity, vertical ground displacement, S_2 response velocity and displacement response, $S_{midceeling}$ velocity and displacement response, (S_2+$S_{midceiling}$) relative displacement, and air blast 38
3.1 Aerial photograph outlining Stiles Road Quarry boundary with blasting area and Connecticut monitoring house encircled 43
3.2 USGS Topographic map outlining Stiles Road Quarry boundary with blasting area and Connecticut monitoring house encircled 43
3.3 Detailed topographic relief maps of blast 1, 8, 9, 14, 15, 18, 19, and 22 locations (outlined in black, numbered in white) on upper and lower bench of Stiles Road Quarry 44
3.4 Borehole geometry and delay timing patterns for blast events 1 and 9 46
3.5 Crack 1 displacement time histories for blast events 1 and 17 compared to longitudinal ground motion, longitudinal S_2 structural response, vertical ground motion, vertical S_2 structural response, and airblast 47
3.6 Borehole geometry and delay timing patterns for blast events 8 and 15 49
3.7 Crack 1 displacement time histories for blast events 8 and 15 compared to longitudinal ground motion, longitudinal S_2 structural response, vertical ground motion, vertical S_2 structural response, and airblast 50
3.8 Borehole geometry and delay timing patterns for blast events 14 and 22 52
3.9 Crack displacement 1 and 3 time histories for blast events 14 and 22 compared to longitudinal ground motion, longitudinal S_2 structural response, vertical ground motion, vertical S_2 structural response, and airblast 53
3.10 Normalized Crack 3 displacement (CD_3/L PPV) versus longitudinal single degree of freedom dominant frequency for blasting in Connecticut 54
3.11 Borehole geometry and delay timing patterns for blast events 18 and 19 57
3.12 Crack displacement 1 and 3 time histories for blast events 18 and 19 compared to longitudinal ground motion, longitudinal S_2 structural response, vertical ground motion, vertical S_2 structural response, event 19 vertical $S_{midceiling}$ structural response, and airblast 58

List of Figures (cont.)

4.1 Single-story house adjacent to Ann Road Construction in Las Vegas, Nevada 59

4.2 (a) Plan view geometry of monitoring house, construction locations, and soil boring location, (b) cross-sectional view of house geometry and excavations (section A-A) 60

4.3 Blow count versus depth for three Ann Road soil borings in vicinity of test house 61

4.4 Photographs of trenching equipment on Ann Road, (a) Hitachi trackhoe with dump truck and (b) Tesmec chain trencher 62

4.5 Photographs of vibratory compaction equipment on Ann Road, (a) Dynapac small single-drum roller and (b) Ingersoll-Rand large single-drum vibratory soil compactor 62

4.6 Roof and truss system for one-story Las Vegas structure 63

4.7 (a) Plan view of monitoring house and (b) profile view of house, showing Cracks and LVDT sensors 1-5, geophone, and weather logger instrument locations 65

4.8 LVDT micro-inch sensors and cracks (a) interior ceiling, Crack 1 and wall, Crack 3 with interior null sensor, (b) exterior west wall Crack 5, and (c) exterior south wall Crack 2 66

4.9 Peak particle velocity versus distance for ground vibration measurements adjacent to trackhoe, trencher, and vibratory roller construction activities 68

4.10 Peak particle velocity versus dominant frequency from fast fourier transform analysis for ground vibration measurements adjacent to trackhoe, trencher, and vibratory roller construction activities 69

5.1 Long-term internal Crack 1 and Crack 3 displacement, indoor temperature and indoor humidity versus time 77

5.2 Long-term external Crack 2 and Crack 5 displacement, outdoor temperature and outdoor humidity versus time 78

5.3 Combined Crack 2 time histories and long-term data triggers showing dominant effect of weather versus vibration induced crack displacements over a one-hour period for trackhoe (top), trencher (middle-top), small vibratory roller (middle-bottom), and large vibratory roller (bottom) 82

5.4 Long-term Crack 2 data showing variability in acquisition periods for trackhoe excavation, trencher excavation, and small roller vibratory compaction 83

5.5 Combined long-term and one-hertz continuous data triggering non-vibratory Crack 2 response over the same one-hour time periods as Figure 5.3, for trencher (top), small vibratory roller (middle), and large vibratory roller (bottom). Example vibratory roller events recorded within this time period are circled 85

5.6 Representation of proposed stick-slip crack displacement effect on external Crack 5 (a) from long-term data taken during a time period without construction activity and (b) trackhoe excavation Event 3 time history on 29 August 2002 86

List of Figures (cont.)

5.7 Three seconds Unfiltered (top) versus filtered (bottom) Crack 2 displacement data for 3 seconds and peak of vibratory roller compaction event #3 on 8 November 2002 88
5.8 Time histories of Crack 1, Crack 2, Crack 3 and Crack 5 from miscellaneous trigger event in August 2002 compared to longitudinal, transverse and vertical ground excitation 89
5.9 Time histories of Crack 1, Crack 2, Crack 3 and Crack 5 from trackhoe excavation event 2 on 29 August 2002 compared to longitudinal, transverse and vertical ground excitation 91
5.10 Frequency Fourier Transform histogram of Crack 2 divided by ground displacement (top), measured Crack 2 displacement (middle), and measured ground displacement (bottom) for trackhoe event #2 on 29 August 2002 92
5.11 Longitudinal, transverse, and vertical single degree of freedom response spectra for trackhoe event #2 on 29 August 2002, showing relative displacement of a 20 Hz structure 93
5.12 Time histories of Crack 1, Crack 2, Crack 3 and Crack 5 from trencher excavation event 2 on 21 November 2002 compared to longitudinal, transverse and vertical ground excitation 94
5.13 (a) Time histories of Crack 1, Crack 2, Crack 3 and Crack 5 from granular trench backfill small single-drum roller compaction Event #3 on 8 November 2002 compared to longitudinal, transverse and vertical ground excitation ground motion 97
5.13 (b) 3-second magnification of granular trench backfill small single-drum vibratory roller event 3 time history showing Crack 1, Crack 2, Crack 3, Crack 5, and longitudinal, transverse and vertical ground motion waveforms 98
5.14 Frequency Fourier Transform histogram of Crack 2 displacement divided by ground displacement ratio (top), measured Crack 2 displacement (middle), and measured ground displacement (bottom) for small vibratory roller event #3 on 8 November 2002 99
5.15 Longitudinal, transverse, and vertical single degree of freedom response spectra for small roller event #3 on 8 November 2002 100
5.16 (a) Time histories of Crack 1, Crack 2, Crack 3 and Crack 5 from granular sub-grade large single-drum roller compaction Event #3 on 18 March 2003 compared to longitudinal, transverse and vertical ground excitation, (b) 3-second close-up of time history showing waveform 102
5.16 (b) 3-second magnification of granular sub-grade large vibratory single-drum roller compaction event 3 time histories showing Crack 1, Crack 2, Crack 3, Crack 5, longitudinal, transverse and vertical ground motion waveforms 103
5.17 Longitudinal, transverse, and vertical single degree of freedom response spectra for large roller event #3 on 18 March 2003 104
5.18 (a) Micro-inch crack 2, 3, and 5 displacement versus directional peak particle velocity correlations for trencher excavation events 108

List of Figures (cont.)

5.18 (b) Micro-inch crack 2, 3, and 5 displacement versus directional integrated particle velocity correlations for trencher excavation events 109
5.18 (c) Micro-inch crack 2, 3, and 5 displacement versus directional 20 Hz SDOF relative displacement correlations for trencher excavation events 110
5.18 (d) Micro-inch crack 2, 3, and 5 displacement versus directional 18-22 Hz average SDOF relative displacement correlations for trencher excavation events 111
5.19 (a) Micro-inch crack 2, 3, and 5 displacement versus directional peak particle velocity correlations for trackhoe excavation events 112
5.19 (b) Micro-inch crack 2, 3, and 5 displacement versus directional integrated particle velocity correlations for trackhoe excavation events 113
5.19 (c) Micro-inch crack 2, 3, and 5 displacement versus directional 20 Hz SDOF realtive displacement correlations for trackhoe excavation events 114
5.19 (d) Micro-inch crack 2, 3, and 5 displacement versus directional 18-22 Hz average SDOF relative displacement correlations for trackhoe excavation events 115
5.20 (a) Micro-inch crack 2, 3, and 5 displacement versus directional peak particle velocity correlations for vibratory roller compaction events 116
5.20 (b) Micro-inch crack 2, 3, and 5 displacement versus directional integrated particle velocity correlations for vibratory roller compaction events 117
5.20 (c) Micro-inch crack 2, 3, and 5 displacement versus directional 20 Hz SDOF relative displacement correlations for vibratory roller compaction events 118
5.20 (d) Micro-inch crack 2, 3, and 5 displacement versus directional 18-22 Hz average SDOF relative displacement correlations for vibratory roller compaction events 119
5.21 Frequency Fourier Transform histogram of Crack 2 displacement divided by longitudinal ground displacement ratio (top), measured Crack 2 displacement (middle), and calculated longitudinal ground displacement (bottom) for small vibratory roller events #3 (left) and #6 (right) on 8 November 2002 121
5.22 (a) Longitudinal single degree of freedom response spectra for large roller events #2 and #7 (low amplitude) 122
5.22 (b) Longitudinal single degree of freedom response spectra for large roller events #3 and #6 (high amplitude) 122
6.1 (a) Global time histories of Connecticut Crack 1 and 3 displacements from blast event 15 and Las Vegas Crack 2 displacement from trackhoe event 2, trencher event 2, small vibratory roller event 3 and large vibratory roller event 3 127

List of Figures (cont.)

6.1 (b) 3-second time history magnification of Connecticut Crack 1 and 3 displacements from blast event 15 and Las Vegas Crack 2 displacement from trackhoe event 2, trencher event 2, small vibratory roller event 3 and large vibratory roller event 3, showing detail of waveforms 128
6.2 (a) Global time histories of longitudinal particle velocity from blast event 15 in Connecticut, and trackhoe event 2, trencher event 2, small vibratory roller event 3 and large vibratory roller event 3 in Las Vegas 129
6.2 (b) 3-second time history magnification of longitudinal particle velocity from blast event 15 in Connecticut, and trackhoe event 2, trencher event 2, small vibratory roller event 3 and large vibratory roller event 3 in Las Vegas, showing detail of waveforms 130
6.3 Time histories of transverse particle velocity from blast event 15 in Connecticut, and trackhoe event 2, trencher event 2, small vibratory roller event 3 and large vibratory roller event 3 in Las Vegas 131
6.4 Time histories of vertical particle velocity from blast event 15 in Connecticut, and trackhoe event 2, trencher event 2, small vibratory roller event 3 and large vibratory roller event 3 in Las Vegas 132
6.5 Vertical single degree of freedom response spectrum for blast event 22 in Connecticut (PPV=0.13 ips) and trackhoe event 2, trencher event 2, small roller event 3 and large roller event 3 in Las Vegas (PPV normalized to 30 feet), and Longitudinal SDOF spectrum for blast event 9 in Connecticut (PPV=0.14) 134
6.6 Visual comparison of geodynamic wavelengths producing individual wall component displacement in Las Vegas (125 ft) and homogenous superstructure displacement in Connecticut (400 ft) 135
6.7 Plane wave theory of radial geodynamic wave motion impacting structures in Connecticut and Las Vegas 137
6.8 Crack 2 and 5 displacement, longitudinal, transverse and vertical time histories of large roller event 6 showing time lag in Crack 5 versus Crack 2 response 138
6.9 Visualization of time lag existing between Crack 5 response and Crack 2 response during large roller event 6, resulting from radial plane wave motion 138
6.10 (a) Connecticut cracks 1 and 3 sensitivity to humidity change 141
6.10 (b) Las Vegas cracks 1, 2, 3, and 5 sensitivity to humidity change 141

List of Tables

2.1 Ground motion, frequency, airblast and crack displacement information for all blast events in Connecticut 6
2.2 Shot timing, scaled distances, explosive characteristics, and other pertinent logistical information for all blast events in Connecticut 7
2.3 Computed crack displacements due to long-term weather phenomena, typical, and maximum ground motion in Connecticut 24
2.4 (a) Traditional structure response and ground motion controls with Crack 1 and 3 displacements for blast events 1 through 12 in Connecticut 28
2.4 (b) Traditional structure response and ground motion controls with Crack 1 and 3 displacements for blast events 13 through 24 in Connecticut 29
3.1 Summary of pertinent blast design and borehole geometry information for blast events 1, 9, 8, 15, 14, 22, 18, and 19 42
4.1 Summary of seismograph arrays employed in attenuation study on Ann Road 67
5.1 Summary of directional measured peak particle velocity, computed displacements by integration of velocity and single degree of freedom methods and measured crack 2, 3, and 5 displacements for all trackhoe events on 29 August 2002 and 13 September 2002 73
5.2 Summary of directional measured peak particle velocity, computed displacements by integration of velocity and single degree of freedom methods and measured crack 2, 3, and 5 displacements for all trencher events on 22 November 2002 and all small roller events on 8 November 2002 74
5.3 Summary of directional measured peak particle velocity, computed displacements by integration of velocity and single degree of freedom methods and measured crack 2, 3, and 5 displacements for all large roller events on 18 March 2003 75
5.4 Summary and comparison of Crack 2, 3, and 5 displacement with weather descriptors, vibratory activity and average and maximum temperature and humidity readings 79
5.5 Summary of rainfall events during monitoring period in 2002. 2003 data not yet available. (National Weather Service) 80
5.6 Summary of R^2 linear regression correlation coefficients of measured Crack 2, 3, and 5 displacement with directional peak particle velocity and computed relative displacement methods for all trackhoe, trencher and vibratory roller events 106
6.1 Summary of information pertaining to time histories and waveforms, frequency response, and crack displacements 126
6.2 Events and crack responses employed in the calculation of crack sensitivity to environmental (humidity) change 140

Chapter 1

Introduction

This thesis summarizes micro-inch crack response to blast-induced ground motions from the Stiles Road Quarry in Southbury, Connecticut, construction equipment-induced ground motions along West Ann Road in North Las Vegas, Nevada, and environmental phenomena at both sites. These structures were instrumented, and their response studied as part of the development of an Autonomous Crack Measurement (ACM) system sponsored by the Infrastructure Technology Institute at Northwestern University through a block grant from the United States Department of Transportation. The objective of the ongoing Autonomous Crack Monitoring study is to record and compare micro-inch crack displacements produced by long-term temperature and humidity changes to those produced by short-term blasting or construction vibrations in a concise and understandable fashion.

Responses of the Connecticut structure were measured with velocity transducers instrumented in the traditional manner of those in the study sponsored by the United States Department of the Interior Office of Surface Mining (OSM) (McKenna, 2002). Ground motions were measured in three orthogonal axes in front of the house. Structural responses were measured with three upper structure velocity transducers, three lower structure velocity transducers, two mid-wall velocity transducers, an air pressure transducer, and for the final month of study, one mid-ceiling velocity transducer. One wall and two ceiling cosmetic drywall cracks were fit with eddie current "Kaman"

sensors to measure micro-inch displacement response to environmental and blast-induced ground vibrations produced by the aggregate quarry approximately 2500 feet away.

Ground motions at the Las Vegas structure were measured via an in-ground tri-axial geophone customary to all ACM structures. Micro-inch displacements were measured across two interior drywall cracks and two exterior stucco cracks with LVDT displacement gages. No velocity response was measured in this structure. Construction adjacent to the house (within 50 feet) involved excavation for the installation of a l0x12 ft. reinforced concrete box culvert by trackhoe, excavation of an 8-inch water service line trench by a chain trencher, and vibratory compaction of trench backfill and granular sub-grade for the reconstruction of West Ann Road.

This thesis is divided into six chapters. Chapter 2 presents traditional OSM velocity and crack instrumentation, and the monitored response in the Connecticut house. The chapter includes the following:

- Description of the structure and location of instruments
- Summary of measurements recorded for each of 24 blast events occurring between May 20th, 2002 and September 20th, 2002.
- Determination of dominant/natural frequency of the structure
- Crack response to long-term and environmental phenomena
- Comparison and correlation of measured crack displacements to traditionally measured and calculated velocity and displacement parameters

Chapter 3 involves a discussion of the effect of blast design on crack displacements. Four time history comparisons are chosen to analyze the effects of differences in:

- Face geometry
- Stemming depth
- Frequency effect
- Total shot time and number of boreholes

Chapter 4 is a discussion of the construction processes and instrumentation for monitoring of construction vibrations at the Las Vegas, Nevada site. The chapter presents:

- Layout and structural details of house and proximity to monitored construction events
- Instruments and locations employed for monitoring purposes
- Soil profile of West Ann Road
- Introduction of construction equipment: trackhoe, trencher, and two vibratory rollers
- Ground attenuation study of trackhoe, trencher and rollers through cemented desert colluvium

Chapter 5 contains the measurement and analysis of heavy construction equipment-induced vibration response at the Las Vegas site. The chapter includes the following:

- Data acquisition, triggering mechanisms, and the challenges presented by construction monitoring
- Long-term response to environmental effects in Las Vegas
- An introduction to "non-vibratory response" monitoring and the proposed stick-slip phenomenon
- Event triggering, ground motions and crack displacements resulting from construction activities of a trackhoe, trencher, and two vibratory rollers
- Determination of dominant/natural frequencies of the Las Vegas structure
- Single degree of freedom response spectra for the trackhoe and vibratory rollers
- Comparison of traditional motion controls to measured crack displacements

Chapter 6 compares blasting response from the Connecticut site to construction equipment response at the Las Vegas site via the following:

- Comparison of time histories from Connecticut blasting and Las Vegas equipment and the number of principal pulses involved

- Introduction to "Normalization Factor" and the effect of 5, 10, 15, and 20 Hz signals on crack displacement
- Effect of construction vibration wavelength on homogenous structural motion versus individual wall component displacement
- Planar wave motion in Connecticut compared to radial wave motion in Las Vegas
- Determination of individual crack sensitivities to changes in humidity

Chapter 2

Blasting Vibration Response, Southbury, Connecticut

Introduction

The Connecticut structure, shown in Figure 2.1, is a one-story house with a walk-out basement and an apartment and garage addition located approximately 2000 to 2500 feet from an aggregate quarry in Southbury, Connecticut. Ground motion and crack data collected on-site from May 20th, 2002 to September 20th, 2002, is summarized in Table 2.1. Table 2.2 summarizes essential descriptors of the ground motion such as number of significant pulses, total shot time, scaled distance factors, shot geometry specifics, etc. These blasts produced peak particle velocities between 0.03 and 0.345 inches per second, peak airblast from less than 100 to 132 db, maximum upper structure responses of 0.030 to 0.480 inches per second, and maximum crack responses between 0 and 90 micro-inches. Weather conditions varied daily with indoor temperatures ranging between 88.7° and 65.9° F and indoor humidity ranging from 76.2 to 32.6 %.

Figure 2.1 Single-Story Connecticut House with Apartment Addition

Shot Date	shot number	GROUND MOTION AND AIRBLAST								CRACK DISPLACEMENT			
		Longitud. PPV	Transverse PPV	Vertical PPV	SDOF Frequency (Long.)	FFT Frequency (Long.)	SDOF Frequency (Vertical)	FFT Frequency (Vertical)	Airblast	Crack 1 (Vertical Plane)	Crack 3 (Long. Plane)	Normalized CD/PPV Crack 1/V	Normalized CD/PPV Crack 3/L
		(in/sec)	(in/sec)	(in/sec)	(Hz)	(Hz)	(Hz)	(Hz)	(dB)	(μin)	(μin)		
5/20/2002	1	0.18	0.165	0.055	21	21.5	24.0	22.0	106	41	N/A	745.5	N/A
5/22/2002	2	0.03	0.05	0.025	20	23.4	24.0	23.6	110	14	N/A	560.0	N/A
5/22/2002	3	0.065	0.05	0.02	19	18.1	40.0	37.6	100	19	N/A	950.0	N/A
5/23/2002	4	0.105	0.15	0.075	18	18.0	25.0	23.4	106	39	N/A	520.0	N/A
5/23/2002	5	0.125	0.085	0.065	21	21.9	24.0	23.0	122	44	N/A	676.9	N/A
5/23/2002	6	0.1	0.085	0.06	18	17.9	25.0	23.5	123	38	N/A	633.3	N/A
6/3/2002	7	0.08	0.08	0.04	19	22.4	27.0	22.8	106	30	N/A	750.0	N/A
6/10/2002	8	0.08	0.07	0.03	22	22.1	23.0	22.8	132	17	N/A	566.7	N/A
6/17/2002	9	0.145	0.125	0.055	22	18.5	25.0	24.9	110	29	25	527.3	172.4
6/18/2002	10	0.08	0.11	0.03	19	19.1	36.0	22.9	112	26	19	866.7	237.5
6/26/2002	11	0.08	0.065	0.05	24	19.0	25.0	23.3	110	25	15	500.0	187.5
7/9/2002	12	0.125	0.16	0.16	23	22.6	25.0	25.0	110	41	31	256.3	248.0
7/12/2002	13	0.08	0.065	0.045	25	24.5	25.0	25.0	122	20	13	444.4	162.5
7/16/2002	14	0.19	0.18	0.095	19	19.0	25.0	25.1	106	60	59	631.6	310.5
7/22/2002	15	0.345	0.255	0.095	23	22.8	25.0	23.6	117	90	50	947.4	144.9
7/26/2002	16	0.14	0.14	0.07	23	20.1	25.0	25.1	122	50	28	714.3	200.0
7/30/2002	17	0.075	0.055	0.035	25	23.5	25.0	25.9	117	23	12	657.1	160.0
8/2/2002	18	0.195	0.155	0.115	25	25.5	25.0	25.3	126	80	37	695.7	189.7
8/15/2002	19	0.215	0.13	0.085	22	23.0	25.0	25.9	119	38	33	447.1	153.5
8/23/2002	20	0.285	0.14	0.095	26	19.9	26.0	25.6	110	47	38	494.7	133.3
9/3/2002	21	0.28	0.21	0.1	23	21.4	25.0	25.8	110	70	60	700.0	214.3
9/10/2002	22	0.27	0.15	0.135	27	26.1	25.0	25.9	112	60	34	444.4	125.9
9/17/2002	23	0.28	0.175	0.095	21	21.5	25.0	31.0	110	57	48	600.0	171.4
9/20/2002	24	0.155	0.06	0.055	24	21.5	25.0	25.4	116	27	28	490.9	180.6

Table 2.1 Ground motion, frequency, airblast and crack displacement information for all blast events in Connecticut

Shot Date	shot number	Distance	Total Shot Weight	Total Number of Holes	Max. Holes per Delay (w/in 8ms)	Total Shot Time	Charge Weight per Hole	Charge Weight/ Delay (Calc.)	Charge Weight/ Delay (Given)	Scaled Distance (Calc.)	Scaled Distance (Given)	Number of Principal Pulses (Radial)	Number of Principal Pulses (Vertical)
		(ft)	(lb)			(ms)	(lb)	(lb)	(lb)	($ft/lb^{1/2}$)	($ft/lb^{1/2}$)		
5/20/2002	1	2429	8280	30	2	352	276	552	290	103.4	142.6	N/A	5
5/22/2002	2	2690	4409	16	1	470	276	276	303	162.0	154.5	N/A	5
5/22/2002	3	3625	8463	53	2	314	160	319	590	202.8	149.2	N/A	4
5/23/2002	4	2200	225	1	1	1	225	225	225	146.7	146.7	N/A	1
5/23/2002	5	2695	4719	27	5	59	175	874	885	91.2	90.6	N/A	3
5/23/2002	6	2260	177	1	1	1	177	177	177	169.9	169.9	N/A	1
6/3/2002	7	2510	7091	42	2	625	169	338	600	136.6	102.5	N/A	3
6/10/2002	8	2217	3920	48		557	147	358	600	117.2	90.5	N/A	4
6/17/2002	9	2693	10271	37	3	428	278	833	810	93.3	94.6	2	4
6/18/2002	10	2460	13216	40	2	287	330	661	800	95.7	87.0	3	2
6/26/2002	11	2430	7637	49	3	301	156	468	800	112.4	85.9	4	4
7/9/2002	12	2700	12261	46	3		267	800	870	95.5	91.5	5	3
7/12/2002	13	2190	4785	50	4		96	383	450	111.9	103.2	1	1
7/16/2002	14	2430	7957	41	3	310	194	582	400	100.7	121.5	5	2
7/22/2002	15	2376	13081	51	3	419	256	769	810	85.7	83.5	7	4
7/26/2002	16	2323	10649	54	N/A		197	N/A	600		94.8	7	5
7/30/2002	17	2240	8965	74	4	441	121	485	800	101.8	79.2	7	6
8/2/2002	18	2441	15345	59	3	436	260	780	660	87.4	95.0	2	5
8/15/2002	19	2490	7495	37	4	215	203	810	840	87.5	85.9	3	3
8/23/2002	20	2420	12804	40	2		320	640	660	95.6	94.2	3	3
9/3/2002	21	2385	12507	38	2		329	658	690	93.0	90.8	1	2
9/10/2002	22	2270	13251	57	3	402	232	697	500	86.0	101.5	3	5
9/17/2002	23	2640	10627	36	3		295	886	825	88.7	91.9	2	3
9/20/2002	24	2693	9780	47	3	430	208	624	720	107.8	100.4	3	1

Table 2.2 Shot timing, scaled distances, explosive characteristics, and other pertinent logistical information for all blast events in Connecticut

Structural Description

Plan and elevation views of the Connecticut structure are shown in Figures 2.2 and 2.3. An apartment addition was constructed over the masonry block garage left of the main portion of the structure labeled "original structure" in Figure 2.2. The wood frame exterior is surfaced with wood shingle clapboard and on the interior with drywall. Photographs of the rear of the house in Figure 2.4 show its position on a hillside exposing the basement.

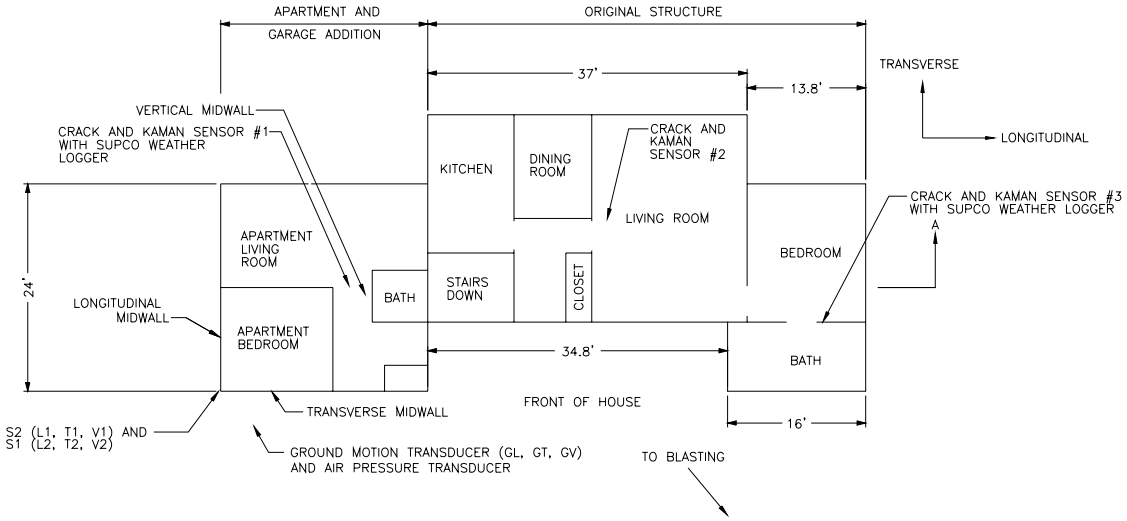

Figure 2.2 Plan View of Connecticut House with Crack and Sensor Locations

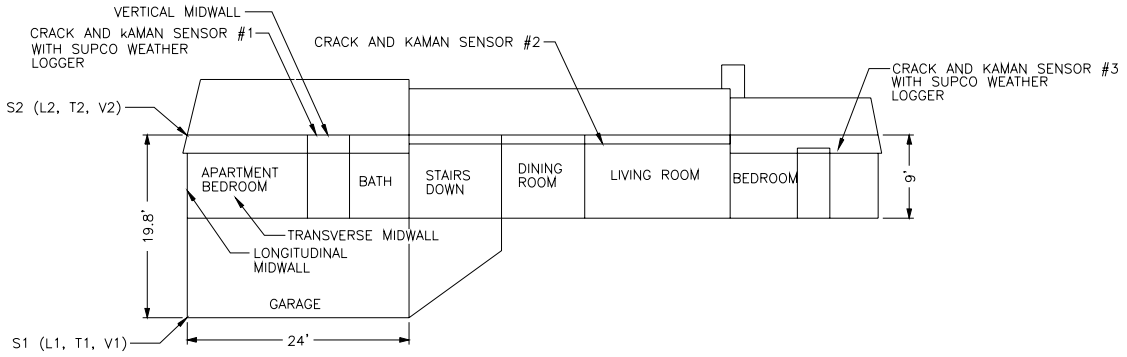

Figure 2.3 Elevation View of Connecticut House with Crack and Sensor Locations

(a) **(b)**

Figure 2.4 Photos of Connecticut house (a) from the rear of the structure, and (b) outside the apartment/garage addition

Figure 2.5 presents photographs of the garage ceiling under the addition, as well as the apartment roof/truss system. The unique feature of the addition is that the floor joists and ceiling joists run perpendicular to each other. Typically floor and ceiling joists are both oriented in the transverse direction of the house, which involves the shortest span. As shown in Figures 2.5 and 2.6, the floor joists between the garage and apartment run parallel to the longitudinal direction supported by a main steel beam in the transverse direction, while the ceiling joists run in the traditional transverse direction and are supported by interior walls. Thus there are several joists in the hallway that span the entire 24' width of the structure, otherwise all joist spans are on the order of twelve feet. This support configuration may have a significant effect on the vertical support of the apartment containing Crack 1.

(a) **(b)**

Figure 2.5 Photos of ceiling joist systems (a) garage ceiling/apartment floor system, (b) apartment addition ceiling truss system

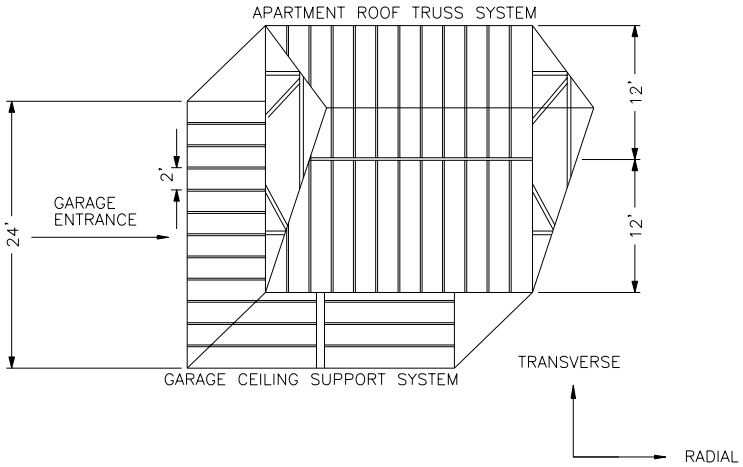

Figure 2.6 Schematic of apartment/garage addition joist systems

Instrumentation

All instrument locations are shown on Figures 2.2 and 2.3. Eight structural velocity transducers were mounted on the southern and western walls of the apartment addition, and an additional transducer was added to the mid-ceiling on August 9th, 2002. A tri-axial seismograph and an airblast transducer were installed outside of the southwest corner of the apartment addition.

Three cracks were instrumented with eddy current "Kaman" micrometer displacement sensors for this case study. Crack #1 was in the apartment ceiling,

identified as Sensor 1 and is shown on the ceiling and in detail in Figure 2.7(a). Two other cracks on a wall and ceiling, were in the main portion of the structure and are identified as sensors 2 and 3, sensor 3 is shown in Figure 2.7(b). Crack 1 runs east-west at the mid-span of the unsupported joists at the beginning of a hallway leading between rooms in the addition. Crack 2 lies in the center of the living room ceiling, and Crack 3 runs vertically up an interior wall in the bedroom of the main portion of the structure.

For each blast, seismograph (ground), and velocity transducer data were collected for eight seconds. Any channel could trigger the entire system. Time correlated time histories of dynamic, blast induced crack displacements were measured by the Kaman sensors for 5 seconds. Temperature and humidity were recorded in each room containing a crack every 10 minutes by independent Supco weather loggers.

One of the challenges involved in this case study is the correlation of the responses. Typically, structure response is measured at the top (S_2) and bottom (S_1) of single-stories or structures with uniform framing and materials. In this case, however, S_1 response is measured near the base of the concrete masonry unit garage wall, while S_2 response is measured near the ceiling at the southwest corner of the wood frame and drywall apartment addition. There was no response data recorded at the junction of these two different wall types. Consequently, the gross wall, in-plane shear distribution cannot be assumed because the distribution of motion will differ due to radically different wall types. This challenge emphasizes the necessity for three sensor locations for two-story structures to ensure that the proper response mode shape is chosen for each story.

Furthermore, structural response was measured only in the southwest corner of the apartment addition. Crack 1 lies within this portion, supported by the garage underneath. Cracks 2 and 3, however, are located some distance away, within the main, un-instrumented portion of the house that includes no underlying basement. Therefore, the structural responses measured at this site are most applicable for the addition and response of Crack 1. Both of these challenges will be explored further when correlations of crack displacements and structural motions are investigated.

Figure 2.7 Wall view and detail photographs of Cracks 1 (top) and 3 (bottom) with sensors

Blast Response

Figure 2.8 shows longitudinal, transverse and vertical time histories of excitation ground velocities, structural response velocities, and the corresponding apartment and bedroom wall crack response for blast 15 with a peak particle velocity of 0.345 ips (8.8 mm/sec), measured in the longitudinal direction. Each waveform includes maximum measured values in parenthesis. These responses are parallel to the plane of the wall containing Crack 3, and therefore are employed to calculate gross wall displacements to compare with directly measured crack displacements. The top two graphs show measured apartment addition Crack 1 displacement and bedroom wall Crack 3 displacement, followed by longitudinal, transverse and vertical particle velocity, upper corner (S_2) longitudinal, transverse, and vertical velocity response, lower corner (S_1) longitudinal, transverse and vertical velocity response, and airblast. This event produced a peak Crack 1 displacement of 90μin (2.29 μm), and peak Crack 3 displacement of 50μin (1.25μm).

Figure 2.9 shows the same Crack 1 and Crack 3 displacements with longitudinal, transverse, and vertical ground, S_2 and S_1 displacements, as well as calculated longitudinal, transverse, and vertical relative (S_2-S_1) displacement time histories, and airblast.

This event produced the largest overall ground motion and largest apartment Crack 1 displacement, but did not produce the largest Crack 3 displacement. Chapter 3 discusses the intricacies of blasting design, and goes further into detail on why certain shot geometries and timing produces relatively larger or smaller crack displacements.

Natural frequency and damping of the structure are important for calculating single degree of freedom response spectra. Thus, the dominant frequency of the structure must be estimated. Dominant frequencies of structure response (natural frequency) are estimated employing either the Fourier Frequency analysis or the zero-point-crossing method during free response (Dowding 1996). The natural frequency of the Connecticut structure was determined via both methods.

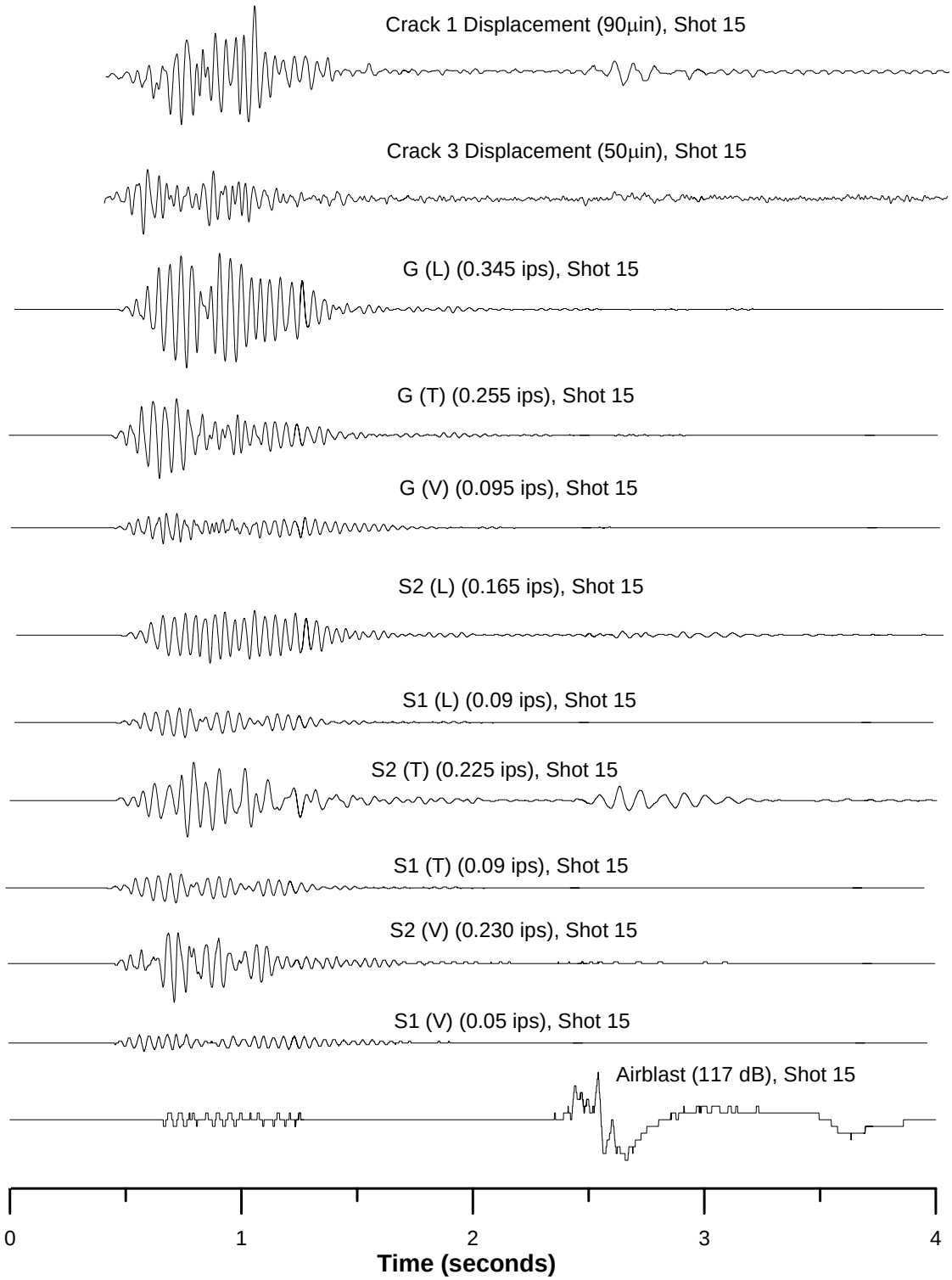

Figure 2.8 Time histories of Crack 1 and 3 displacements from blast event 15 on July 22nd, 2002 at 11:49 AM compared to longitudinal, transverse, and vertical velocity ground excitation, S_2 response velocity, S_1 response velocity, and air blast.

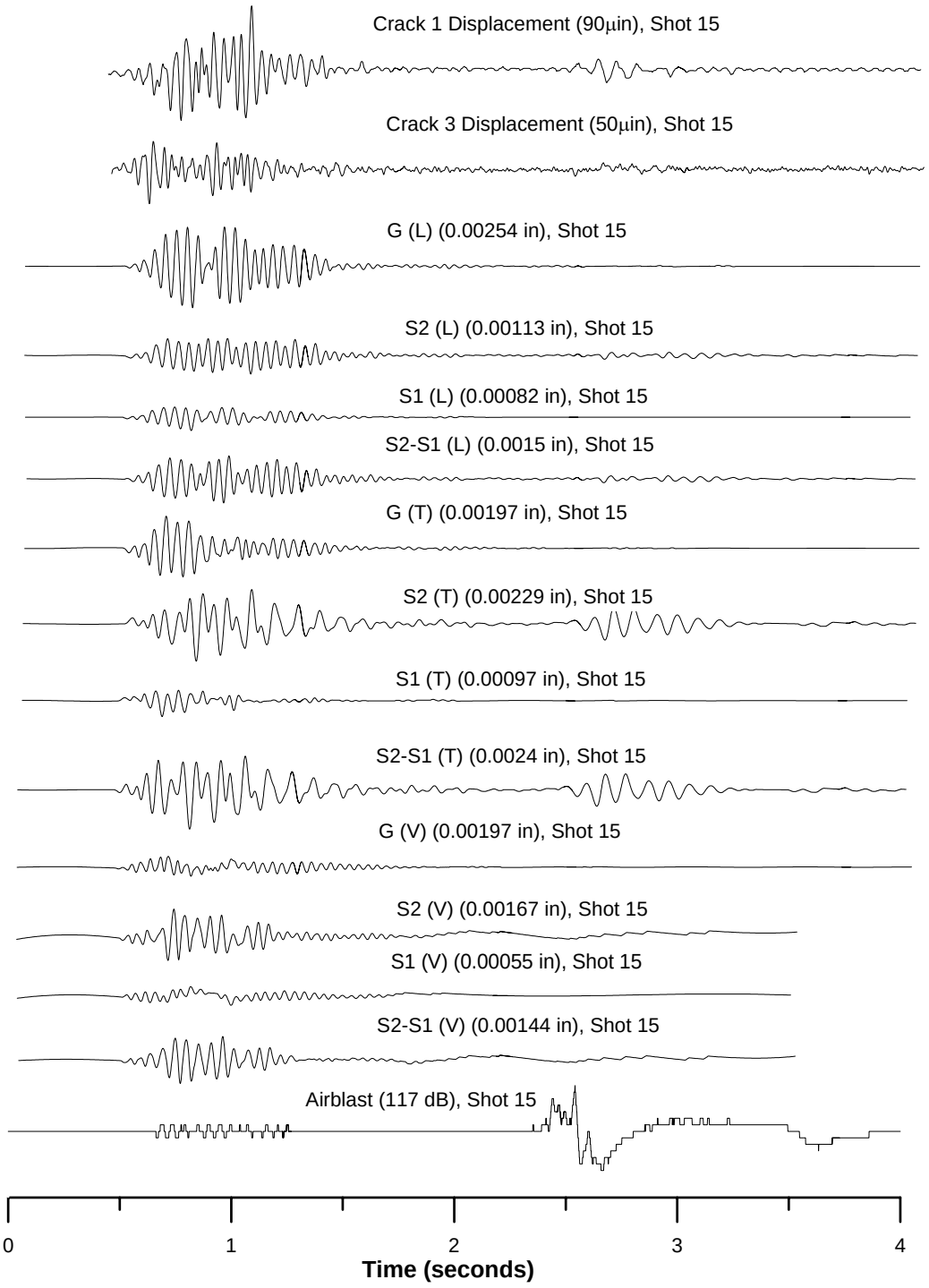

Figure 2.9 Time histories of Crack 1 and 3 displacements from blast event 15 on July 22nd, 2002 at 11:49 AM compared to longitudinal, transverse, and vertical ground displacements, S_2 displacement response, S_1 displacement response, (S_2-S_1) relative displacement, and air blast.

"Free response" is defined as structural response continuing after the cessation of ground motion. Where free response occurs, as shown in Figure 2.10, the zero-point-crossing method may be employed. Free response is necessary for the development of this method because the natural frequency of a structure is most easily identified when it is no longer excited by ground motion. The inverse of twice the time between successive zero-crossings, or the period, results in an estimated dominant/natural frequency of the structure. Natural frequencies estimated from $S_{2,}$ horizontal, radial time histories, during free response averaged 11-12 Hz.

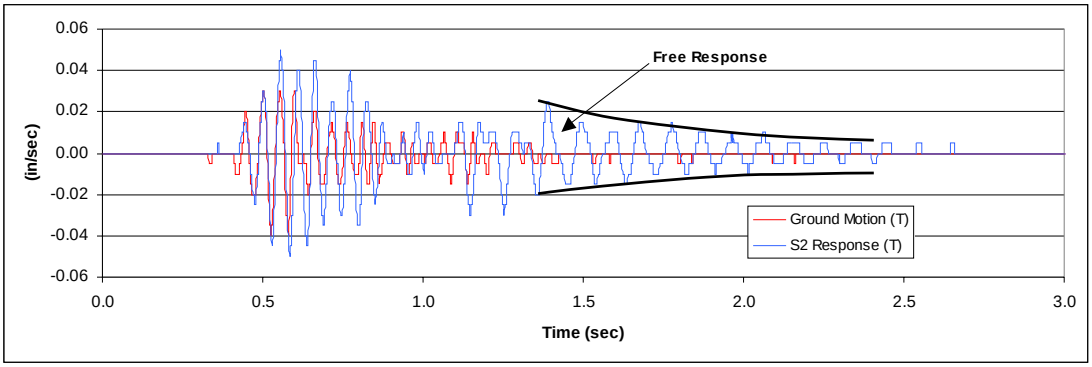

Figure 2.10 Free response of an S_2 velocity time history in the Connecticut house

The Fourier Frequency Spectra approach must be employed when little or no free response is detected in a S_2 time history. For the purposes of this case study, Fourier Frequency Transforms (FFT) are calculated with the dedicated software White Seismograph Data Analysis (White Industrial Seismology 1998), and Northwestern University Vibration Analysis, or NUVIB (Huang 1994). White Seismograph Data analysis only accepts data files secured from White seismographs. Therefore, NUVIB must be employed to transform crack displacement time histories. The ratio of structural response and ground motion FFT amplitudes of the same component provides the means to determine the dominant frequency of the structure, and is shown in Figure 2.11 (a) for blast event 15 on July 22nd in the longitudinal direction, and Figure 2.11 (b) for event 8 on June 10th in the vertical direction. In this figure, the longitudinal S_2 velocity spectra (middle), is divided by the longitudinal ground motion spectra (bottom) to obtain the dominant frequency spectra ratio (top). False peaks may develop when small structural amplitudes are divided by much smaller ground motion amplitudes. To prevent these large ratios of insignificant response and excitation, broad-frequency band, low amplitude

noise should be added to both the structural and ground motion amplitudes (Dowding 1996). Alternately, these false peaks can be filtered out by replacing spectra amplitudes less than ten percent of the peak amplitude with a value of exactly ten percent of the peak. This latter approach was followed in this case.

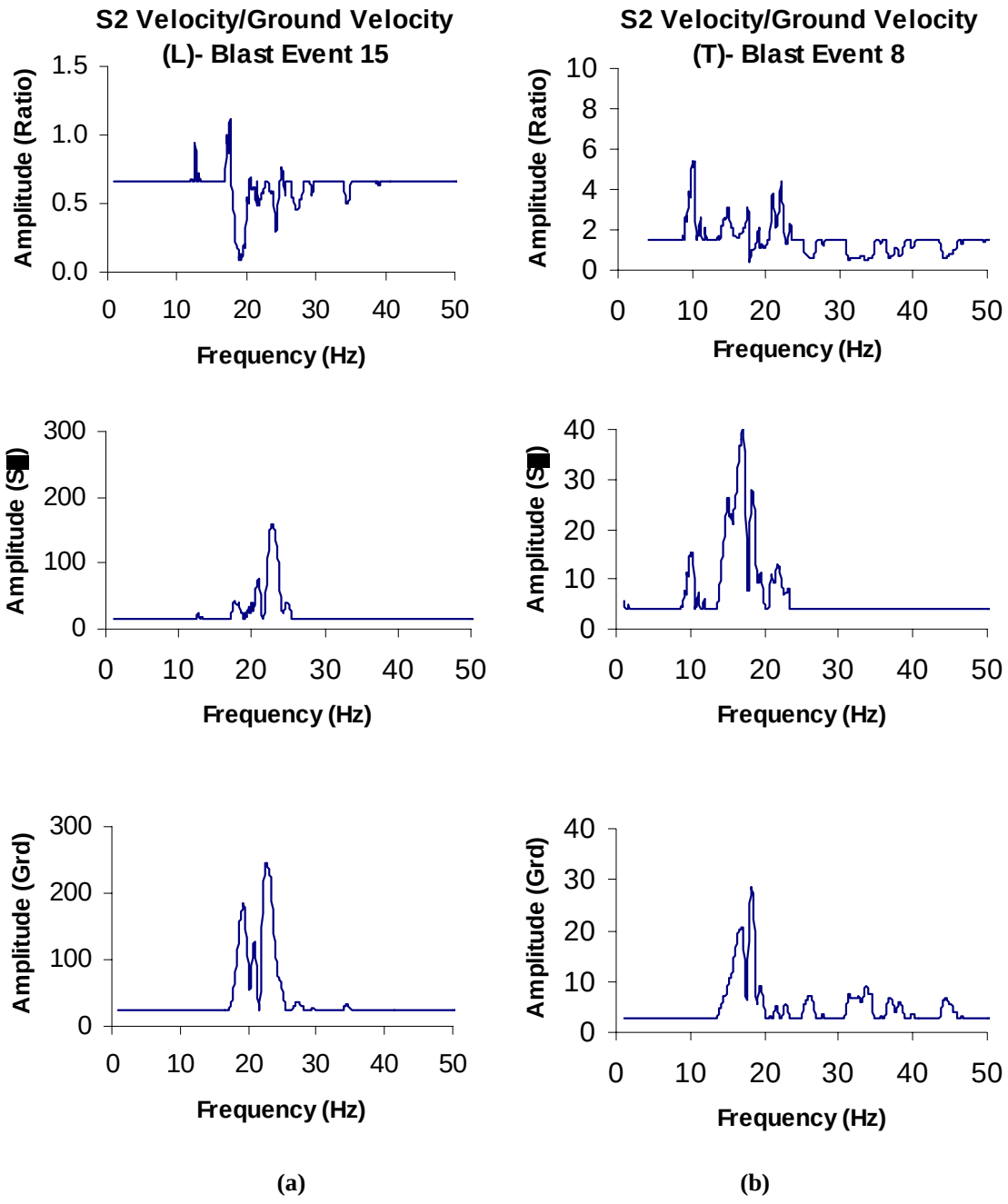

Figure 2.11 Spectra of S_2 velocity frequency fourier transform with ground velocity frequency fourier transform ratio (top), S_2 velocity frequency fourier transform (middle) and ground velocity frequency fourier transform (bottom) (a) for longitudinal response, Blast 15 and (b) for transverse response, Blast 8

Single degree of freedom (SDOF) responses were calculated for all longitudinal and vertical ground motions produced by the blast events to estimate relative displacements of the structure. A pseudo velocity response spectrum curve is generated from SDOF analyses that represent the response of structures, of varying natural frequencies, to the same ground motion (Dowding 1996).

The SDOF response spectrum for the longitudinal ground motion produced by blast event 15 is shown in Figure 2.12. A damping coefficient of 5% was assumed in determining the response spectra for all of the ground motions analyzed, based on average values from previous studies (Dowding, 1996). The estimated natural frequency of the superstructure is 10 to 12 Hz, while the estimated natural frequency of the wall is 17 to 18 Hz. Therefore the calculated displacement of the structure relative to the ground at 11 Hz is 7000 μin (178 μm), while the average displacement between 10 and 18 Hz. is 13620 μin (346 μm) via the SDOF spectrum in Figure 2.12.

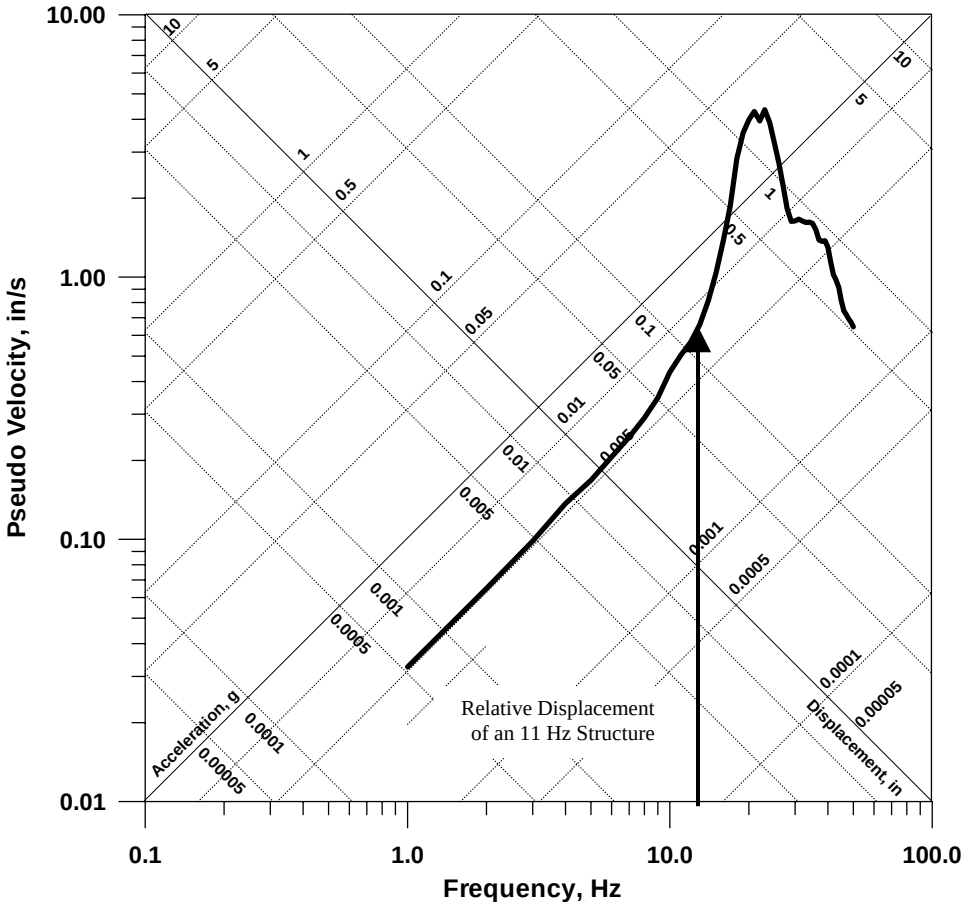

Figure 2.12 Single degree of freedom response spectrum of longitudinal ground motion produced by Blast 15 on July 22nd, 2002 at 11:49 AM, showing the estimated relative displacement of an 11 Hz structure

Figure 2.13 shows longitudinal, transverse, and vertical time histories of excitation ground motion, S_2 structural response, airblast, and the corresponding addition ceiling Crack 1 response associated with blast 8 (June 10th, 2002). One of the inherent challenges in Connecticut was establishing correlation criteria for Crack 1, which lies in the ceiling of the apartment. The same analysis employed for the longitudinal responses and correlated to the bedroom wall Crack 3 in the longitudinal plane, was performed for all three axes of excitation and response, and correlated with Crack 1 response. Figure 2.11 (b) above shows the transverse FFT spectra for blast 8 and Figure 2.14 shows the longitudinal, transverse and vertical single degree of freedom response spectrum.

The response of Crack 1 illustrates the importance of airblast control. For many of the shots involved in this study there are two separate Crack 1 responses, one resulting from the relatively low amplitude vertical ground motions (compared to the longitudinal motions), and another resulting from the trailing airblast. Blasting at the quarry was roughly 2500 feet from the house, therefore the airblast arrives roughly 1.8 to 1.9 seconds after the ground motion, causing a completely independent displacement in Crack 1. Crack 3 did not respond with nearly the same vigor to airblast events as Crack 1. The quarry is situated such that the trailing air pressure impacts the long face of the structure, causing a significant transverse response. Figure 2.13 clearly shows the effect of this transverse motion on Crack 1.

The time history in Figure 2.13 shows the effect of a 132 dB airblast pressure intersecting the structure. The corresponding 90 μin peak-to-peak Crack 1 displacement is the largest recorded single crack displacement for this project. Of the 24 blast events recorded, 11 of them produced airblast events over 115 dB, and 7 of them over 120 dB. Crack 1 was far more sensitive to these airblast events than Crack 3, and was typically more sensitive to them than the ground motion. The existence of large airblast over-pressures is often a significant concern in mining and quarry operations.

Midway through the course of the project, it became apparent, however, that the methods of measuring structural displacement, S_2 and S_1 due to ground motions, do not accurately represent the true relative displacement of the ceiling, or of Crack 1 under these conditions. For the final six events, a transducer was placed next to Crack 1, in the center of the ceiling, to measure vertical mid-ceiling response, and obtain an out-of-plane

ceiling response. The correlation of displacements calculated from motions at this ceiling velocity transducer to Crack 1 displacement will be presented and evaluated later in the chapter.

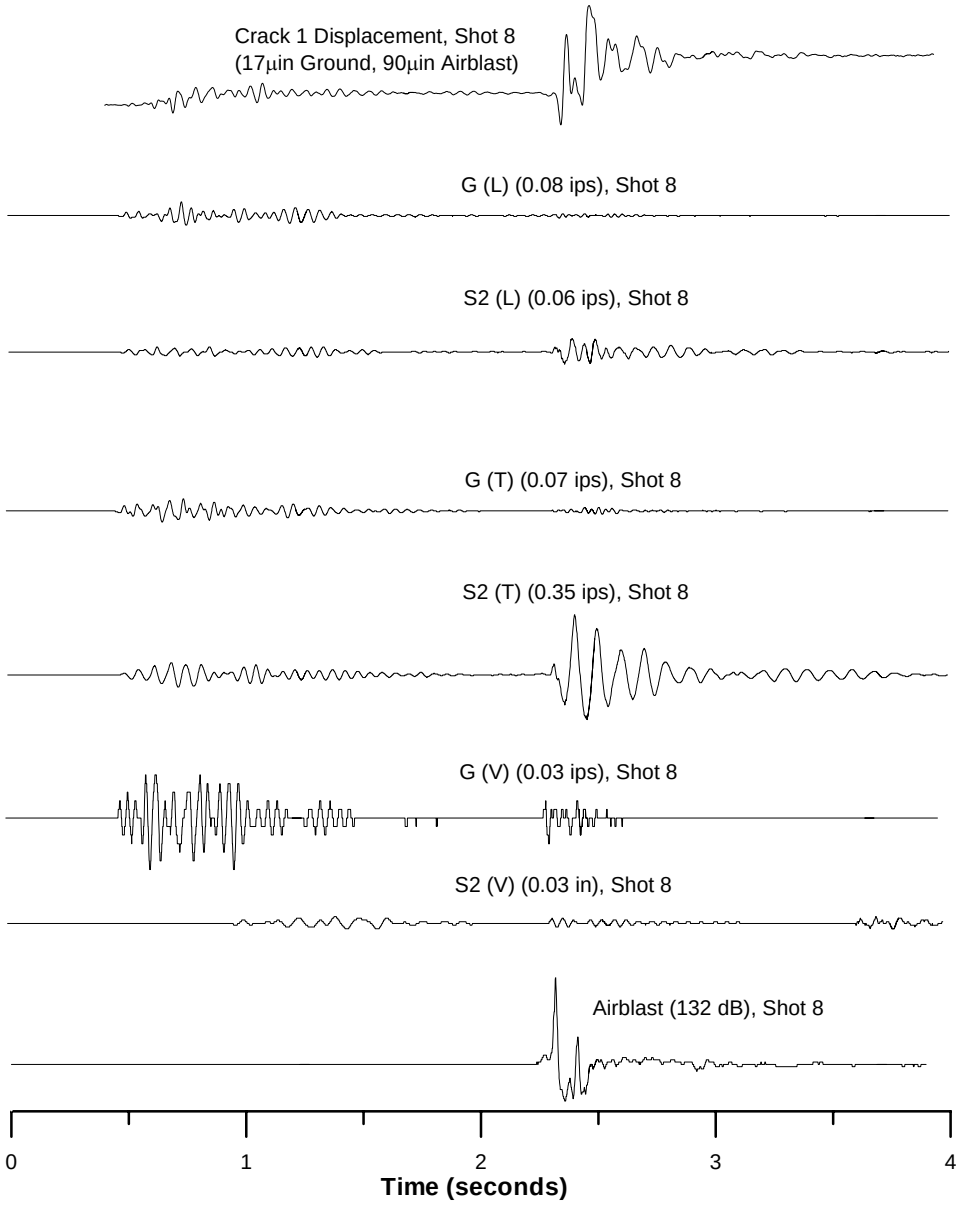

Figure 2.13 Time history of Crack 1 displacement from Blast event 8 on June 10th, 2002 at 11:49 AM compared to longitudinal, transverse, and vertical ground excitation, longitudinal, transverse, and vertical S_2 response, and air blast.

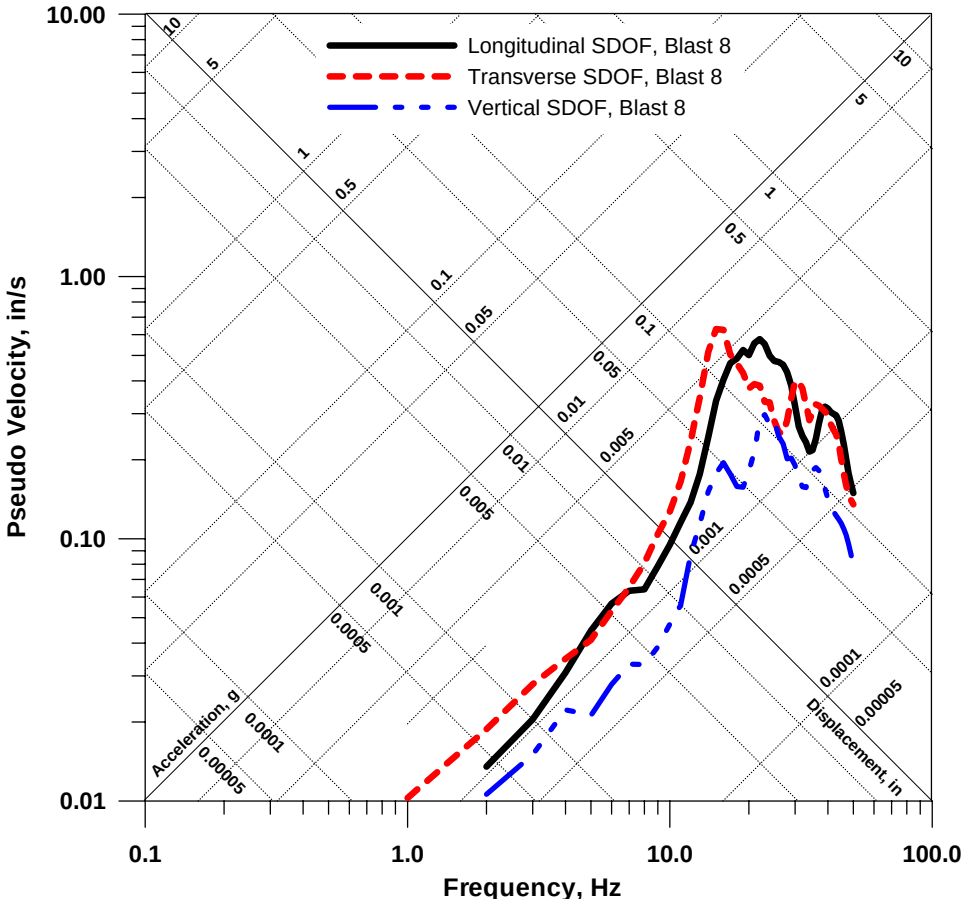

Figure 2.14 Single degree of freedom response spectrum of longitudinal, transverse, and vertical ground motion produced by Blast 8 on June 10th, 2002 at 11:49 AM

Crack Response to Environmental Effects

Figure 2.15 compares the long-term response of the bedroom wall crack to the long-term fluctuation of temperature and humidity. Long-term crack displacement was measured hourly for the duration of the monitoring period, while temperature and humidity were measured every ten minutes and averaged to obtain one sample per hour. Some sharp changes are observed in the temperature, humidity and crack displacement during the monitoring period. Large, simultaneous changes in temperature and humidity, such as those on July 5th, July 12th, and July 24th, produce the largest changes in crack displacement.

A 24-hour rolling average of temperature, humidity and crack displacement were systematically calculated at each hourly measurement by averaging the data 12 hours before and 12 hours after (24 hours in total) each individual sample. See McKenna (2002) for details. Overall averages of crack displacement, temperature and humidity for the duration of the monitoring period are presented as horizontal solid lines in Figure 2.15.

Field measurements, 24-hour and overall averages are employed collectively to quantify micro-inch crack response to weather effects. Weather effects are analyzed for three different effects; frontal movements that change overall temperature and humidity for periods of several days to weeks, daily response to changes in average temperature and solar radiation, and extremes of unusual weather or other environmental effects (McKenna 2002). Table 2.3 lists average and maximum values for the frontal, daily, and total weather effects alongside values of crack response to maximum ground motions associated with quarry blasting to compare the difference in magnitude of environmentally induced and blasting induced crack response.

The frontal effect is defined as the deviation of a peak 24-hour average value from the overall average. In other words, between instances of a 24-hour average curve and overall average curve crossing, the frontal effect is measured as the peak, absolute deviation of the 24-hour average from the overall average. The daily effect is defined as the deviation of a peak field measurement from the corresponding 24-hour average. Between each crossing of the field measurement curve and the 24-hour average, the daily effect is measured as the peak, absolute deviation of the field curve from the 24-hour

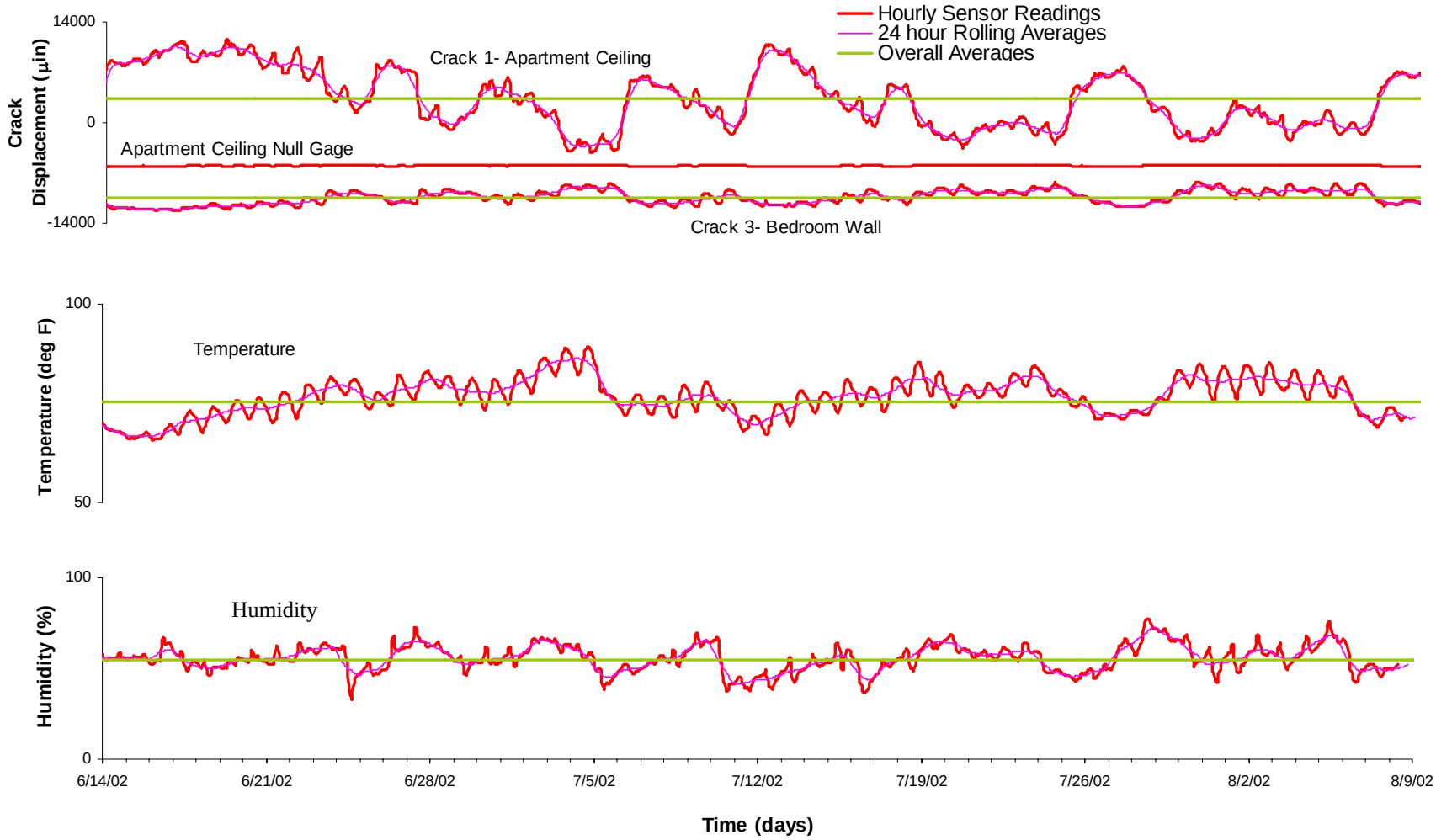

Figure 2.15 Long-term Crack 1, Crack 3, and null gage displacement, temperature, and humidity versus time

average. The final descriptor, the total weather effect, is defined as the difference in the peak field measurement from the overall computed average. Between each crossing of the field measurement curve and the overall average the weather effect is computed as the peak, absolute value of the field measurement minus the overall average. The average and maximum values of these three effects on crack displacement, temperature and humidity are presented in Table 2.3.

Crack Sensor 1- Apartment Ceiling	Temperature Change (DegF)	Humidity Change	Crack Displacement (μin)	Crack Displacment (μm)
Frontal Effect				
Average deviation of 24-hour average from overall average	5	4	3346	85
Maximum deviation of 24-hour average from overall average	12	14	7283	185
Daily effect				
Average deviation of field measurement from 24-hour average	1.5	1.5	669	17
Maximum deviation of field measurement from 24-hour average	5	11	5748	146
Weather Effect				
Average deviation of field measurement from overall average	5	4	3543	90
Maximum deviation of field measurement from overall average	15	15	8307	211
Blsting Effect				
Typical vertical ground motion (PPV=0.10 ips)	-	-	35	0.89
Maximum ground motion (PPV= 0.345 ips)	-	-	90	2.89

Crack Sensor 3- Bedroom Wall	Temperature Change (DegF)	Humidity Change	Crack Displacement (μin)	Crack Displacment (μm)
Frontal Effect				
Average deviation of 24-hour average from overall average	4	6	669	17
Maximum deviation of 24-hour average from overall average	13	23	1693	43
Daily effect				
Average deviation of field measurement from 24-hour average	2	2	217	5.5
Maximum deviation of field measurement from 24-hour average	6.5	15	1142	29
Weather Effect				
Average deviation of field measurement from overall average	4	6	748	19
Maximum deviation of field measurement from overall average	14	26	2165	55
Blsting Effect				
Typical Radial ground motion (PPV=0.10 ips)	-	-	30	0.74
Maximum ground motion (PPV= 0.345 ips)	-	-	72	1.82

Table 2.3 Computed crack displacements due to long-term weather phenomena, typical ground motion and maximum ground motion in Connecticut

Figure 2.16 displays in detail the relatively dominant effect of weather phenomena on crack displacement versus that of blast-induced ground excitation. This Figure shows the response of Crack 1 in the apartment over two full days, June 10th and 11th, 2002, during which significant blast event #8, time histories of which are shown in Figure 2.17, occurred with a peak particle velocity of 0.08 ips and airblast of 132 dB. This daily response is compared with the response during the entire period of observation. The blast effect on Crack 1 is circled and labeled on Figure 2.16.

Blast event 8 and its resultant displacement time history for Crack 1 are unique to those previously analyzed for two reasons. First, the 132 dB airblast that occurs approximately 2 ½ seconds into the monitoring period produces a peak crack displacement of 180 micro-inches, far exceeding the 35 micro-inch displacement induced by the ground motion. Second, this airblast also produces what appears to be a 90 micro-inch offset during the 8-second record. However, the magnified hourly crack response in Figure 2.16 shows that the daily weather phenomena on June 10th produced a maximum crack displacement in the apartment ceiling of 1500 micro-inches, which is an order of magnitude greater than that produced by the event. This crack, even if it were offset by 90 micro-inches, was returned to its pre-blast displacement less than four hours later as a result of the temperature and humidity change.

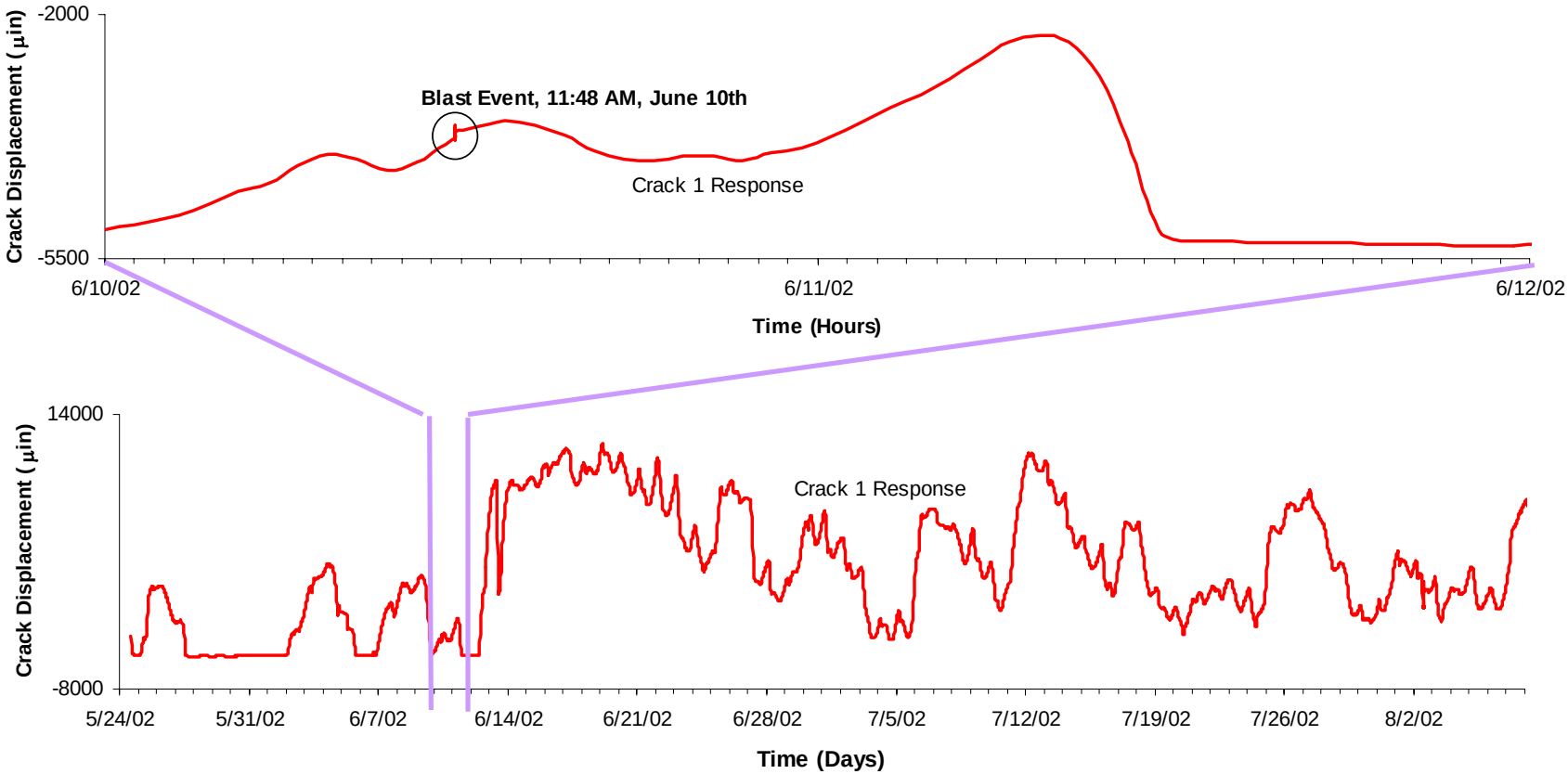

Figure 2.16 Long-term Crack 1 displacement magnified to show 48-hours of response data surrounding blast event 8 on June 10th, 2002

Comparison of Computed and Measured Crack Displacements

The maximum measured crack displacement produced by each shot is compared in the longitudinal and vertical directions in Table 2.4 (a) and (b) to various computed wall displacements based on structure response and peak ground motions. Structure/wall displacements were computed using a number of methods such as the integration of velocity time histories and the single degree of freedom response spectrum method. Response of bedroom wall Crack 3 correlated best with ground motions and displacements in the longitudinal direction, and displaced with zero correlation to airblast. Crack 3 is on an interior wall, so this poor correlation is expected. Apartment ceiling Crack 1, however, responded better to certain ground motion and structural displacements in various axial directions. Correlations of Crack 3 responses are presented in Figure 2.17. Correlations of Crack 1 displacement in the longitudinal direction are presented in Figure 2.18, transverse in 2.19, and vertical in 2.20. In addition, Figure 2.20 presents the correlation between Crack 1 displacement and measured airblast. Details pertaining to the aforementioned methods in the computation of structural displacement are presented below.

	Relative Displacement of Structure, δ, by Method (μin)										Velocities (in/sec)			Crack Displacements	
	Integration of Velocities							SDOF Method							
Date Shot #	Vertical ($S_{midceiling}$)	Vertical $(S_2)_{max}$ $(S_2\text{-}S_1)_{max}$	Vertical $(G)_{max}$ $(S_2\text{-}G)_{max}$	Transverse $(S_2)_{max}$ $(S_2\text{-}S_1)_{max}$	Transverse $(G)_{max}$ $(S_2\text{-}G)_{max}$	Longitud. $(S_2)_{max}$ $(S_2\text{-}S_1)_{max}$	Longitud. $(G)_{max}$ $(S_2\text{-}G)_{max}$	Vertical f_n = 12Hz f_n = 10-20Hz	Transverse f_n = 12Hz f_n = 10-20Hz	Longitudinal f_n = 12Hz f_n = 10-20Hz	Peak Particle Velocity	Upper Structure $(S_2)_{max}$	Vertical Midceiling $(S_{mid})_{max}$	Crack 1 (μin)	Crack 3 (μin)
5/20/2002 1	N/A	1000 1100	460 900	2600 1300	1690 1700	1600 1600	1460 2200	3243 2726	8816 10678	6529 10600	0.180 (L) 0.165 (T) 0.055 (V)	0.160 (L) 0.240 (T) 0.115 (V)	N/A	41	N/A
5/22/2002 2	N/A	300 800	210 1000	1200 1200	410 1300	400 400	260 500	1422 931	2430 2426	1221 2055	0.030 0.050 0.025	0.035 0.090 0.040	N/A	14	N/A
5/22/2002 3	N/A	600 800	80 800	700 800	400 500	300 290	500 600	300 389	1600 2638	2097 3352	0.065 0.050 0.020	0.035 0.065 0.030	N/A	19	N/A
5/23/2002 4	N/A	1300 N/A	600 1300	2300 N/A	1100 2110	600 N/A	800 1100	1800 2100	4500 7117	3571 5268	0.105 0.150 0.075	0.070 0.160 0.180	N/A	39	N/A
5/23/2002 5	N/A	900 N/A	700 950	2000 N/A	900 2050	900 N/A	1400 1270	2000 1962	3000 4000	3200 4242	0.125 0.085 0.065	0.060 0.140 0.070	N/A	44	N/A
5/23/2002 6	N/A	700 1000	560 1000	2000 2000	780 2000	900 1000	780 1200	2000 2300	3990 6000	4400 6553	0.100 0.085 0.055	0.080 0.135 0.060	N/A	38	N/A
6/3/2002 7	N/A	1150 1700	300 1900	1100 1300	660 1100	500 500	640 800	1300 1345	3561 4754	2000 3768	0.080 0.080 0.040	0.045 0.110 0.070	N/A	30	N/A
6/10/2002 8	N/A	600 700	300 600	4700 4500	720 4700	1000 1000	520 1000	1154 1400	3132 4300	1827 3059	0.080 0.070 0.030	0.030 0.035 0.030	N/A	17	N/A
6/17/2002 9	N/A	660 580	380 740	2520 3000	1000 1640	620 730	1000 1130	2300 1700	4852 7175	3553 5647	0.145 0.125 0.055	0.070 0.195 0.080	N/A	29	25
6/18/2002 10	N/A	830 770	310 970	1270 1510	900 1020	400 430	600 800	544 698	3300 6140	2014 3605	0.080 0.110 0.030	0.040 0.125 0.060	N/A	35	19
6/26/2002 11	N/A	510 580	410 560	790 910	500 750	360 340	600 670	1737 1619	2578 2918	1800 2905	0.080 0.065 0.050	0.035 0.080 0.050	N/A	25	15
7/9/2002 12	N/A	1390 1060	910 1380	1910 2280	120 1640	1170 1120	1000 1350	2600 3331	3421 6984	3185 5103	0.125 0.160 0.160	0.135 0.185 0.190	N/A	41	31

Table 2.4 (a) Traditional structure response and ground motion controls with Crack 1 and 3 displacements for blast events 1 through 12 in Connecticut

Date Shot #		Relative Displacement of Structure, δ, by Method (μin)									Velocities (in/sec)			Crack Displacements	
		Integration of Velocities						SDOF Method							
		Vertical $(S_2)_{max}$ $(S_2-S_1)_{max}$	Vertical $(G)_{max}$ $(S_2-G)_{max}$	Transverse $(S_2)_{max}$ $(S_2-S_1)_{max}$	Transverse $(G)_{max}$ $(S_2-G)_{max}$	Longitud. $(S_2)_{max}$ $(S_2-S_1)_{max}$	Longitud. $(G)_{max}$ $(S_2-G)_{max}$	Vertical f_n = 12Hz f_n = 10-20Hz	Transverse f_n = 12Hz f_n = 10-20Hz	Longitudinal f_n = 12Hz f_n = 10-20Hz	Peak Particle Velocity	Upper Structure $(S_2)_{max}$	Vertical Midceiling $(S_{mid})_{max}$	Crack 1 (μin)	Crack 3 (μin)
7/12/2002 13	N/A	750 460	460 850	1480 1470	700 1500	570 580	700 700	976 1066	1734 2700	2236 2421	0.080 (L) 0.065 (T) 0.045 (V)	0.050 (L) 0.085 (T) 0.060 (V)	N/A	20	13
7/16/2002 14	N/A	1810 1690	640 1700	2280 2810	1600 2580	1290 1000	1500 1730	2614 3000	6839 11053	5365 9647	0.190 0.180 0.095	0.145 0.230 0.230	N/A	60	59
7/22/2002 15	N/A	1670 1440	660 1710	2290 2400	1970 2720	1130 1480	2540 3150	1965 2244	6709 11907	7494 13620	0.345 0.255 0.095	0.165 0.220 0.230	N/A	90	50
7/26/2002 16	N/A	980 910	670 1270	1540 1640	1180 1770	1100 1040	910 1290	1411 1843	4441 6719	3170 4524	0.140 0.140 0.070	0.145 0.180 0.130	N/A	50	28
7/30/2002 17	N/A	290 250	370 200	730 810	510 830	510 360	650 570	1078 1223	1632 2600	1447 2460	0.075 0.055 0.035	0.050 0.080 0.040	N/A	23	12
8/2/2002 18	N/A	1390 1060	840 1690	3000 3090	1430 3030	1010 980	1510 1500	2338 3529	6481 9649	4682 6670	0.195 0.155 0.115	0.130 0.225 0.180	N/A	80	37
8/15/2002 19	3490	3080 1600	660 3700	1880 1950	880 2300	1230 1260	1500 1640	2051 1987	3859 4200	3671 4712	0.215 0.130 0.085	0.155 0.170 0.180	0.460	38	33
8/23/2002 20	4420	2920 2180	870 2940	1640 1680	1130 2340	1180 110	1950 2160	2125 2484	4000 5100	6433 10316	0.285 0.140 0.095	0.115 0.175 0.320	0.590	47	38
9/3/2002 21	2000	5080 3050	730 4990	2220 3050	1620 1890	920 1060	2220 2290	4334 3679	9721 12111	7020 9627	0.280 0.210 0.100	0.100 0.195 0.480	0.250	70	60
9/10/2002 22	3290	2440 1650	940 2490	1360 1610	930 1900	810 870	1880 2160	3290 3364	5017 5300	6230 8795	0.270 0.150 0.135	0.105 0.155 0.320	0.445	60	34
9/17/2002 23	2820	3170 1910	720 3260	2980 2990	1190 2730	1560 1680	1830 2050	4253 3189	5000 7254	5366 8468	0.280 0.175 0.095	0.185 0.235 0.330	0.385	57	48
9/20/2002 24	1470	2240 1430	360 2240	1190 1200	470 1010	720 670	920 1100	1328 1238	1885 3235	2400 4334	0.155 0.060 0.055	0.090 0.105 0.210	0.220	27	28

Table 2.4 (b) Traditional structure response and ground motion controls with Crack 1 and 3 displacements for blast events 13 through 24 in Connecticut

Velocity Time History Integration

Displacement time histories are calculated by integrating velocity time histories. By subtracting time correlated (±0.001 sec) pairs of integrated time histories, a relative displacement time history is produced. This difference was calculated for two pairs of displacement time histories: 1) upper corner response, S_2, minus lower corner response, S_1, and 2) S_2 minus ground motion, G. Comparisons between measured crack displacements and the peak values of these resulting displacement time histories, $(S_2-S_1)_{max}$ and $(S_2- G)_{max}$, are presented graphically in Figures 2.17 through 2.20.

Displacements were also estimated from the integrated ground velocity time histories exclusively. The comparison between measured crack displacement and the peak of these displacement time histories, S_{2max} and G_{max}, are presented in Figures 2.17 through 2.20.

Single Degree of Freedom Response Spectrum Method

As described earlier in the chapter, by analyzing SDOF response spectra of blast-induced ground motions, relative displacements can be estimated for structures of different dominant frequencies. Two approaches were employed in estimating relative displacements via this method. The first was to run an SDOF at 11 Hz to calculate the relative displacement associated with the estimated natural frequency of the structure. These computed relative displacements are then compared with measured crack displacements and shown in Figures 2.17 through 2.20.

The second approach in estimating relative displacements based on the SDOF method was to average the relative displacements of structures with natural frequencies of 10-15 HZ found most likely from previous studies. Comparisons between the measured crack displacements and these average relative displacements are also presented in Figures 2.17 through 2.20.

Correlations to Ground and Structural Motions

The square of the correlation coefficient, R^2, is employed to describe correlations. Microsoft Excel defines R^2 as the square of the Pearson product moment correlation coefficient, which is the proportion of the variance in the value of measured crack response, depending on the variance in the estimator.

In previous case studies (McKenna, 2002), the best correlations with measured crack displacement were those produced by structural motion, S_2 and S_2-S_1 for single-story structures. These measured responses correlate the best because they give the most accurate representation of in-plane wall strains and relative wall displacements. S_2-G is less accurate than S_2-S_1 as there is some transfer of energy between the ground and the house.

S_2-S_1 relative displacement calculations in this case, however, are less applicable because of the large construction and material differences between the lower concrete masonry unit garage walls and the upper wood frame apartment walls. Thus, values calculated for S_2-S_1 response in the Connecticut house represent relative displacements of wall components of two different construction techniques and the mode shapes and response cannot be properly estimated without a transducer, $S_{1.5}$, at the interface between the upper and lower stories. In addition, structural response data were recorded only in the apartment/garage addition and Crack 3 is located on an interior wall in the bedroom at the east, opposite end of the main unit of the house. This portion of the house is founded differently. Therefore it will experience an S_2 response different than that measured above the garage. Were these situations to be corrected (S_1 recorded at the base of the apartment wall and structural response recorded in the bedroom of the main unit), these correlations would be expected to improve significantly.

Crack 3 displacement responds best to ground and structural motions in the longitudinal direction, and does not correlate at all to airblasts, as shown in Figure 2.17. This result is expected, as Crack 3 lies in the longitudinal plane and sits on an interior wall, thus negating the relative effect of airblasts. The highest correlations are those that involve peak particle velocity and integrated ground velocity. The best structural correlations are the single degree of freedom response spectra relative displacement calculations.

Crack 1 displacement correlates with both longitudinal and transverse motions almost equally; being highly responsive, it is most likely to give the appearance of responding to axial motions that produce significantly greater particle velocities. Crack 1 displacements are also divided into two separate categories; those resulting from ground motion, and those resulting from airblasts. The correlation between airblast-induced

Crack 1 displacement and airblast-induced transverse S_2 response (also divided into two categories), is very good, R^2=0.94. The correlation between airblast-induced Crack 1 displacement and airblast decibel level is also quite good, R^2=0.82.

The highest correlation (0.96) for Crack 1 response occurs with the summation of integrated velocities, S_2+$S_{midceiling}$ shown in Figure 2.21 in the vertical direction. Figure 2.22 shows time histories of Crack 1 displacement, Crack 3 displacement, longitudinal, transverse, and vertical particle velocity, vertical ground displacement, vertical S_2 velocity and displacement, $S_{midceiling}$ velocity and displacement, vertical S_2+ $S_{midceiling}$ relative displacement and airblast for Shot 20. The midceiling responses were obtained only for the final six shots. Figure 2.22 shows time histories for blast event 20, and includes ground velocities in all three directions, ground displacements in the long and vertical directions, upper corner structure (S_2) velocity and displacement in the long and vertical directions, and vertical midceiling ($S_{midceiling}$) velocity and displacement. The midceiling response during this event is greater than that at the corner (S_2), and it can be seen that Crack 1 displaces more in tandem with the S_2+$S_{midceiling}$ response than to any other time history. Thus, a continuing displacement at approximately the 1-second mark is seen for both the measured crack displacement and that calculated as S_2+$S_{midceiling}$.

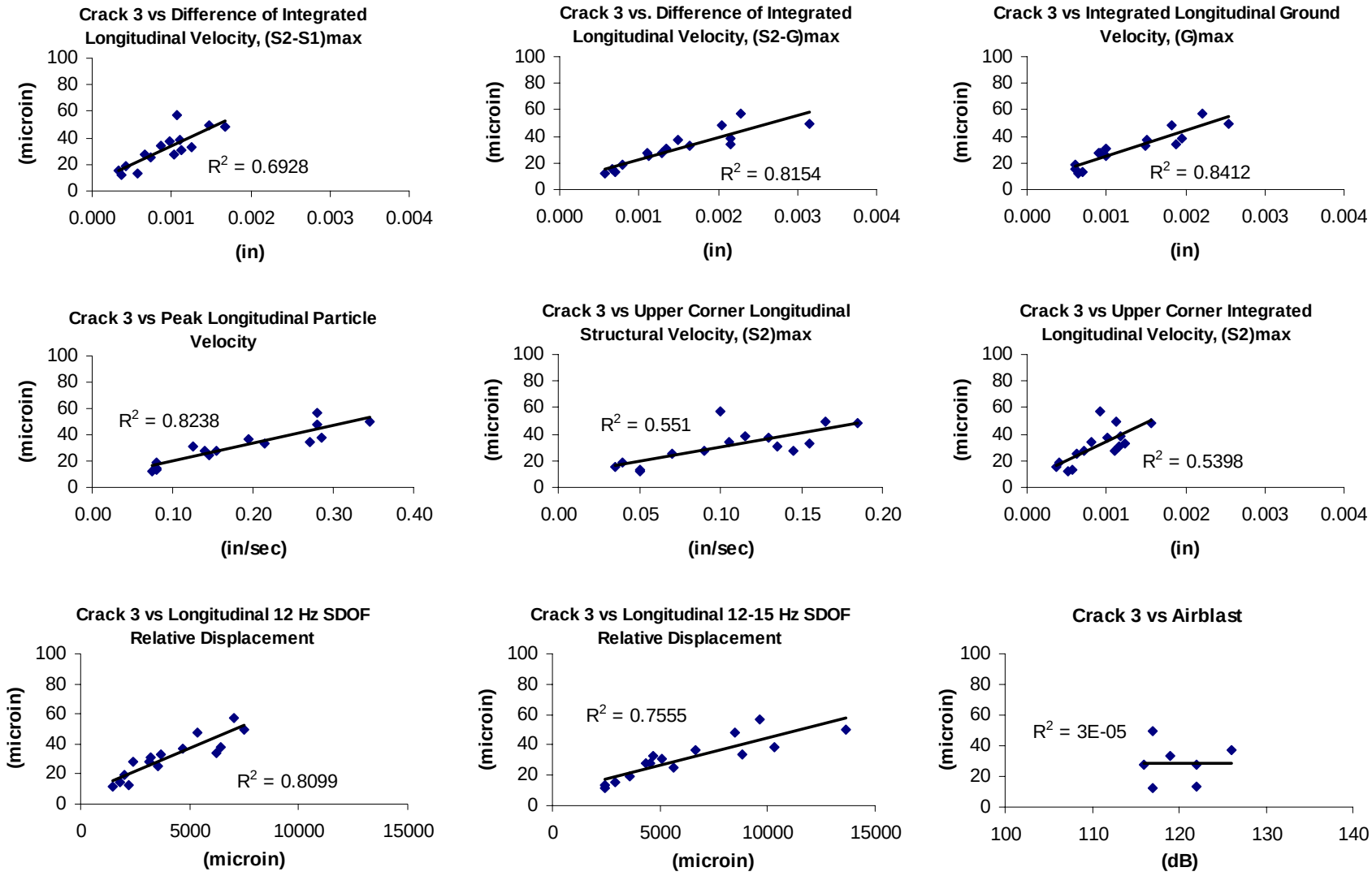

Figure 2.17 Correlations between measured Crack 3 displacement and longitudinal ground motions, relative structural displacements, and airblast

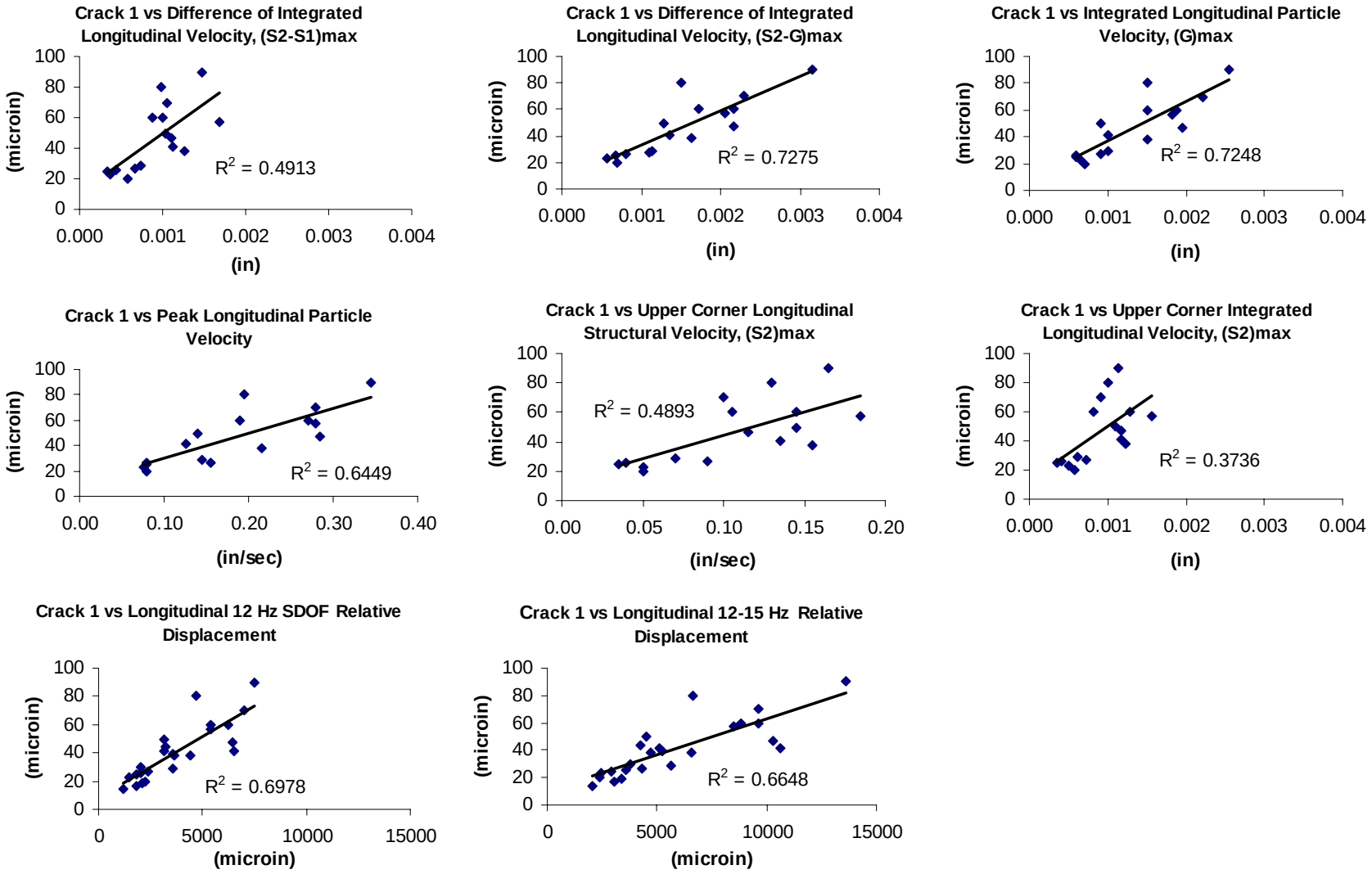

Figure 2.18 Correlations between measured Crack 1 displacement and longitudinal ground motions and relative structural displacements

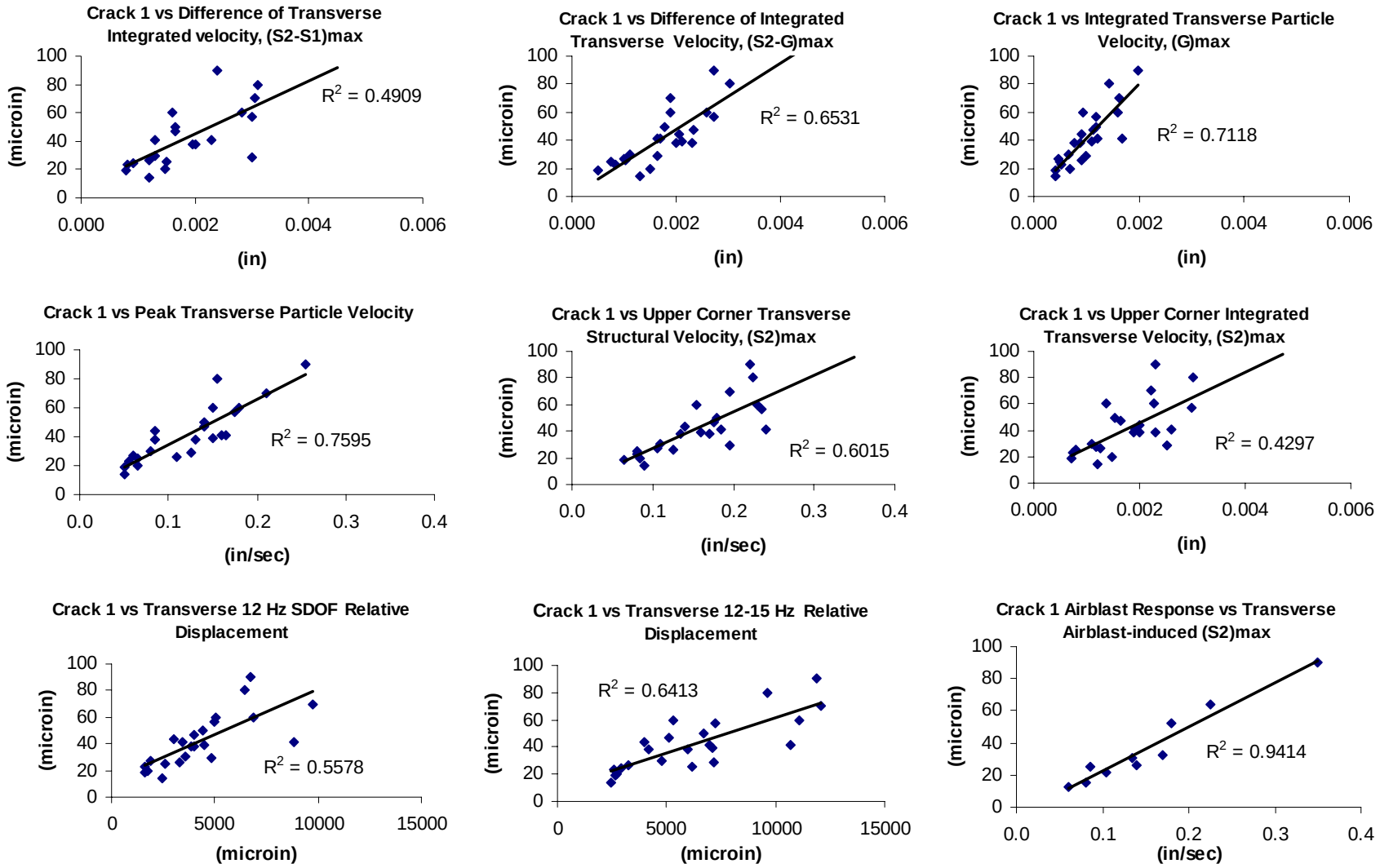

Figure 2.19 Correlations between measured Crack 1 displacement and transverse ground motions, relative structural displacements, and Crack 1 airblast response versus airblast induced upper structure response

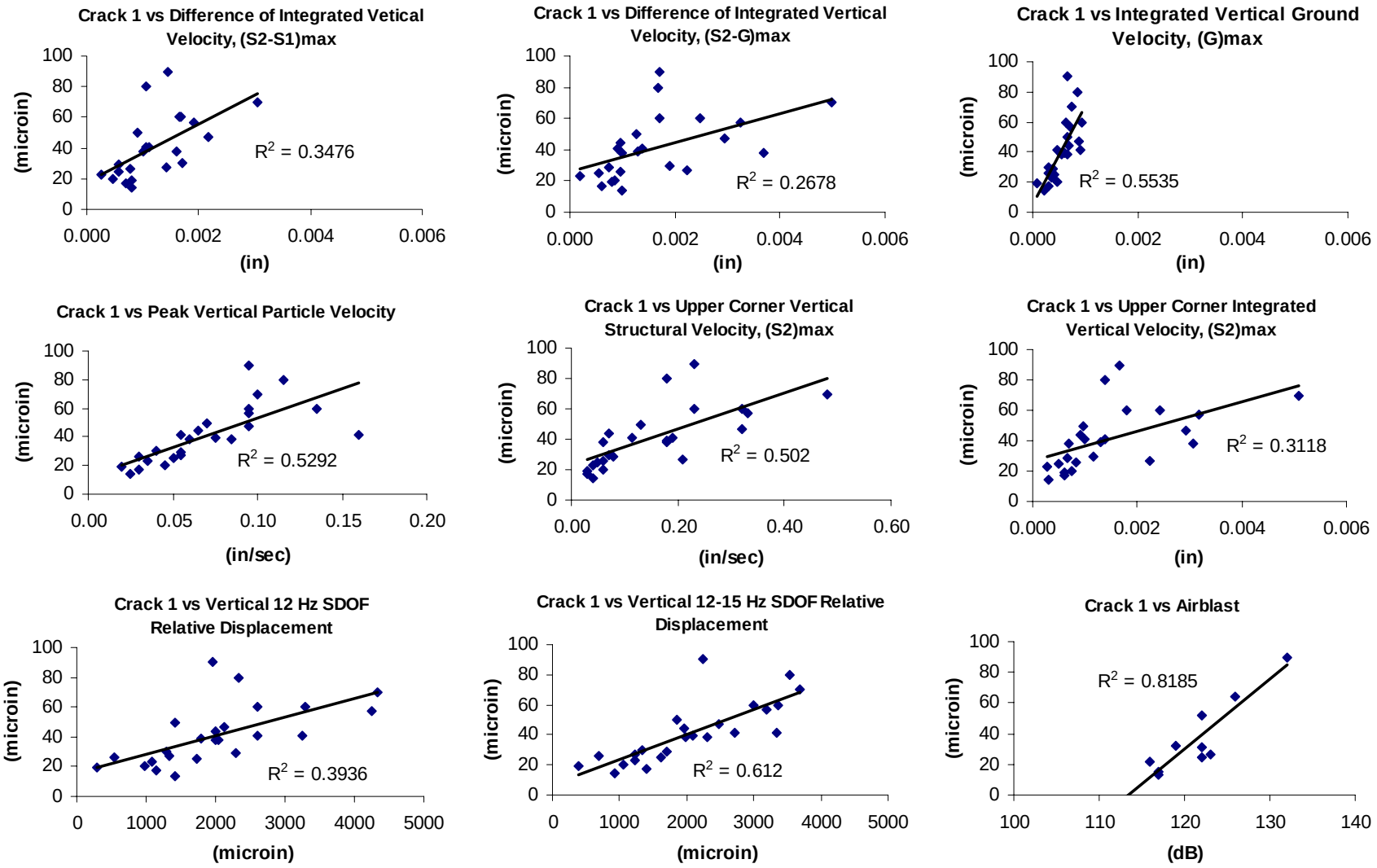

Figure 2.20 Correlations between measured Crack 1 displacement and vertical ground motions, relative structural displacements, and airblast

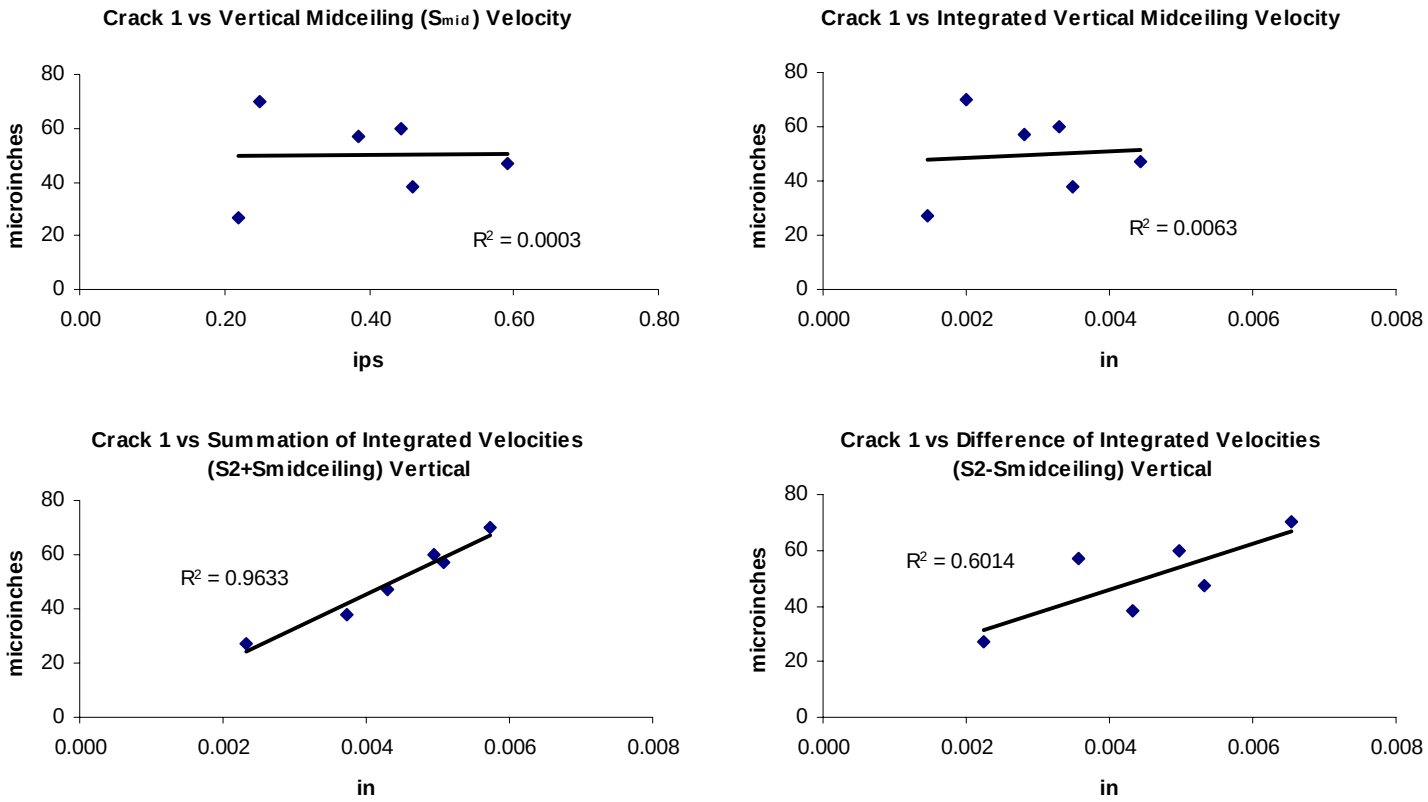

Figure 2.21 Correlations between measured Crack 1 displacement and vertical structural and midceiling velocity and displacements

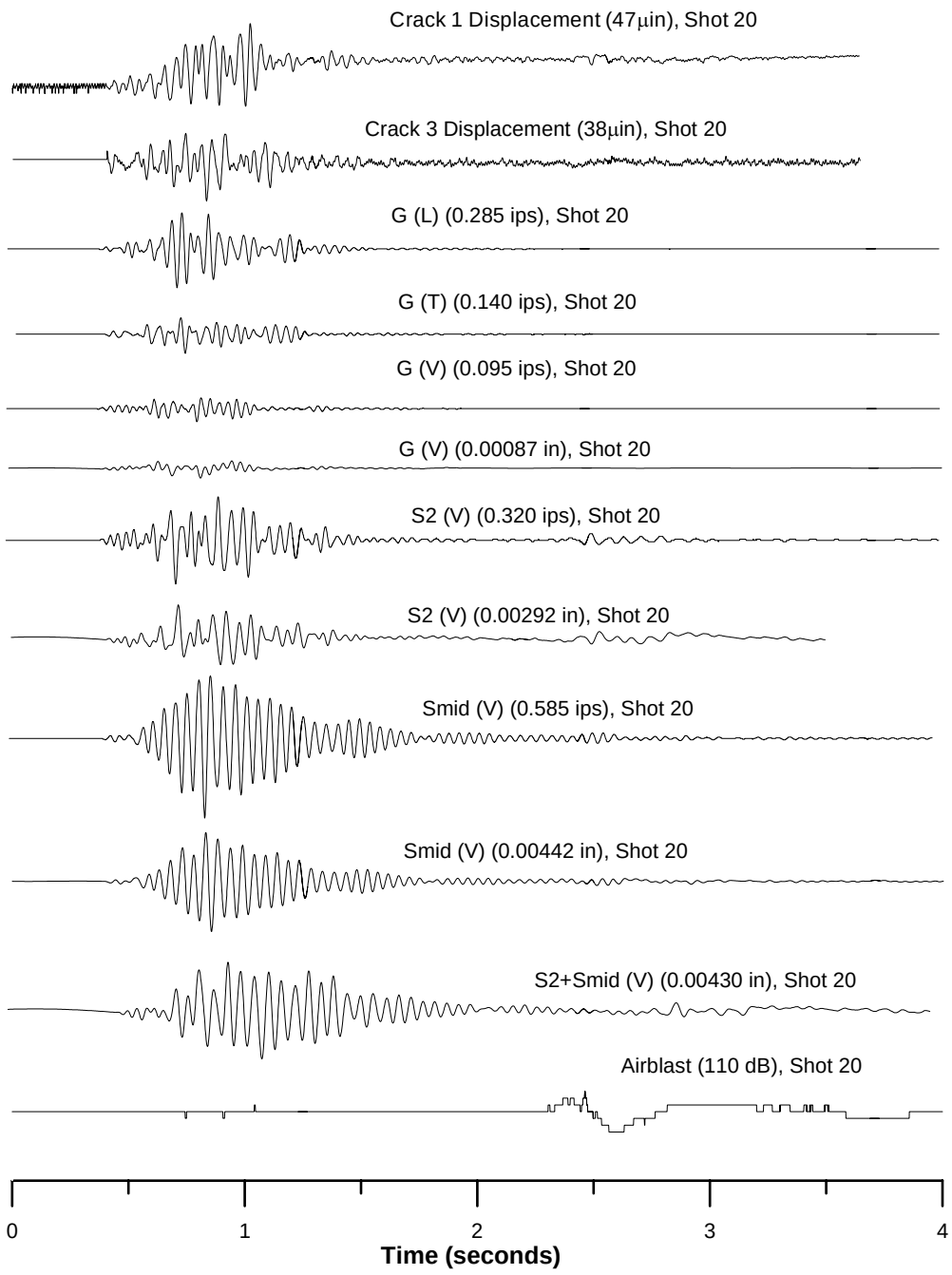

Figure 2.22 Time histories of Crack 1 and 3 displacements from blast event 20 on August 23rd, 2002 at 11:49 AM compared to longitudinal, transverse, and vertical ground velocity, vertical ground displacement, S_2 response velocity and displacement response, $S_{midceeling}$ velocity and displacement response, (S_2+$S_{midceiling}$) relative displacement, and air blast.

Chapter 3

Effect of Blast Design on Crack Displacement

Introduction

Two principal factors determine peak particle velocities from blasting; 1) maximum charge weight detonated per delay, or the quantity of energy released into the ground at any moment, and 2) the absolute distance between the blast and the target. These two parameters are normalized by dividing the distance by the square root of the charge weight per delay ($ft/lbs^{1/2}$). The smaller the scaled distance factor, the larger the ratio of explosive energy to distance and the "stronger" the shot. There are, however, many other secondary factors that have significant effects on peak particle velocity, structural response and crack displacements in target structures. These factors include propagation velocity and attenuation characteristics of the soil, borehole layout and timing patterns, the distance between charges at the source, the direction and orientation in which the detonation progresses, and the coupling of the released energy with the transmitting soil.

This chapter describes differences in structural and crack responses that resulted from blasts at similar scaled distance or expected particle velocities. Interest in this investigation stems from the results of a previous study (Aimone, 2000) that involved measurement of structural and ground responses at the Stiles Road quarry. This study concluded with the following suggestions for modification of blasting practices:

increased stem length, increased front row burden, minimum 25 millisecond delay time per hole, elimination of base primers, initiation of blast events from north to south for benches on north high walls, and design of blasts on south faces. Since the first study, the ACM system has been developed and additional house response measurement techniques have been adopted, both of which allow more efficient measurement. Installation of the ACM system and additional velocity transducers has allowed measurement of the effects of some of these blast design changes on house and crack response. This chapter describes these effects.

This chapter will focus on 4 primary components of blast design that have significant effects on resulting crack displacements in structures. These four components are borehole and free face geometry, designs that produce significant ground motions versus significant airblasts, blasts at different dominant frequencies, and shot timing and overlapping delay times which result in differences in the number of significant pulses.

Four pairs of blast events and their respective ground, structure and crack responses at the Connecticut structure described in Chapter 2 will be compared to describe the effects of variable blast designs. Table 3.1 summarizes the pertinent information associated with the following events comparing differences in:

- Face geometry (Shot 1, narrow V, single face versus Shot 9, wide V, two face)
- Stemming depth (Shot 8, shallow stemming with 132 dB air overpressure versus Shot 15, 0.345 ips ground motion)
- Frequency effect (Shot 14, 19 Hz versus Shot 22, 27 Hz in the longitudinal direction)
- Total shot time and number of boreholes (Shot 18, 436ms total shot time, 59 holes versus Shot 19, 215ms total shot time, 37 total holes)

Figure 3.1 is an aerial photograph of the quarry and the surrounding area with the location of the Connecticut house within the smaller circle, and the location of the blasts in the larger circle to the south. Figure 3.2 is the USGS topographic relief map of the same area shown in Figure 3.1 with the same location identification and Figure 3.3 shows close-up relief maps on both benches of the blasting area with the locations of each blast outlined in black and the shot numbers adjacent in red. In general, all blast events were

approximately 762 m (2500 ft) from the test structure. They were located on the same side of the quarry as the house and shot on either south or east facing high-walls.

Scaled distance factors for these shots had to be calculated from information received via the blasting company. Borehole geometries and timing patterns were pieced together to calculate maximum charge weights per delay. Unless otherwise noted (as in comparison 4), it will be assumed that one "delay" consists of any number of holes within 8 ms of each other. Time delay in detonations is for the most part dependent of timing delays within the blasting caps, up-hole delays and non-electric shock tubes. However, often times these planned timing patterns are not achieved due to errors in the blasting caps (Dowding, 1996). The errors are a function of several various sources, including human error and manufacturing, and at one time were as high as 7 to 8% for the 500 ms in-hole delay. These timing issues play an important role in accurately calculating and assessing scaled distance factors.

Shot #	Date/Time	Raw Distance (ft)	# of Holes	Total Weight (lbs)	Weight Per Hole (lbs)	Charge Wt. Per Delay (Calculated) (lbs)	Charge Wt. Per Delay (Given) (lbs)	Scaled Distance (Calculated) (ft/lb1/2)	Scaled Distance (Given) (ft/lb1/2)	Pattern	Maximum Holes/Delay (w/in 8ms)	Total Shot Time (ms)
1	20-May	2429	30	8280	276	552	290	103	143	Wide "V"	2	352
9	17-Jun	2693	37	10271	278	833	810	93	95	Row	3	428
8	10-Jun	2217	48	3920	147	358	600	117	91	Row		557
15	22-Jul	2376	51	13081	256	769	810	86	84	Wide "V"	3	419
14	16-Jul	2430	41	7957	194	582	400	101	122	Row	3	310
22	10-Sep	2270	57	13251	232	697	500	86	102	Wide "V"	3	402
18	2-Aug	2441	59	15345	260	780	660	87	95	Wide "V"	3	436
19	15-Aug	2490	37	7495	203	810	840	87.5	86	Tight "V"	4	215

Table 3.1 Summary of pertinent blast design and borehole geometry information for blast events 1, 9, 8, 15, 14, 22, 18, and 19

Figure 3.1 Aerial photograph outlining Stiles Road Quarry boundary with blasting area and Connecticut monitoring house encircled

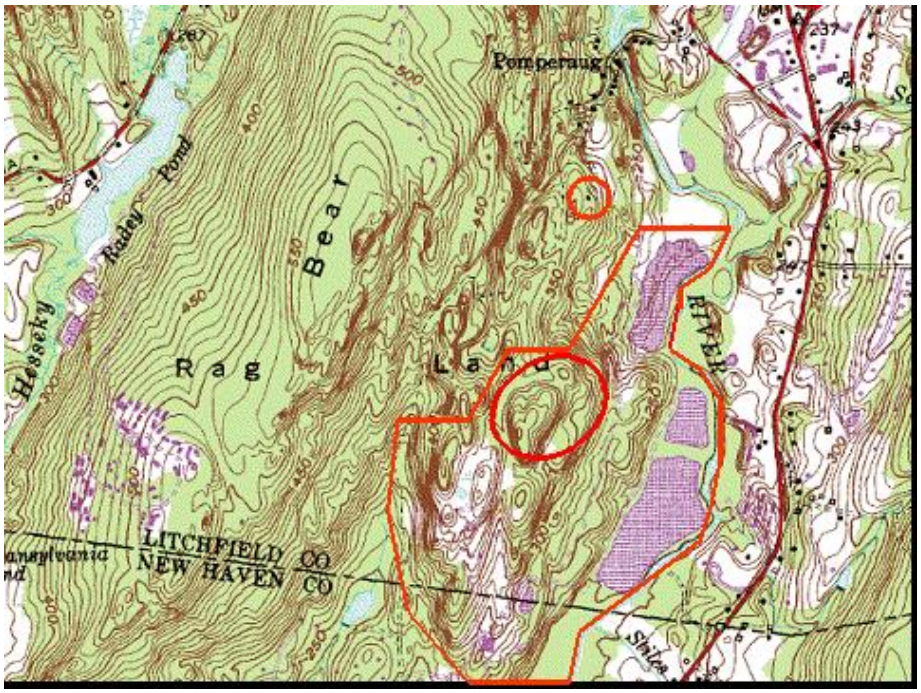

Figure 3.2 USGS Topographic map outlining Stiles Road Quarry boundary with blasting area and Connecticut monitoring house encircled

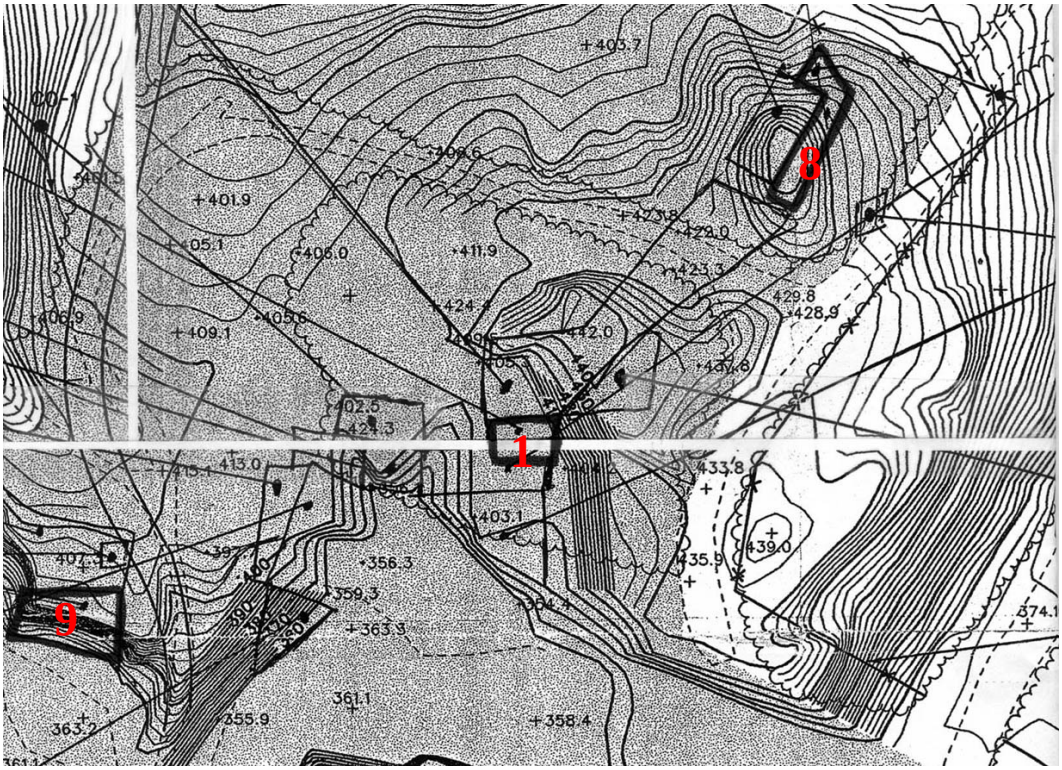

Upper Bench

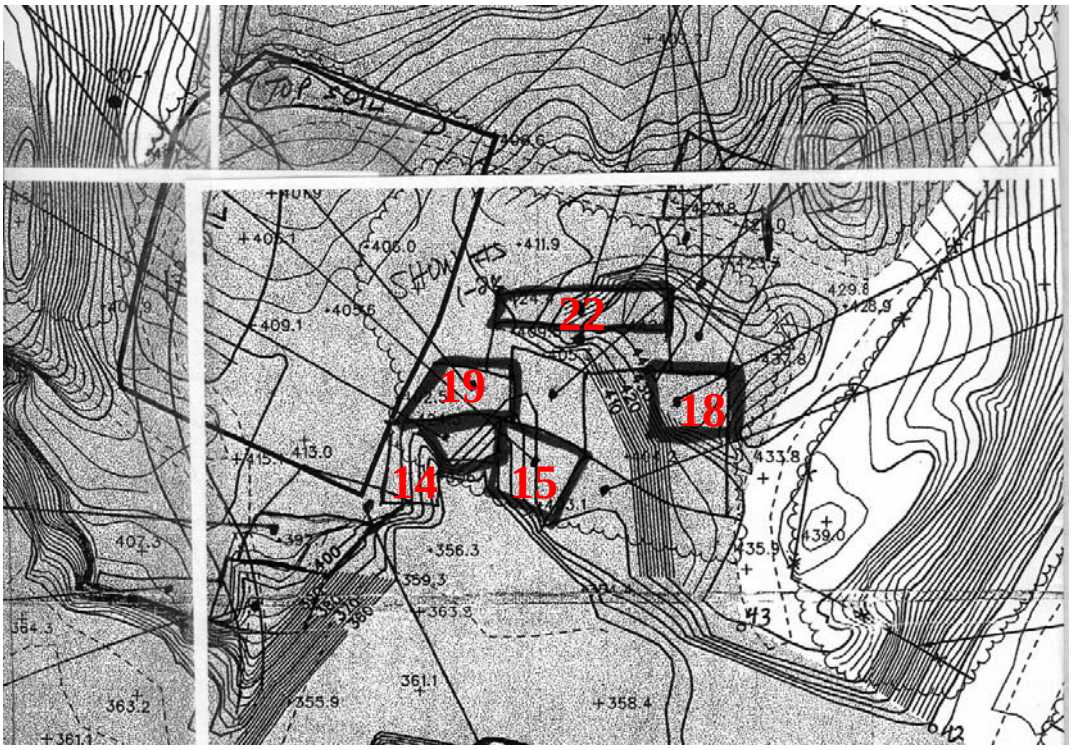

Lower Bench

Figure 3.3 Detailed topographic relief maps of blast 1, 8, 9, 14, 15, 18, 19, and 22 locations (outlined in black, numbered in red) on upper and lower bench of Stiles Road Quarry

Shot 1 (Narrow V, single face) vs. Shot 9 (Wide V, double face)

Shot 1 involved a maximum charge weight of 550 lb/delay at a distance of 2429 feet from the house, for a scaled distance factor of 104 ft/lb$^{1/2}$. It produced a peak particle velocity of 0.18 ips (longitudinal) and a Crack 1 displacement of 41μin. Shot 9 involved a charge weight of 833 lb/delay at a distance of 2693 ft for a scaled distance of 94 ft/lb$^{1/2}$, a peak particle velocity of 0.145 ips (longitudinal) and a Crack 1 displacement of 29μin. Both of these were standard production shots, and occurred at the same time of day.

The borehole layouts and timing patterns for these two shots are shown in Figure 3.4. Shot 1 is a narrow V pattern on a single face and maximum shot delay of 352ms (plus 500ms in hole). Accounting for the 8ms timing error discussed previously, there were a maximum of 2 holes per delay throughout the duration of the shot. With a total shot weight of 8280 lbs of explosive and 30 total holes, there are 276 lbs of explosive per hole. Shot 9 is a row-by-row or wide V pattern with two free faces and a maximum shot delay of 428ms (with 500ms in hole). There are a maximum of 3 holes per 8 ms delay, total shot weight of 10,271 lbs, 37 total holes and 278 lbs of explosive per hole.

Figure 3.5 shows longitudinal and vertical time histories corresponding to shots 1 and 9, the top six show responses to Shot 1. Time histories are shown for Crack 1 response, longitudinal and vertical ground motion, longitudinal and vertical S_2 structural response and decibel level airblast for shot 1, while those for Shot 9 are one the bottom. The peak longitudinal particle velocities for both these events are shown with shot 1 having a slightly higher value of 0.18 ips than 0.145 ips for shot 9. Both of these shots have identical peak particle velocities in the vertical direction of 0.55 ips. Despite these measurements, shot 1 produced a vertical structural response 44% higher (0.115 ips vs. 0.08 ips) and Crack 1 displacement 25% greater (41μin vs. 29μin) than Shot 9.

The significant structural and crack response differences in this comparison shows the effect of borehole layout, shot progression, free face employment and general shot design criteria. Under standard blast design criteria, the lower scaled distance factor for shot 9 should produce larger ground motions and more significant structural and crack response. However, the row-by-row geometry, shot progression and the existence of a curved/multi-face for shot 9 may have provided more relief. The timing progression in Figure 3.4 for Shot 9 shows five total rows, wherein each row contains only one

overlapping delay (within 8ms). Even though there are a maximum of three holes per delay, the holes are spread out and progress in opposite directions. Shot 1 is a narrower "V" pattern, which is also traditionally employed to distribute explosive energy in multiple directions, but there is only one free face for relief.

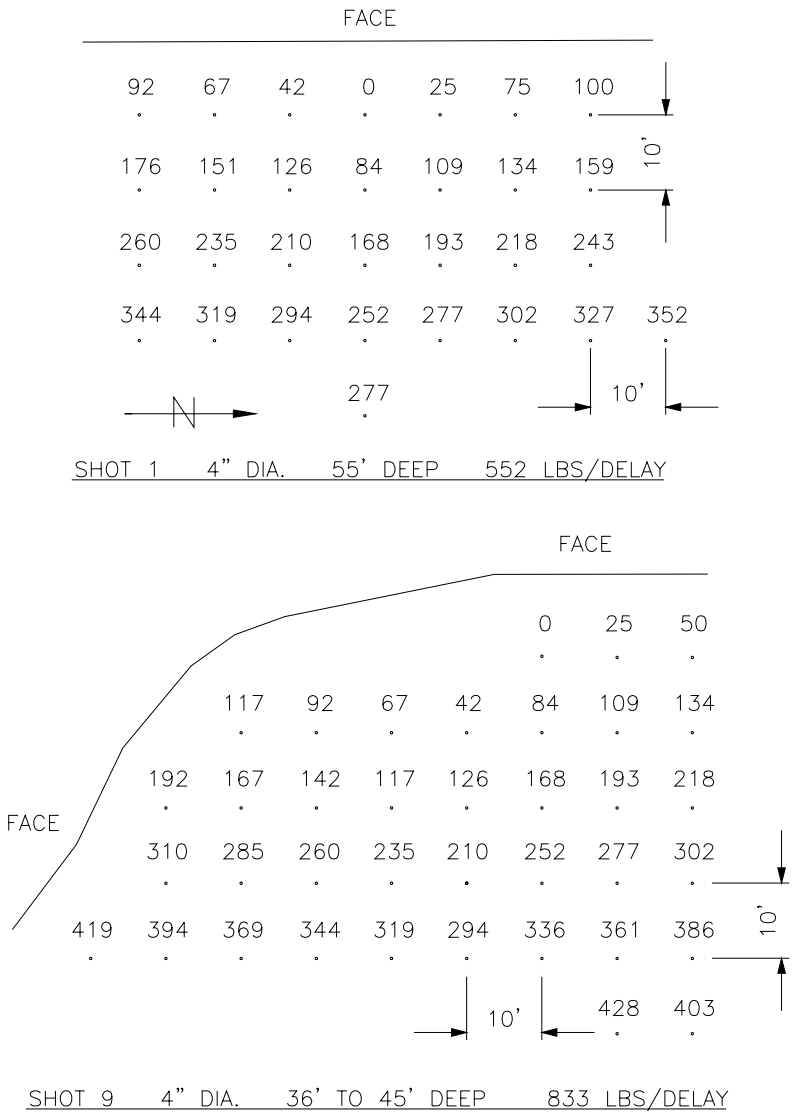

Figure 3.4 Borehole geometry and delay timing patterns for blast events 1 and 9

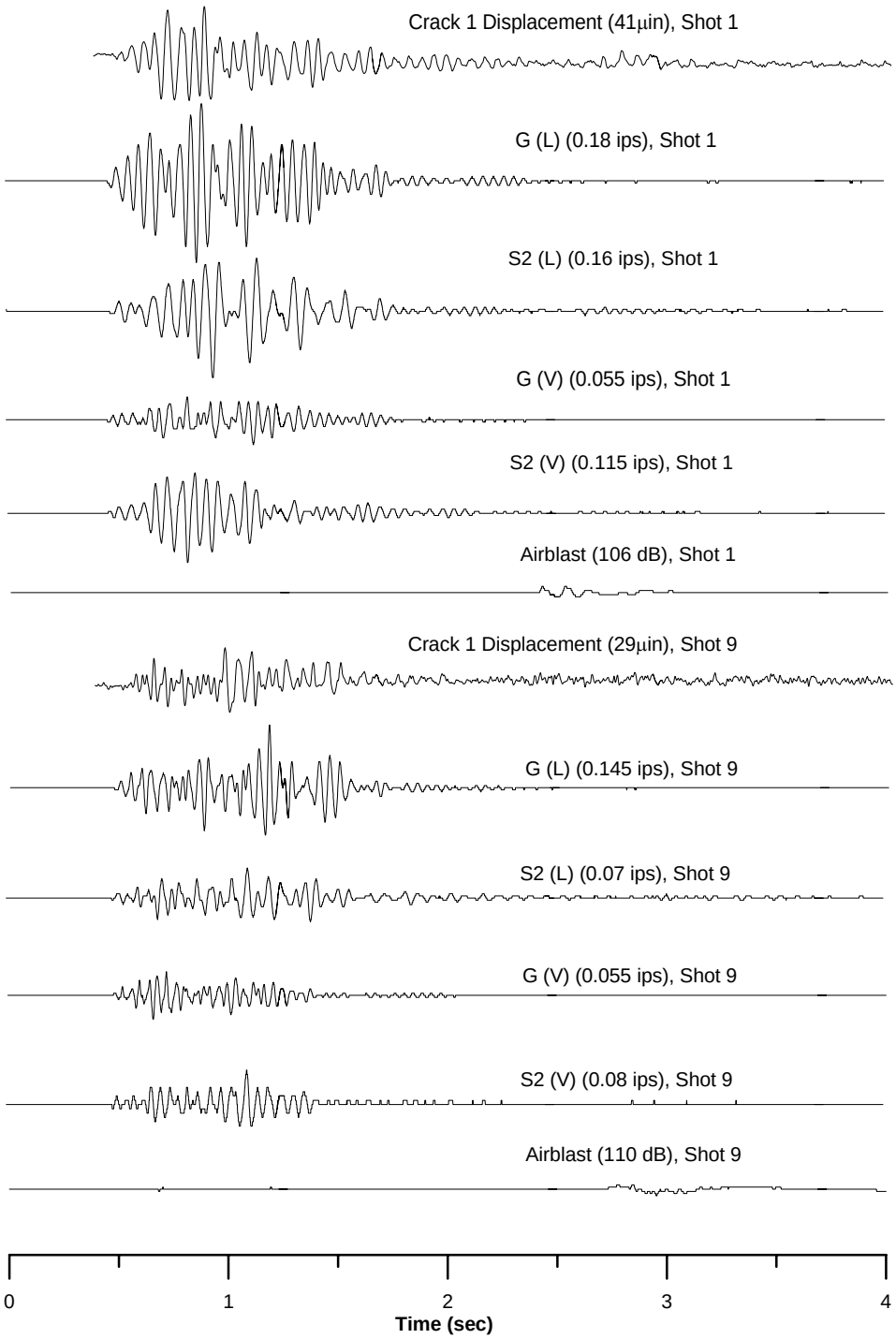

Figure 3.5 Crack 1 displacement time histories for blast events 1 and 17 compared to longitudinal ground motion, longitudinal S_2 structural response, vertical ground motion, vertical S_2 structural response, and airblast

Shot 8 (Shallow stemming) vs. Shot 15 (Normal stemming)

Shot 8 involved a charge per delay of 600 lbs, at a distance of 2217 feet, with a scaled distance factor of 91 $ft/lb^{1/2}$. It produced a peak particle velocity of 0.08 ips. Shot 15 with a charge per delay of 810 lbs, at a distance of 2376 feet, has a scaled distance factor of 84 $ft/lb^{1/2}$ and the largest monitored peak particle velocity of 0.345 ips.

The borehole layouts and timing patterns for these two shots are included as Figure 3.6, and their respective time histories are presented as Figure 3.7 in the same format as Figure 3.5. Shot 8 produced a rare, maximum 132 dB airblast that caused a great deal of response in Crack 1. The reasons for this air pressure are unknown, but is most likely the result of a combination of blasting a knoll on the north end of the quarry whose free-face was at an elevation well above the structure and stemming too short to effectively contain the explosive gases. The blasting log for this event shows a grouping of 16, 3.5" holes drilled to an eight-foot depth with five feet of stemming. Conventional blasting design calls for stemming of approximately 30 times the diameter of the hole, or 7 to 8 feet for 3.5" holes.

In contrast to Shot 8, Shot 15, elicited the maximum peak particle velocity of any recorded event, 20% higher than the next highest PPV, but did not have the smallest scaled distance factor. This shot was designed with 4" holes drilled to 36 to 45 feet with 12 feet of stemming in a "V" pattern. Although this shot progressed to the north in the general direction of the structure and provided what appears to be an ideal circumstance for high-energy transfer. Typically the "V" pattern employed in this situation with a standard 25 ms delay and 10 foot burden usually directs the seismic energy in two directions, and consequently keeps vibrations to a minimum.

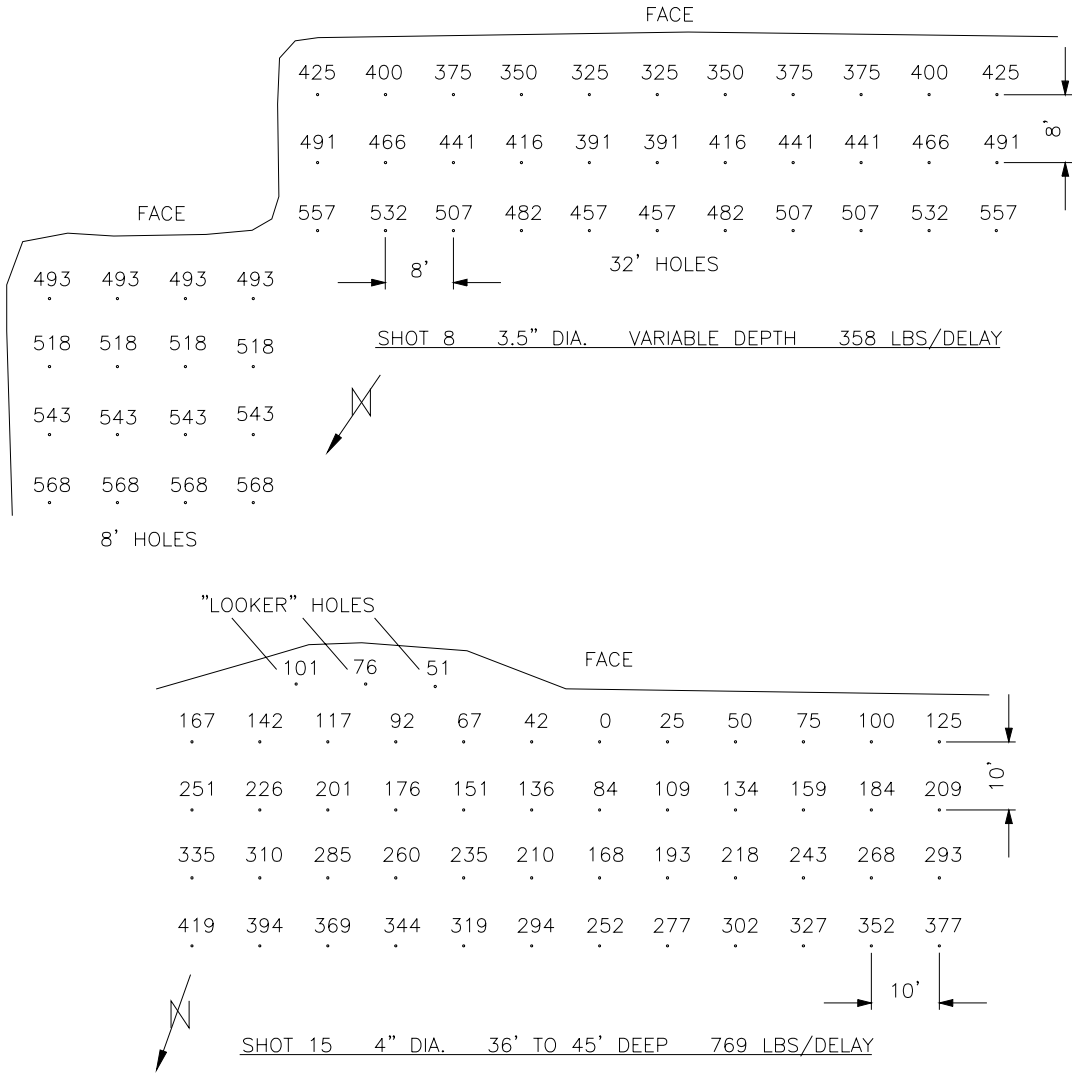

Figure 3.6 Borehole geometry and delay timing patterns for blast events 8 and 15

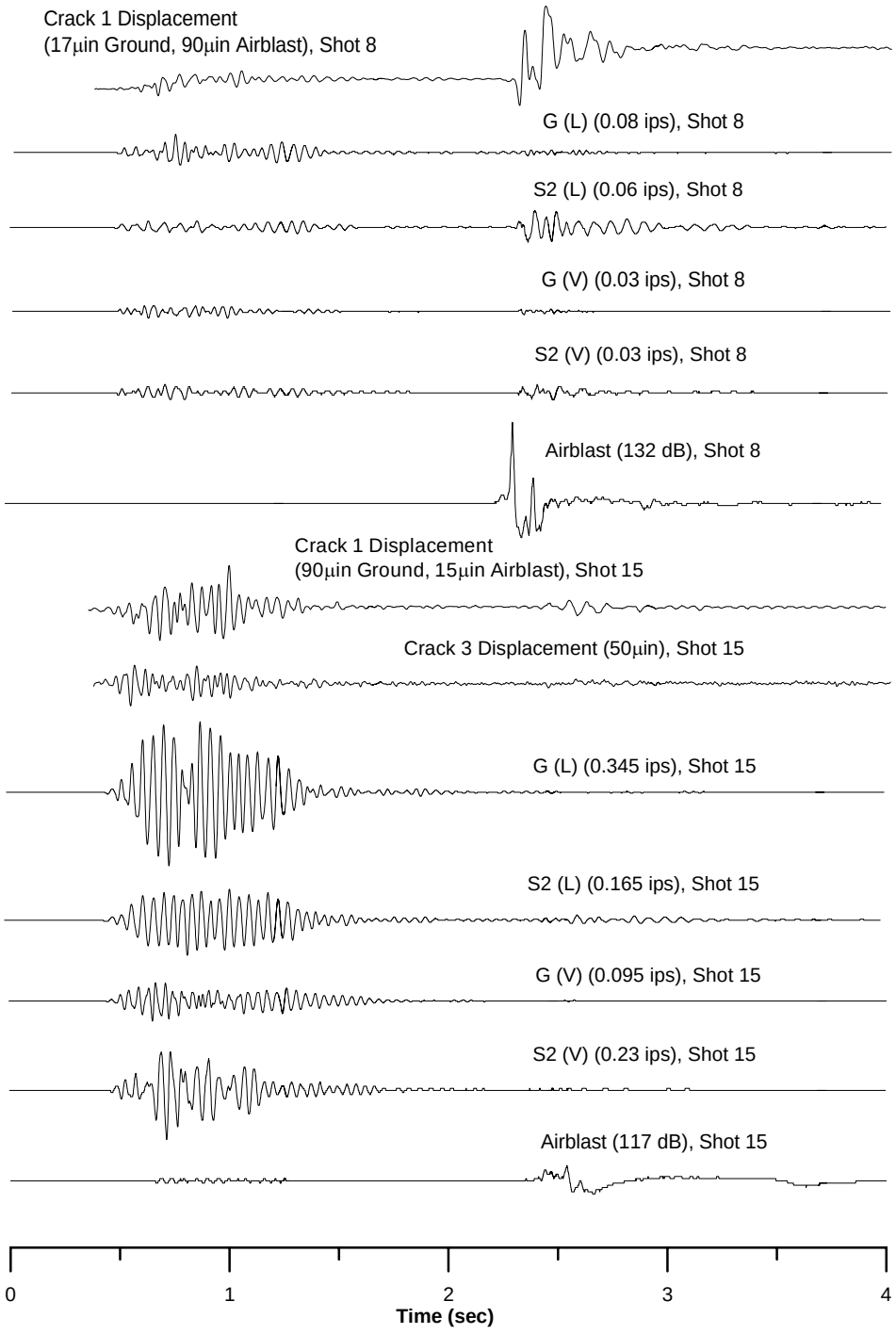

Figure 3.7 Crack 1 displacement time histories for blast events 8 and 15 compared to longitudinal ground motion, longitudinal S_2 structural response, vertical ground motion, vertical S_2 structural response, and airblast

Shot 14 (19 Hz in long. direction) vs. Shot 22 (27 Hz in long. direction)

Shot 14 involved a maximum charge weight of 582 lb/delay at a distance of 2430 feet from the house, for a scaled distance factor of 101 ft/lb$^{1/2}$. It produced a peak particle velocity of 0.19 ips (longitudinal), Crack 1 displacement of 60μin and Crack 3 displacement of 59μin. Shot 22 involved a charge weight of 697 lb/delay at a distance of 2270 ft for a scaled distance of 86 ft/lb$^{1/2}$. It produced a peak particle velocity of 0.27 ips (longitudinal), Crack 1 displacement of 60μin and Crack 3 displacement of 34μin. Both of these were standard production shots, and occurred at the same time of day.

The borehole layouts and timing patterns for these two shots are shown in Figure 3.8. Shot 14 is a diagonal row pattern on a single face and maximum shot delay of 310ms (plus 500ms in hole). Accounting for the 8ms timing error discussed previously, there were a maximum of 3 holes per delay throughout the duration of this shot. With a total shot weight of 7957 lbs and 41 total holes, there are a relatively low 194 lbs of explosive per hole. Shot 22 is a classic wide V pattern on a single face and a maximum shot delay of 410ms (with 500ms in hole). There are a maximum of 3 holes per 8 ms delay, total shot weight of 13,251 lbs, 57 total holes and 232 lbs of explosive per hole.

Figure 3.9 shows longitudinal and vertical time histories corresponding to shots 14 and 22; the top seven time histories Crack 1 response, Crack 3 response, longitudinal and vertical ground motion, longitudinal and vertical S_2 structural response and decibel level airblast for shot 14. The bottom seven show identical information for shot 22. The peak particle velocities for both these events occur in the longitudinal direction, with shot 22 producing 0.27 ips versus 0.19 ips for shot 14.

This comparison introduces the concept of crack displacement normalized to peak particle velocities for the purpose of showing the effect of alternatively significant measured data. For the purposes of normalization, individual crack displacements are divided by the peak particle velocities, Crack 1 with vertical and Crack 3 with longitudinal, in order to divide out or normalize the effect of peak particle velocity. This comparison demonstrates the effect of differences in dominant frequency.

There are three primary methods of establishing the dominant excitation frequency of a blast event; the zero-peak crossing, fourier frequency transform (FFT), and single-degree of freedom methods described in Chapter 2. As the single-degree of

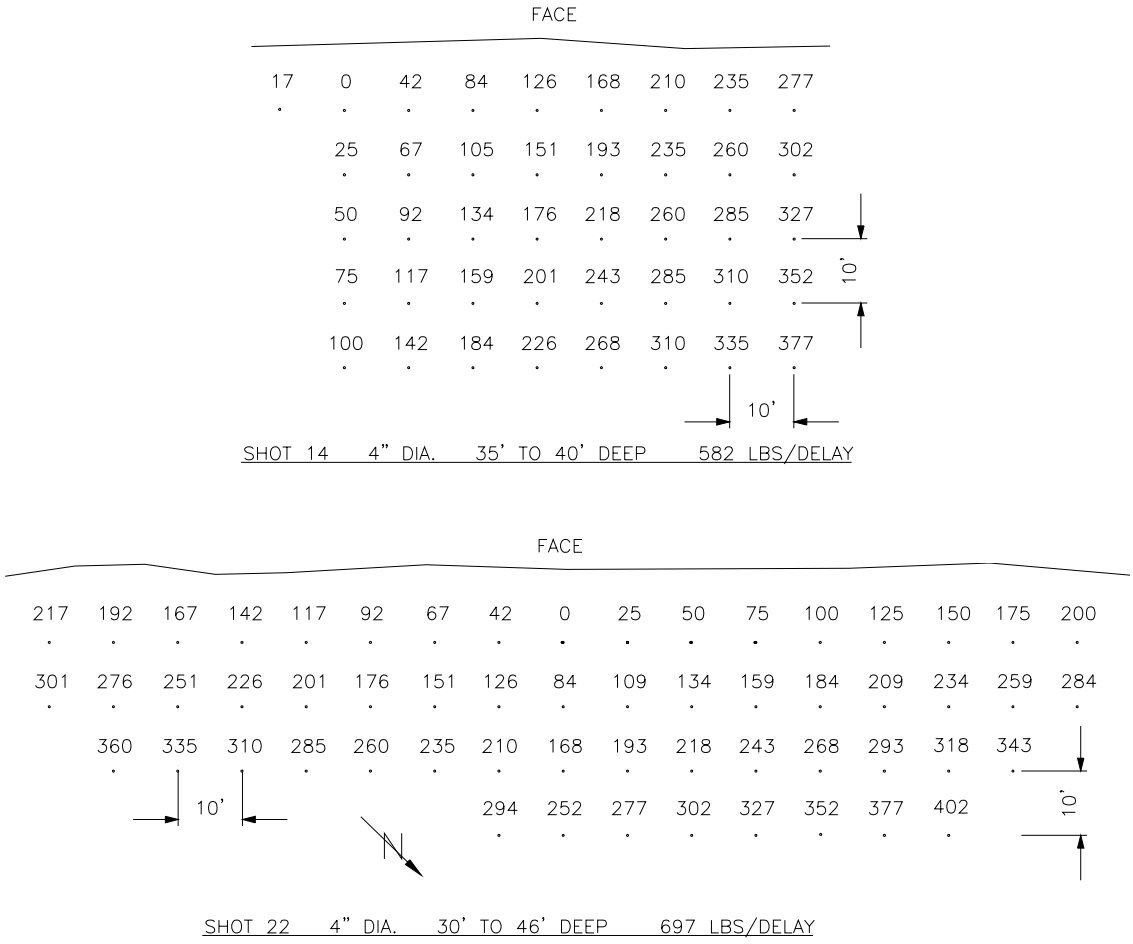

Figure 3.8 Borehole geometry and delay timing patterns for blast events 14 and 22

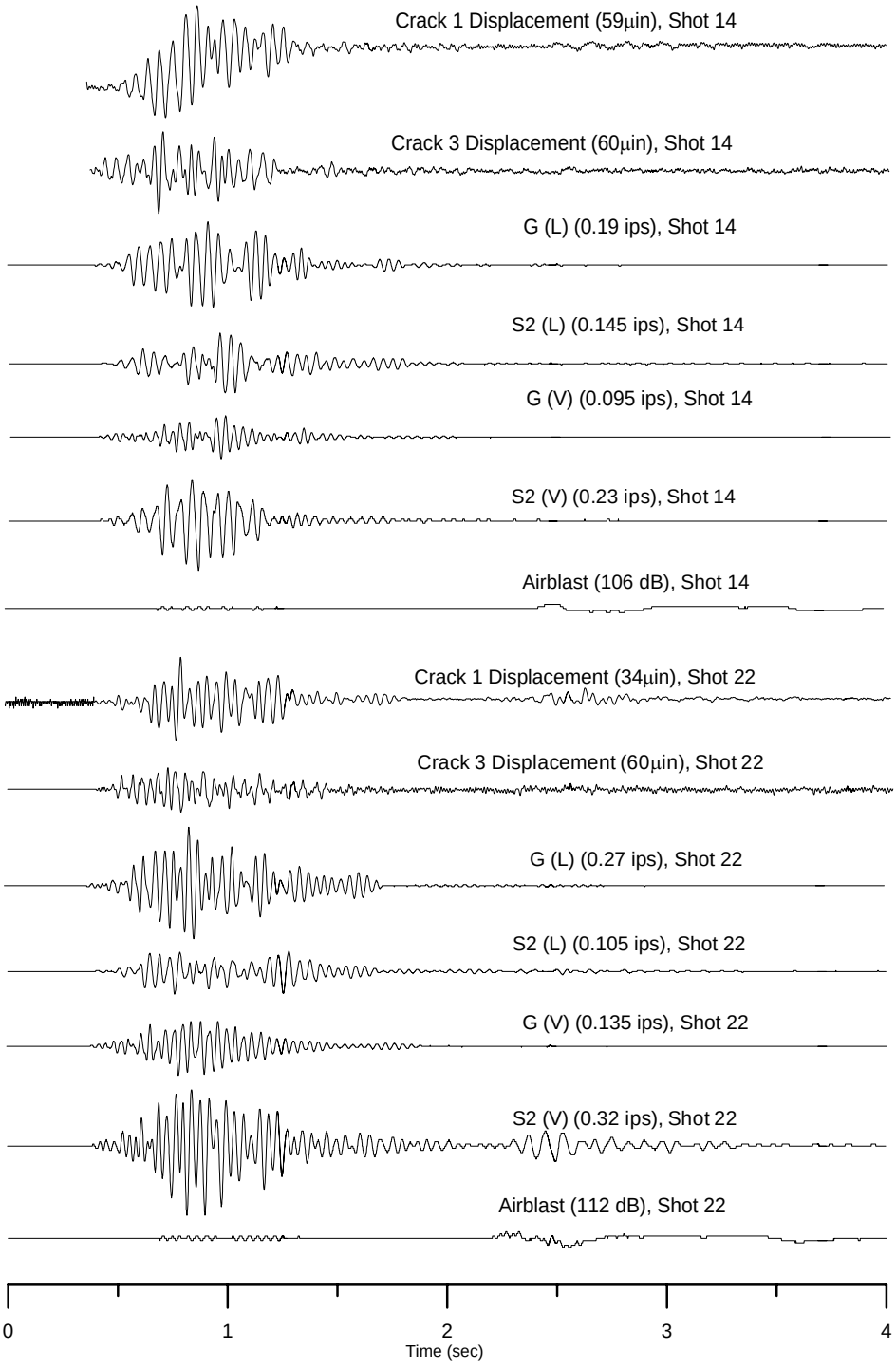

Figure 3.9 Crack displacement 1 and 3 time histories for blast events 14 and 22 compared to longitudinal ground motion, longitudinal S_2 structural response, vertical ground motion, vertical S_2 structural response, and airblast

freedom method best describes structure displacement as a function of frequency, it will be employed for the purposes of this discussion. Furthermore, only longitudinal frequencies and Crack 3 will be examined, as the frequencies in the vertical direction did not vary significantly for the shots monitored in this time period. In terms of measured ground motions and peak particle velocities, these two shots performed as expected. Shot 22 had a lower scaled distance factor and was a wide V, thereby producing a relatively high peak particle velocity of 0.27 ips versus 0.19 ips for shot 14. Crack 3 displacement normalized to longitudinal peak particle velocity for shot 22, however, was 126μin/ips, the lowest among any recorded shot. By comparison, normalized Crack 3 displacement of Shot 14 was 145μin/ips, falling somewhere in the middle of normalized response. A possible reason for this low relative response for shot 22 is the dominant frequency of 27 Hz in the longitudinal direction, as compared to a 19 Hz frequency from shot 14. In Chapter 2 the dominant frequency of the structure is shown to be lie between 11 and 15 Hz, closer to the dominant frequency of Shot 14. Thus greater structural and crack response is expected for the shot whose excitation frequency more nearly matches the natural frequency of the structure. Figure 3.10 shows a plot of normalized Crack 3 displacement to dominant SDOF frequencies for all shots.

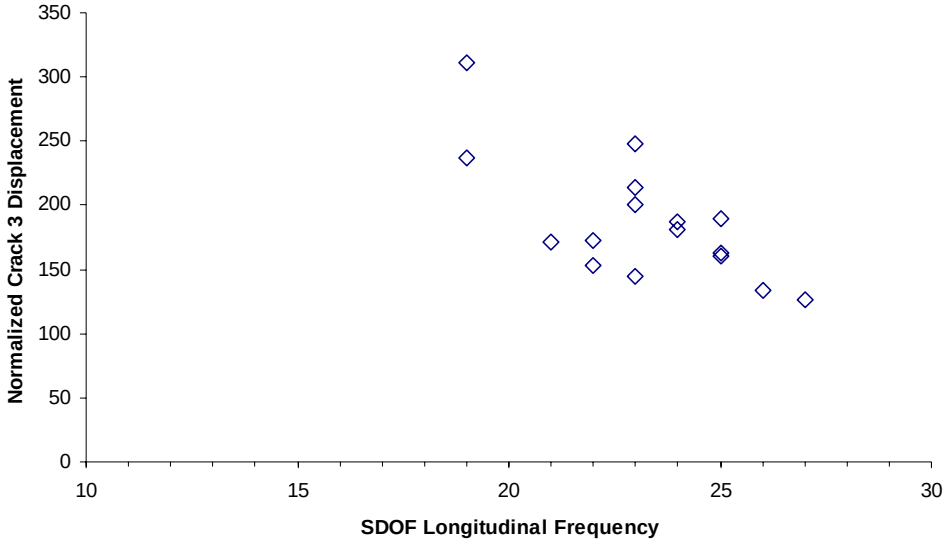

Figure 3.10 Normalized Crack 3 displacement (δ_3/L PPV) versus longitudinal single degree of freedom dominant frequency for blasting in Connecticut

Shot 18 (Total shot time of 436ms) vs. Shot 19 (Total shot time of 215ms)

Shot 18 involved a maximum charge weight of 780 lb/delay at a distance of 2441 feet from the house, for a scaled distance factor of 88 ft/lb$^{1/2}$. It produced a peak particle velocity of 0.195 ips (transverse), a Crack 1 displacement of 80μin and a Crack 3 displacement of 37μin. Shot 19 involved a charge weight of 810 lb/delay at a distance of 2490 ft for a scaled distance factor of 88 ft/lb$^{1/2}$. It produced a peak particle velocity of 0.215 ips (longitudinal) a Crack 1 displacement of 38μin and a Crack 3 displacement of 33μin. Both of these were standard production shots, and occurred at the same time of day.

The borehole layouts and timing patterns for these two shots are shown in Figure 3.11. Shot 18 is a wide V pattern on a single face and maximum shot delay time of 410ms (plus 500ms in hole). Accounting for a possible 8ms timing error discussed previously, there were a maximum of 3 holes per delay throughout the duration of the shot. With a total shot weight of 15,345 lbs of explosive and 59 total holes, there are 260 lbs of explosive per hole. Shot 19 is a tight V pattern on a single face, but with a maximum shot delay of 215ms (with 500ms in hole). There are a maximum of 4 holes per 8 ms interval, total shot weight of 7495 lbs, 37 total holes and 203 lbs of explosive per hole.

Figure 3.12 shows time histories for shots 18 and 19; the top eight time histories are Crack 1 response, Crack 3 response, longitudinal ground motion, longitudinal S_2 structural response, vertical ground motion, vertical S_2 structural response, vertical S_{mid} mid-ceiling structural response and decibel level airblast for shot 19. The bottom seven time histories show identical information, minus the $S_{midceiling}$ structural response for shot 18, as it was installed after the shot. The peak particle velocities for both these events lie in the longitudinal direction, with shot 19 producing a slightly higher value of 0.215 ips versus 0.195 ips for shot 18. Vertical PPV was 0.115 ips for shot 18, and for shot 19 only slightly lower at 0.085.

This comparison explores the final design component: total shot time, percentage error in delay timing and coupled seismic energy producing significant pulses in ground motion. Both shots 18 and 19 are designed for 3 and 4 holes per delay respectively, and have almost identical scaled distance factors. The frequencies of the shots are nearly

identical, the longitudinal SDOF frequencies being 22 and 25 Hz, vertical 25 and 26 Hz. Shot 19 is a tighter V pattern, but they were both shot on single faces and have identical spacing and burden, so the borehole layouts themselves should not significantly affect the results at the house. The issue here is the shot timing, and the question of "whether 15,000 lbs of explosive shot in 60 holes versus 7,500 lbs of explosive shot in 30 holes, with similar scaled distance factors will produce different displacement responses in the same crack"?

A factor that should always be considered carefully in blast design is the possibility for coupled seismic energy. Previous studies have shown that, with the use of non-electric delays, the error in delay timing increases as the number of holes and/or shot duration increases. Longer shot durations and timing errors also may involve larger numbers of significant pulses. Significant pulses (called principal pulses) are defined as ground motions in excess of 75% of the peak value. Shots 18 and 19 both produced 3 principle pulses in the longitudinal direction, but the additional coupled energy later in Shot 18 resulted 5 principal pulses in the vertical direction versus only 3 for Shot 19. This difference may also be a consequence of the longer duration in Shot 18. The normalized Crack 1 displacement from Shot 18 was 700μin/ips, as compared to 450μin/ips for Shot 19. Even with the same number of principal pulses, however, the normalized Crack 3 displacement from Shot 18 of 190μin/ips was still greater than the 154μin/ips for Shot 19.

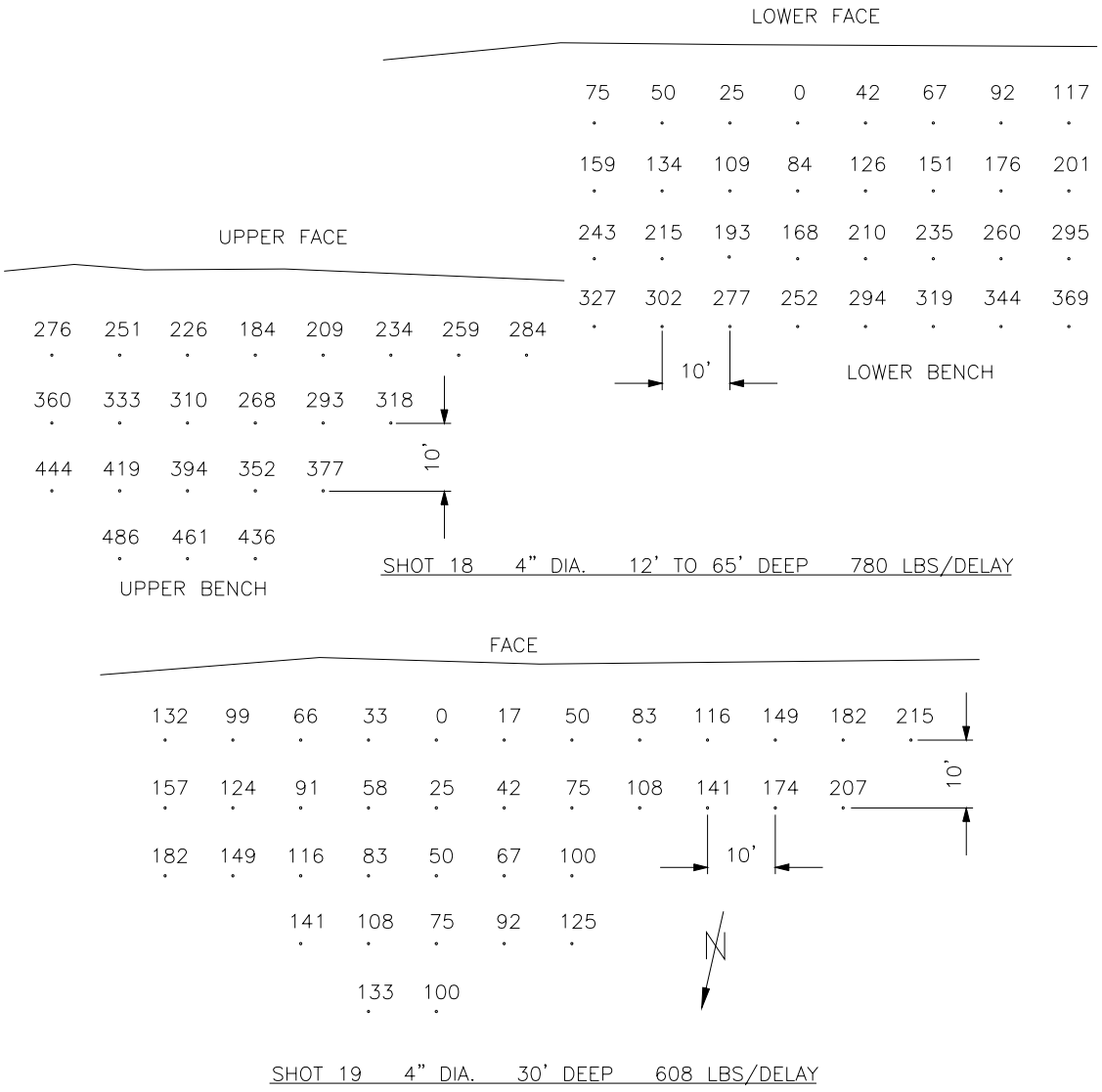

Figure 3.11 Borehole geometry and delay timing patterns for blast events 18 and 19

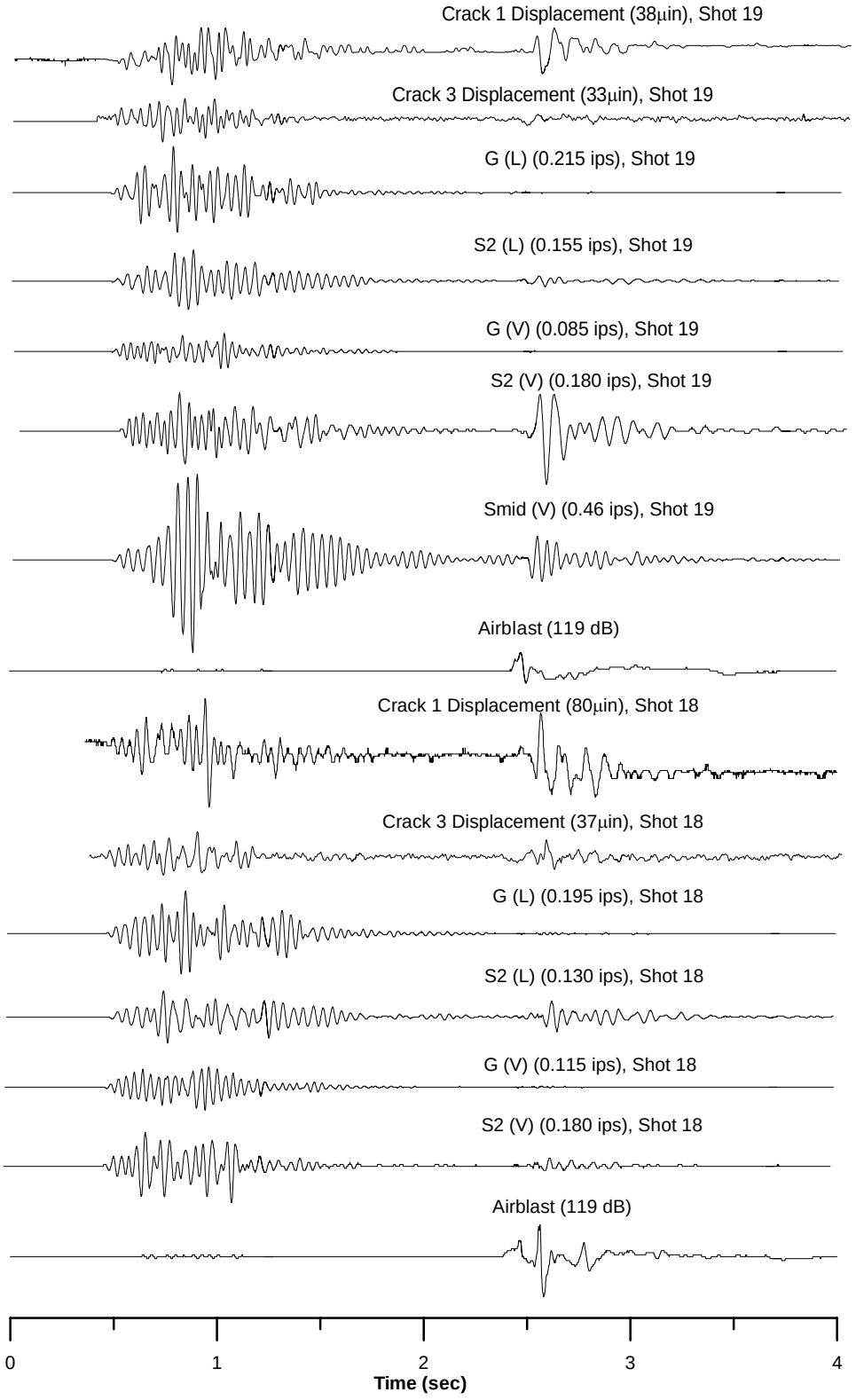

Figure 3.12 Crack displacement 1 and 3 time histories for blast events 18 and 19 compared to longitudinal ground motion, longitudinal S_2 structural response, vertical ground motion, vertical S_2 structural response, event 19 vertical $S_{midceiling}$ structural response, and airblast

Chapter 4

Construction Vibrations, Las Vegas, Nevada

Introduction

The one-story residential test structure, shown in Figure 4.1, is located immediately adjacent to the widening and reconstruction of West Ann Road in Las Vegas, Nevada. Vibratory crack deformation resulted from ground motion produced by backhoe excavation, trenching and vibratory rolling on cemented desert colluvium.

Figure 4.1 Single-story house adjacent to Ann Road Construction in Las Vegas, Nevada

Figure 4.2 shows plan and cross-sectional views of the test structure and its position relative to the construction activities on Ann Road. This slab-on-grade founded, one-story house is approximately 60 feet long, 36 feet wide, and eight feet tall, floor to ceiling. As shown in Figure 4.2 (a) two trenches were excavated: a 12-foot wide, 20-foot deep trench approximately 46 feet from the front of the house, and an 8-inch wide utility trench approximately 32-feet away. These excavations will be discussed in detail later in the chapter.

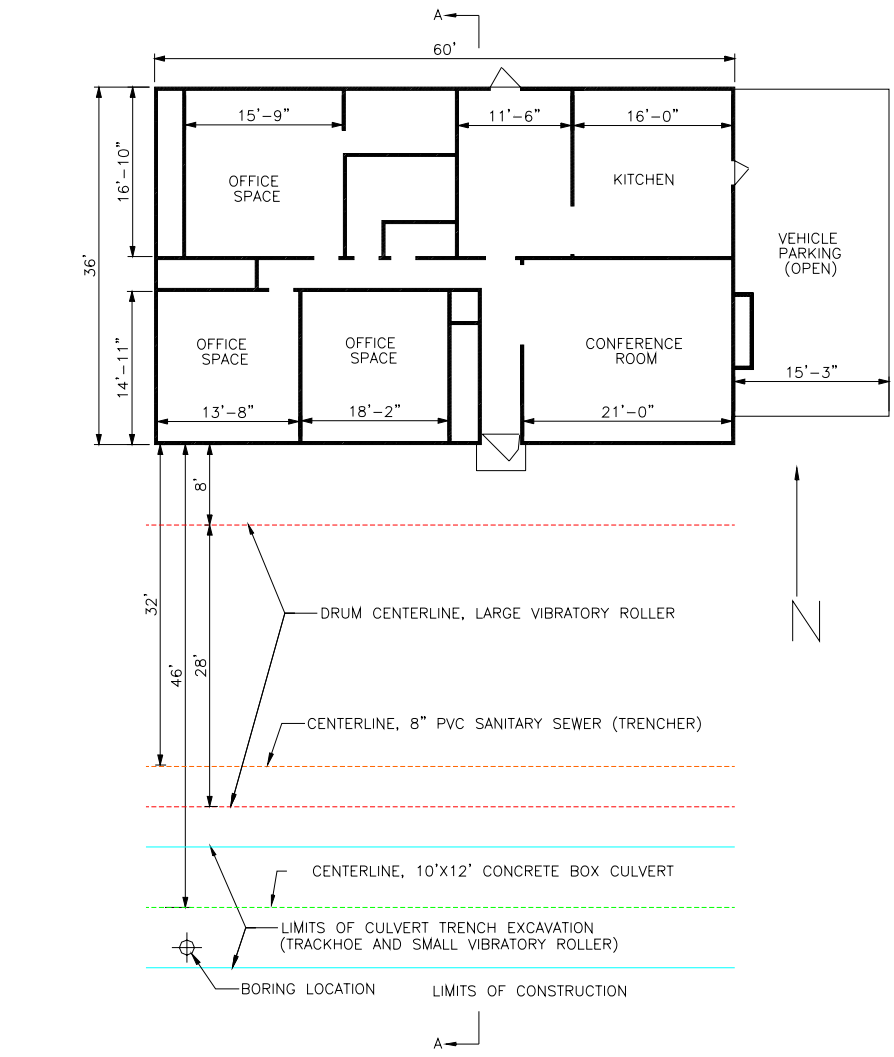

(a)

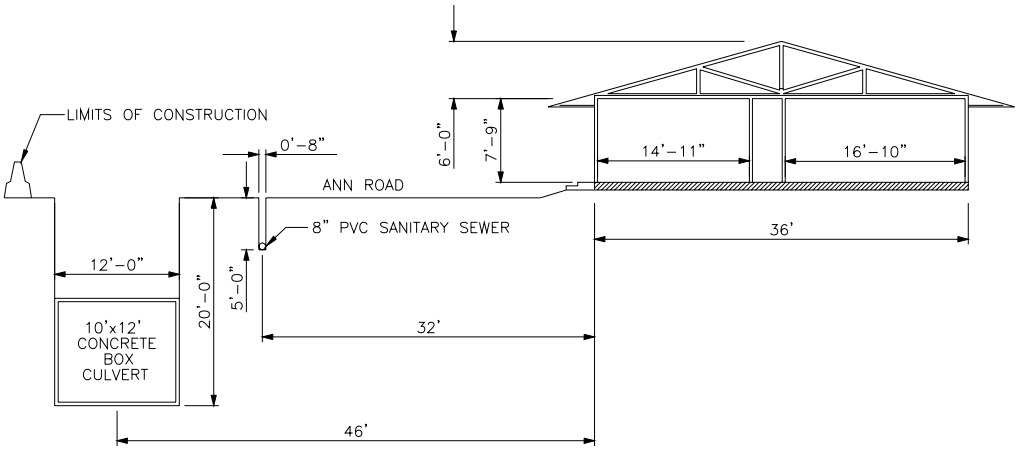

(b)

Figure 4.2 (a) Plan view geometry of monitoring house, construction locations, and soil boring location, (b) cross-sectional view of house geometry and excavations (section A-A)

Ann Road Soil Profile

Three, 20-foot deep soil-borings along the centerline of Ann Road in the vicinity of the test structure reveal the soil conditions. Figure 4.2 shows the location of the boring directly in front of the house; the other two approximately 500 feet in either direction along the construction centerline. Figure 4.3 compares the standard penetration blow count versus depth for the three borings. While the penetration resistance varies widely, all three borings reveal variable depth, and at times thick, layer of caliche, a calcium-rich cemented soil formed by the evaporation of alluvial groundwater in desert climates. Above and between these random caliche deposits, the borings show thin layers of sandy gravel to silty clay fill over natural silty clay and sandy clay layers. These variable caliche deposits are important to this case study because of the relative energy necessary for their excavation, as well as their energy transfer characteristics. These topics will be covered in detail later in this chapter during the ground attenuation study discussion.

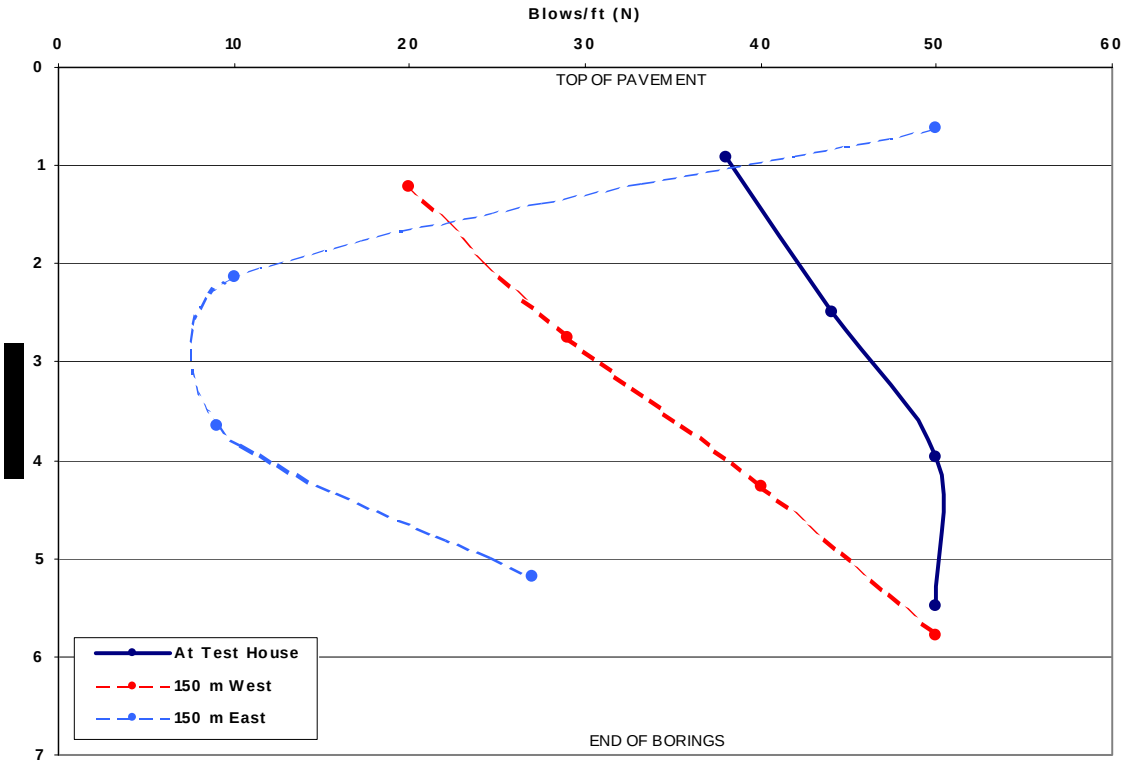

Figure 4.3 Blow count versus depth for three Ann Road soil borings in vicinity of test structure

Construction Equipment

Reconstruction and roadway improvements are divided into excavation and vibratory compaction activities for the purposes of monitoring construction vibrations. Excavation activities include excavation for a 10'x12' reinforced box storm culvert with a Hitachi 1200 EX Super trackhoe and excavation for an 8" PVC sanitary line by Tesmec TRS-1175XL "chainsaw" trencher. Photos of both are shown in Figures 4.4 (a) and (b). Vibratory compaction activities include compaction of backfill materials employed in the 12' wide culvert trench with a Dynapac CC 522 single-drum vibratory roller, and the compaction of roadway subgrade with an Ingersoll-Rand Pro-Pac Series SD-115F single-drum vibratory soil compactor. Figures 4.5 (a) and (b) show photos of both vibratory roller compaction machines. Specifications for all machines are found in Appendix B.

(a) **(b)**

Figure 4.4 Photographs of trenching equipment on Ann Road, (a) Hitachi trackhoe with dump truck and (b) Tesmec chain trencher

(a) **(b)**

Figure 4.5 Photographs of vibratory compaction equipment on Ann Road, (a) Dynapac small single-drum roller and (b) Ingersall-Rand large single-drum vibratory soil compactor

Structural Details

The interior walls of the Las Vegas structure are constructed of drywall over a wood-frame and the exterior is covered by southwestern-style stucco. The house is in generally good condition, with the majority of the cosmetic cracking is on the exterior stucco material.

Photographs of the roof and truss system are shown in Figure 4.6. This system consists of a series of 2"x4" ceiling joists placed at 2'6" centers. These joists are supported by a central 2"x8" beam running the 60-foot longitudinal length of the house.

(a) **(b)**

Figure 4.6 Roof and truss system for one-story Las Vegas structure

Instrumentation

Instrument locations are indicated on the plan and elevation views in Figure 4.7. A tri-axial geophone block was installed approximately two feet from the South (construction) face of the structure to measure excitation ground motions in the longitudinal, transverse, and vertical directions. As with previous studies, the longitudinal direction is defined as parallel to the long axis of the structure. Four cracks were instrumented with Macro-sensor LVDT micro-inch crack displacement gages for this study. Three of the cracks and the interior null were in place for the full monitoring period. On August 12th, 2002, the external null sensor (#5) was moved to an external crack on the transverse west wall for the remainder of the project.

All of the crack sensors, as well as the geophone were wired to a Somat eDAQ data acquisition system. This eDAQ provides simultaneous triggering of crack sensors to acquire transient response whenever the geophone exceeds a predetermined excitation

trigger threshold, as well as readings every hour to acquire long-term response to environmental effects. Hourly temperature and humidity were recorded internally and externally with independent Supco weather loggers. The data from these loggers was manually downloaded and correlated with the field measured crack data.

Three indoor sensors monitor cosmetic wall and ceiling cracks, plus the null wall response. The ceiling and wall cracks are labeled "Sensor 1" and "Sensor 3" in Figure 4.7 and the null gage, adjacent to sensor 3, is labeled "Sensor 4". As shown by the detailed photographs of these three sensors in Figure 4.8, the wall crack is located high on the wall.

The two external stucco cracks are also located in Figure 4.7. Sensor 2, shown in Figure 4.8(b), spans a crack near the door running vertically up the southern wall, which is the closest, parallel wall to Ann Road. Sensor 5 in Figure 4.8(c) (originally selected as an external null gage until August 12th, 2002), spans a vertical stucco crack on the west, transverse face of the house.

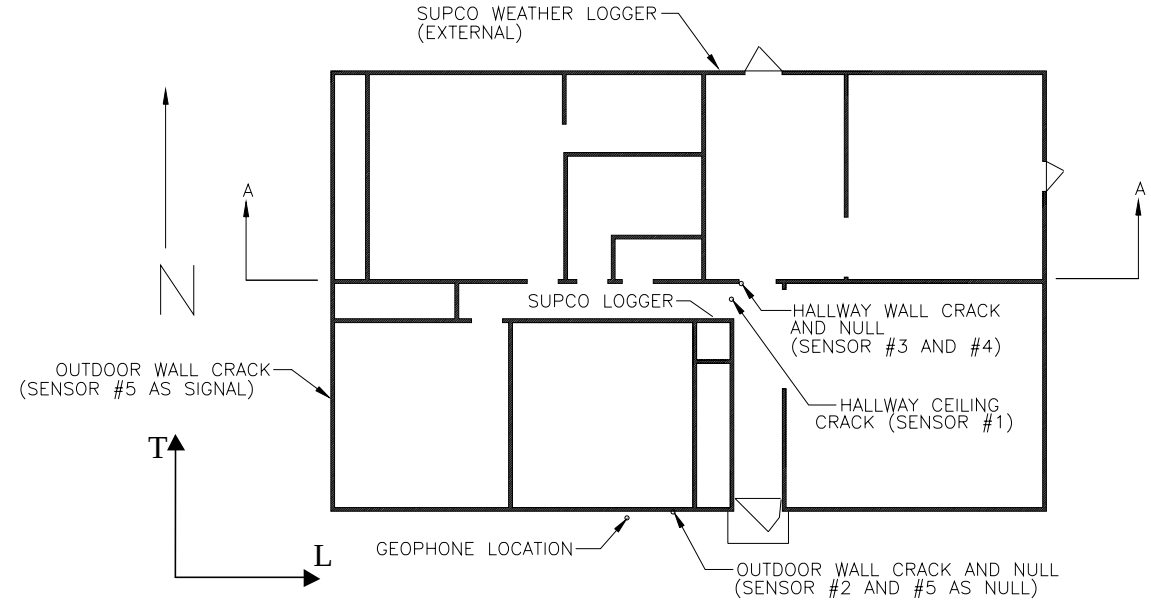

(a)

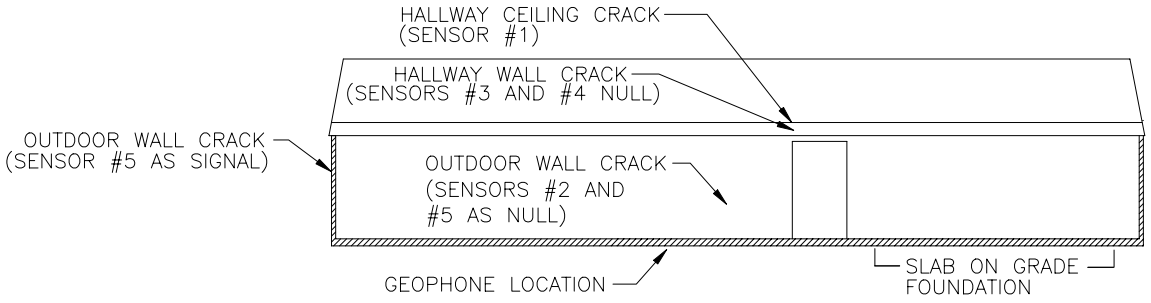

(b)

Figure 4.7 (a) Plan view of monitoring house and (b) profile view of house, showing Cracks and LVDT sensors 1-5, geophone, and weather logger instrument locations

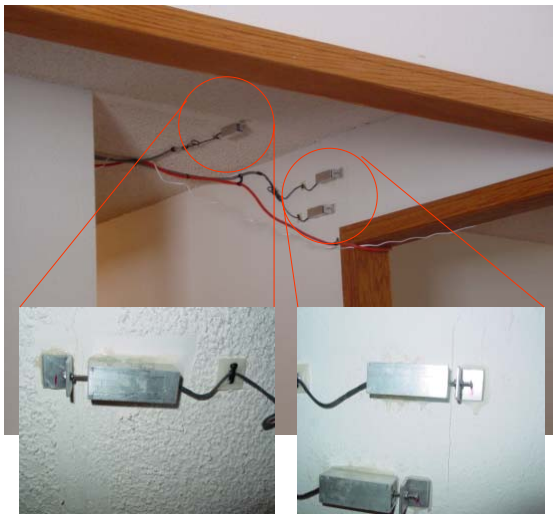

(a)

(b)

(c)

Figure 4.8 LVDT micro-inch sensors and cracks (a) interior ceiling, Crack 1 and wall, Crack 3 with interior null sensor, (b) exterior west wall Crack 5, and (c) exterior south wall Crack 2

Ground Attenuation Study

Attenuation of motions produced by representative construction equipment was measured in early September 2002 (Aimone-Martin, 2002). Equipment included a Dynapac model CA 151D vibratory roller running on both high and low frequency settings, a Tesmec TRS-1175 trencher, and an Hitachi EX 1200 Super trackhoe. Vibrations were monitored with linear arrays of either four or seven LARCOR seismographs oriented parallel and/or perpendicular to the direction of activity, recording longitudinal, transverse and vertical ground motions. Table 4.1 summarizes the three seismograph arrays employed for each machine monitored in this study. All the seismographs were wired in series, with the instrument closest to the monitored equipment acting as a trigger for the entire system. Trackhoe activities were monitored during the removal of existing asphalt pavement and the upper caliche soil level along Ann Road. The vibratory roller was placed in service specifically for this study, and thus was not monitored during construction activities along Ann Road. It was, however, operated over similar desert colluvial soils.

Machine Type and Model	Parallel Distances	Perpendicular Distances
	(ft)	(ft)
Hitachi 1200 Trackhoe	Variable 27 31	6 32 60 100
Tesmec TRS-1175 Trencher	None	7 27 43 57
Dynapac CA 151-D Roller	None	10 16 25 36

Table 4.1 Summary of seismograph arrays employed in attenuation study on Ann Road

Figure 4.9 is a log-log plot of peak particle velocity versus distance for the trackhoe, trencher and roller. A best-fit linear regression relationship determined for each machine describes the site-specific attenuation of the peak particle velocity. The attenuation of particle velocity in the ground is characterized by the negative exponent of

the distance term in the linear regressions shown on Figure 4.9. The y-intercept of this line, or the point representing a distance of 1 is proportional to the amount of relative energy transferred from the equipment to the ground. The trackhoe excavating the caliche layer imparts the highest level of energy into the ground, followed by the vibratory roller on the low frequency setting, high frequency setting (both operating over the caliche layer) and finally the trencher operating in relatively uncemented soils. The trencher was not excavating through the caliche layer at the time of monitoring.

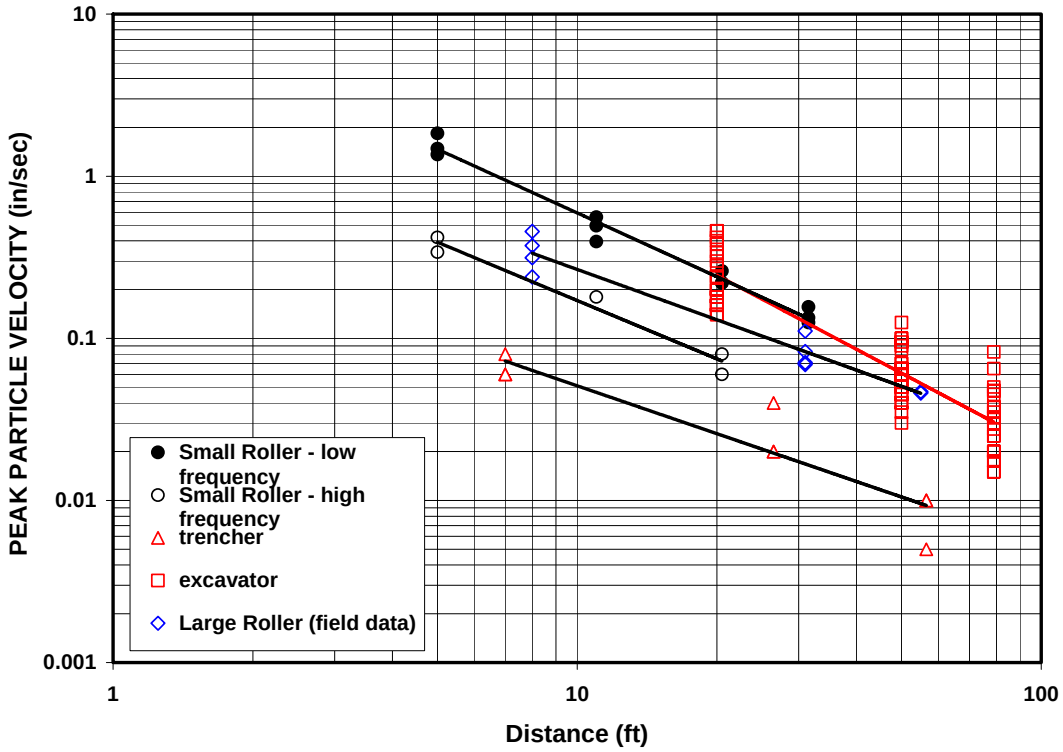

Figure 4.9 Peak particle velocity versus distance for ground vibration measurements adjacent to trackhoe, trencher, and vibratory roller construction activities

Figure 4.10 is a log-log plot of peak particle velocity versus dominant frequency. The dominant frequency for each data set was calculated by Fast Fourier Transform (FFT) spectral analysis of velocity time histories. The trackhoe produced ground motions with dominant frequencies between 16 and 25 Hz. The factory prescribed operating frequencies for the Dynapac small roller are 29 Hz (low frequency) and 40 Hz (high frequency). The dominant frequencies of the resulting ground motions were 27.5 Hz low and 45.2 Hz high. The Ingersoll-Rand large vibratory roller has a frequency dial that adjusts from 18 to 32 Hz. The field data taken for this roller were recorded at either 23 or

32 Hz. Dominant frequencies presented in Figure 4.10 are constant out to the greatest distance measured for all data (up to 56 feet). Thus, frequency is shown to be relatively independent of distance, for activity within 60 feet. Excitation frequency at short distances should be considered constant when considering the frequency response characteristics of structures described in Chapter 2.

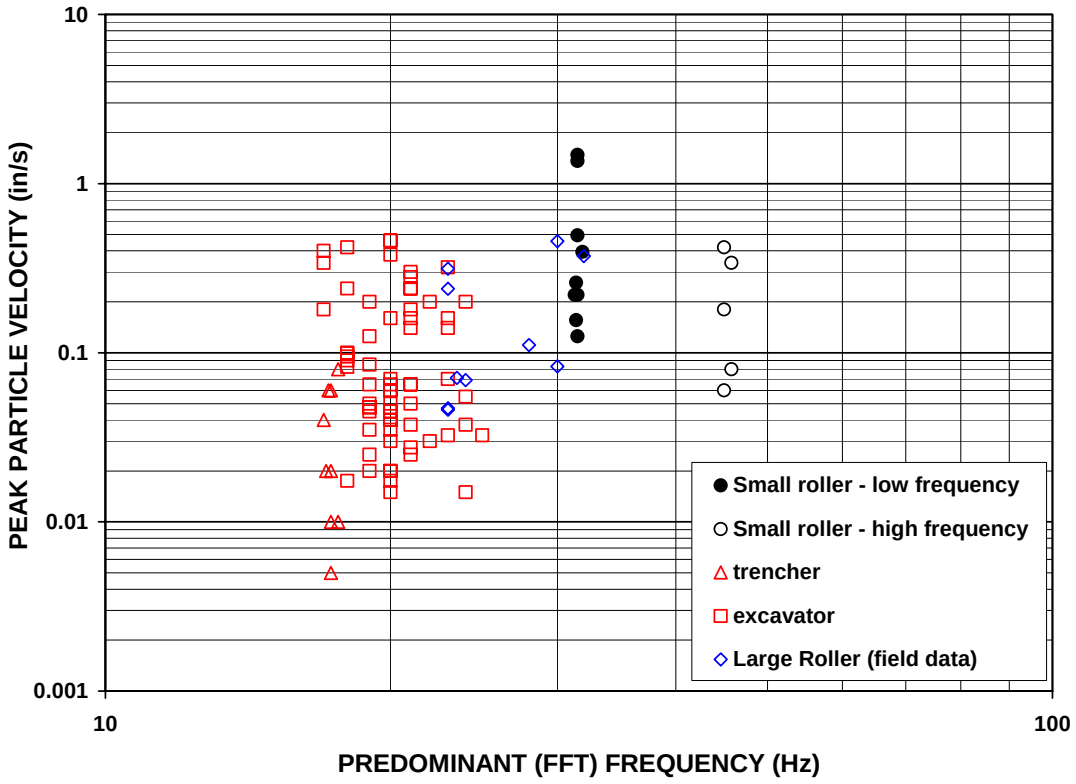

Figure 4.10 Peak particle velocity versus dominant frequency from fast fourier transform analysis for ground vibration measurements adjacent to trackhoe, trencher, and vibratory roller construction activities

Chapter 5

Construction Vibration Response Analysis and Recording

Introduction

One of the challenges of recording construction vibrations not found with blast vibrations is the necessity of measuring many (possibly hundreds) of daily events. While blasting vibrations typically occur only a few times a day or week, last for only a few seconds, and involve relatively standard ground motions and time histories, ground vibrations from construction machinery are less predictable and can last for relatively extensive periods of time. These differences in vibration environment brings forth the need for various and much more elaborate systems for data collection and triggering protocols to capture the full extent of ground and structural response.

Four different triggering mechanisms were employed to autonomously record the vibrations produced by construction on West Ann Road. This project, unfortunately, did not involve daily on-site inspection or personnel. Therefore it was of great importance that the instruments autonomously measure the varied and often continuous activity in the vicinity of the structure. Roadway reconstruction and utility improvements involve the services of several different heavy machines, thus the ability to differentiate each machine by waveform and correlated proximity and response are important to the success of any autonomous construction vibration study.

The first triggering mechanism enables long-term data collection. This mechanism triggers the system at a specific, pre-set time to collect one second of data at a frequency of 1000 Hz each hour for the duration of the test. Each one-second of data (1000 points) is then averaged, and becomes one data point, which is employed to define crack response to long-term and environmental effects. Only crack sensors will display long-term response, as velocity transducers are normally at rest and produce no measurable output.

A second triggering mechanism enables collection of ground velocity and crack displacement time histories of vibratory events. Collection begins when any component of ground motion exceeds the "trigger level" of 0.04 ips. While Somat data collection systems have enough memory to collect a significant number of time histories in a given run, the capacity is not infinite, but dependant on the size of PC data card available. For the purposes of this project and the equipment involved, the Somat eDAQ system was programmed to collect a maximum of 8 channels of 100, three-second time histories at 1000 Hz, or 2,400,000 data points. This system not only records individual time histories, but also allows collection of continuous time histories if events last longer than 3 seconds. This ability to continuously record is important in the monitoring of continuous vibrations produced by trenching and vibratory rolling.

The third triggering mechanism enables the collection of absolute peak values on each channel at either 1 or 10 Hz (depending on the situations that will be discussed later in detail) for the duration of the test run. These data allow an assessment of activity level for continuously vibrating sources such as vibratory rollers and trenching machines. This data stream will define the level of activity that produces vibrations less than the event trigger level of 0.04 ips. It can also define the occurrence of single-event activity (the second triggering mechanism) if the activity exceeds the 100-event data system capacity.

The final triggering mechanism involves the collection of significant events by manual trigger. This mechanism allows on-site personnel to collect data while construction occurs immediately adjacent to the test structure. Unfortunately, this manual assistance did not occur, and a summary had to be established through an unanticipated and heavy reliance on triggering mechanism three.

Vibratory crack and ground motion data collected between 9 June 2002 and 18 March 2003 is summarized in Tables 5.1, 5.2 and 5.3. The trackhoe, trencher and two vibratory roller activities produced peak particle velocities (PPV) between 0.03 and 0.456 inches per second and maximum crack response from 0 to 450 micro-inches. Weather conditions varied daily with indoor temperatures ranging between 62° and 86° F, humidity ranging from 14% to 35%, outdoor temperatures ranging from 27° to 124° F, and outdoor humidity ranging from 2% to 86%.

Machine Date Event #	Peak Particle Velocity (in/sec)	Relative Displacement of Structure, δ, by Method (μin)			Crack 2 Displacement (μin)	Crack 3 Displacement (μin)	Crack 5 Displacement (μin)
		Integration of Velocities G_{max}	SDOF MEthod f_n = 20 Hz	SDOF Method f_n = 18-22 Hz			
Trackhoe	0.034 (L)	300 (L)	580 (L)	580 (L)			
8/29/2002	0.035 (T)	200 (T)	320 (T)	350 (T)	44	2.8	16
Event 1	0.073 (V)	460 (V)	1110 (V)	1190 (V)			
Trackhoe	0.048	270	670	690			
8/29/2002	0.038	210	320	350	63	7.3	26
Event 2	0.08	580	1510	1460			
Trackhoe	0.041	180	620	590			
8/29/2002	0.033	120	360	370	41	8.1	25
Event 3	0.076	330	1160	1110			
Trackhoe	0.037	260	160	160			
9/13/2002	0.03	190	250	230	18	2.6	11
Event 4	0.051	350	200	220			
Trackhoe	0.034	110	600	550			
9/13/2002	0.02	60	190	220	11	2.5	7
Event 5	0.049	230	960	920			
Trackhoe	0.049	200	690	640			
9/13/2002	0.037	100	310	280	9.4	6	17
Event 6	0.049	240	990	910			
Trackhoe	0.043	190	160	150			
9/13/2002	0.044	130	150	150	7.1	2.6	6.4
Event 7	0.03	220	490	480			
Trackhoe	0.054	290	360	380			
9/13/2002	0.03	130	240	260	20	10	11
Event 8	0.061	440	590	580			

Table 5.1 Summary of directional measured peak particle velocity, computed displacements by integration of velocity and single degree of freedom methods and measured crack 2, 3, and 5 displacements for all trackhoe events on 29 August 2002 and 13 September 2002

Machine Date Event #	Peak Particle Velocity (in/sec)	Relative Displacement of Structure, δ, by Method (μin)			Crack 2 Displacement (μin)	Crack 3 Displacement (μin)	Crack 5 Displacement (μin)
		Integration of Velocities G_{max}	SDOF Method f_n = 20 Hz	SDOF Method f_n = 18-22 Hz			
Trencher	0.052 (L)	240 (L)	400 (L)	430 (L)			
11/22/2002	0.052 (T)	190 (T)	1010 (T)	940 (T)	13	8	17
Event 1	0.045 (V)	160 (V)	600 (V)	510 (V)			
Trencher	0.069	200	470	430			
11/22/2002	0.049	220	1130	1040	15	12	22
Event 2	0.048	210	540	480			
Trencher	0.064	190	420	410			
11/22/2002	0.044	210	670	700	14	10	21
Event 3	0.044	220	460	520			
Small Roller	0.059	270	480	500			
11/8/2002	0.019	70	160	170	15	7	12
Event 1	0.043	240	480	480			
Small Roller	0.05	230	390	400			
11/8/2002	0.025	110	170	180	23	11	17
Event 2	0.05	240	430	440			
Small Roller	0.146	560	950	920			
11/8/2002	0.063	220	430	420	48	16	34
Event 3	0.147	540	840	830			
Small Roller	0.05	250	460	470			
11/8/2002	0.02	90	140	150	13	10	15
Event 4	0.045	230	470	470			

Table 5.2 Summary of directional measured peak particle velocity, computed displacements by integration of velocity and single degree of freedom methods and measured crack 2, 3, and 5 displacements for all trencher events on 22 November 2002 and all small roller events on 8 November 2002

Machine Date Event #	Peak Particle Velocity (in/sec)	Relative Displacement of Structure, δ, by Method (μin)			FFT Excitation Frequency (Hz)	Crack 2 Displacement (μin)	Crack 3 Displacement (μin)	Crack 5 Displacement (μin)
		Integration of Velocities G_{max}	SDOF Method f_n = 20 Hz	SDOF Method f_n = 18-22 Hz				
Large Roller	0.041 (L)	240 (L)	940 (L)	1010 (L)				
3/18/2003	0.046 (T)	250 (T)	860 (T)	900 (T)	23	25	14	15
Event 1	0.069 (V)	250 (V)	1380 (V)	1560 (V)				
Large Roller	0.071	420	1450	1710				
3/18/2003	0.039	240	760	900	23	39	15	18
Event 2	0.062	390	1380	1570				
Large Roller	0.193	820	2400	2950				
3/18/2003	0.091	480	1620	1940	23	110	40	32
Event 3	0.237	1140	3740	4280				
Large Roller	0.229	940	2850	3450				
3/18/2003	0.147	740	2230	2650	23	175	42	38
Event 4	0.314	1950	6640	7950				
Large Roller	0.106	500	990	1010				
3/18/2003	0.05	300	520	530	32	25	20	22
Event 5	0.111	580	1040	1120				
Large Roller	0.367	1740	3570	3840				
3/18/2003	0.138	610	1020	1060	32	450	70	100
Event 6	0.456	1960	3390	3440				
Large Roller	0.083	420	1080	1080				
3/18/2003	0.027	140	230	240	32	40	18	21
Event 7	0.069	330	630	660				
Large Roller	0.354	1490	2990	3080				
3/18/2003	0.113	480	830	840	32	350	55	85
Event 8	0.373	1620	3400	3560				

Table 5.3 Summary of directional measured peak particle velocity, computed displacements by integration of velocity and single degree of freedom methods, excitation frequency by FFT method, and measured crack 2, 3, and 5 displacements for all large roller events on 18 March 2003

Long-term Triggering and Crack Response to Environmental Effects

Figures 5.1 and 5.2 compare long-term crack response with long-term weather indicators for each crack. Figure 5.1 shows long-term indoor Crack 1 and Crack 3 displacement compared to indoor temperature and humidity, while Figure 5.2 shows outdoor Crack 2 and Crack 5 displacement compared with external temperature and humidity. Temperature, humidity, and crack displacement are plotted on the same time scale. Crack displacement along with indoor and outdoor temperature and humidity were measured every hour for the duration of the monitoring period. Large daily changes in temperature, particularly outdoors, are characteristic of Nevada's desert climate, as is the generally low and relatively slow changing humidity. These weather phenomena correlate well with large, sharp daily changes in displacement of exterior cracks 2 and 5. The interior of the house is air-conditioned, which controls temperature and humidity, which thus reduces weather fluctuations and crack displacements relative to those outside.

Employing the same methodology established for the Connecticut structure in Chapter 2, 24-hour rolling and overall averages were calculated for all four cracks. The average and maximum of each weather descriptor, the frontal, daily, and maximum weather (in this study, seasonal) effects, for the four cracks are presented in Table 5.4. These weather-induced effects on external Cracks 2 and 5 were noticeably larger than for the internal cracks. This disparity in magnitude between internal and external crack displacement is expected, as the interior of the house is temperature and humidity controlled and out of the influence of direct sunlight. The weather-induced crack displacement for all cracks as defined by the three aforementioned descriptors was at least a factor of ten larger than any vibration-induced displacement, and often much more. The external cracks are subjected to greater changes in weather effects as well as the intense heat of the desert sun, and these factors are recognized as 24-hour temperature changes of as much as 50 degrees Fahrenheit and humidity changes of as much as 40 percent.

Several notable weather events occurred during the collection of the long-term data. Significant increases in humidity and decreases in temperature, such as those seen

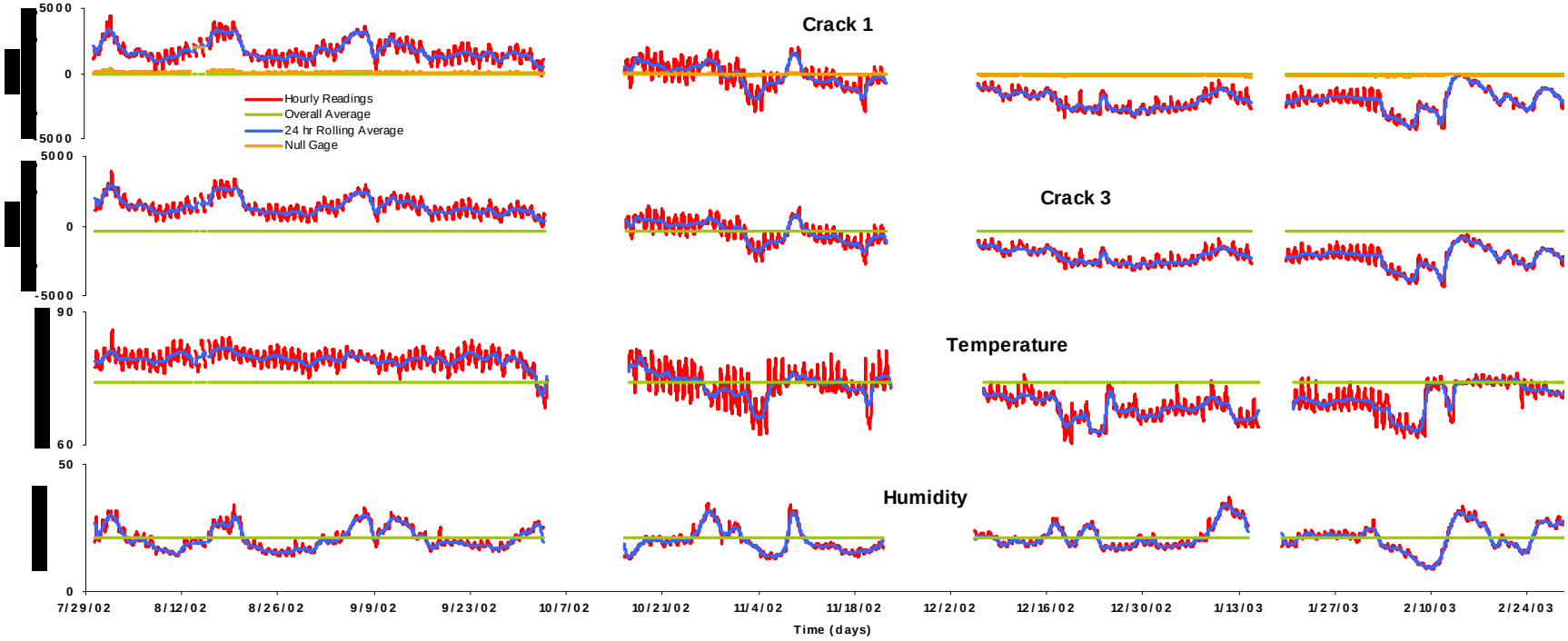

Figure 5.1 Long-term internal Crack 1 and Crack 3 displacement, indoor temperature and indoor humidity versus time

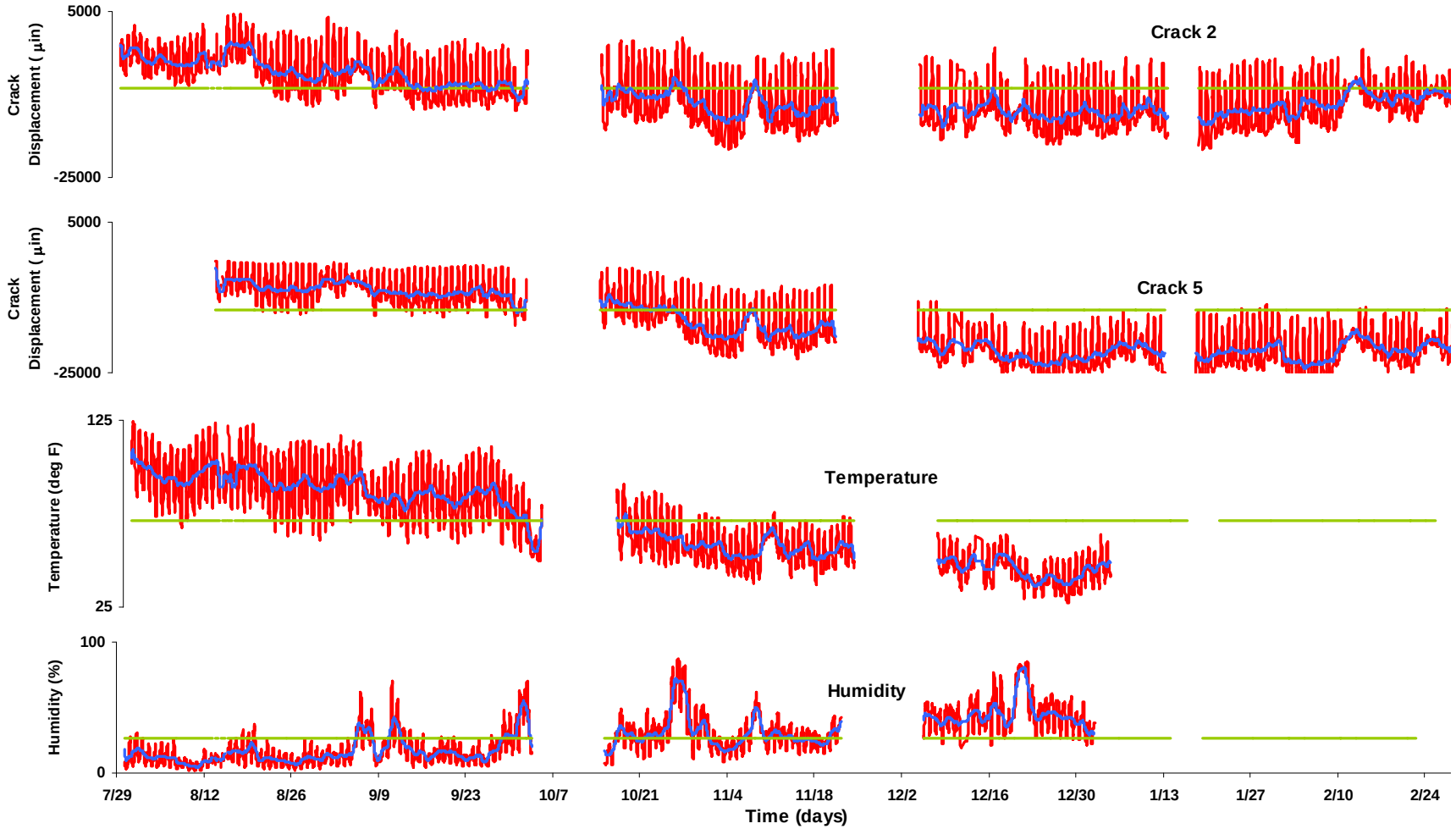

Figure 5.2 Long-term external Crack 2 and Crack 5 displacement, outdoor temperature and outdoor humidity versus time

Crack Sensor 2- External South Wall	Temperature Change (DegF)	Humidity Change	Crack Displacement (μin)	Crack Displacment (μm)
Frontal Effect				
Average deviation of 24-hour average from overall average	18.3	12.3	3300	84
Maximum deviation of 24-hour average from overall average	37.9	54.3	8800	224
Daily effect				
Average deviation of field measurement from 24-hour average	9.3	6.3	3200	81
Maximum deviation of field measurement from 24-hour average	45.9	38.2	10700	272
Weather Effect				
Average deviation of field measurement from overall average	19.5	13.8	4600	117
Maximum deviation of field measurement from overall average	71.2	61	13200	335
Construction Effect				
Maximum ground motion (PPV= 0.08 ips Trackhoe)	-	-	63	1.60
Maximum ground motion (PPV= 0.055 ips Trencher)	-	-	15	0.38
Maximum ground motion (PPV= 0.148 ips Small Roller)	-	-	48	1.22
Maximum ground motion (PPV= 0.456 ips Large Roller)	-	-	450	11.43

Crack Sensor 3- Hallway Wall	Temperature Change (DegF)	Humidity Change	Crack Displacement (μin)	Crack Displacment (μm)
Frontal Effect				
Average deviation of 24-hour average from overall average	4.6	3.8	1600	41
Maximum deviation of 24-hour average from overall average	11.5	13	3600	91
Daily effect				
Average deviation of field measurement from 24-hour average	1.3	0.9	270	7
Maximum deviation of field measurement from 24-hour average	9.5	23.2	1250	32
Weather Effect				
Average deviation of field measurement from overall average	4.5	4	1600	41
Maximum deviation of field measurement from overall average	14.2	17	4300	109
Construction Effect				
Maximum ground motion (PPV= 0.08 ips Trackhoe)	-	-	10	0.25
Maximum ground motion (PPV= 0.055 ips Trencher)	-	-	12	0.30
Maximum ground motion (PPV= 0.148 ips Small Roller)	-	-	16	0.41
Maximum ground motion (PPV= 0.456 ips Large Roller)	-	-	70	1.78

Crack Sensor 5- External West Wall	Temperature Change (DegF)	Humidity Change	Crack Displacement (μin)	Crack Displacment (μm)
Frontal Effect				
Average deviation of 24-hour average from overall average	18.3	12.3	5700	145
Maximum deviation of 24-hour average from overall average	37.9	54.3	13000	330
Daily effect				
Average deviation of field measurement from 24-hour average	9.3	6.3	2100	53
Maximum deviation of field measurement from 24-hour average	45.9	38.2	10000	254
Weather Effect				
Average deviation of field measurement from overall average	19.5	13.8	6100	155
Maximum deviation of field measurement from overall average	71.2	61	15500	394
Construction Effect				
Maximum ground motion (PPV= 0.08 ips Trackhoe)	-	-	26	0.66
Maximum ground motion (PPV= 0.055 ips Trencher)	-	-	22	0.56
Maximum ground motion (PPV= 0.148 ips Small Roller)	-	-	34	0.86
Maximum ground motion (PPV= 0.456 ips Large Roller)	-	-	100	2.54

Table 5.4 Summary and comparison of Crack 2, 3, and 5 displacement with weather descriptors, vibratory activity and average and maximum temperature and humidity readings

around the 7th of September, 27th of October and 21st of December suggest rainfall events occurred during these time periods. Weather stations in Las Vegas confirm that rainfall events did take place, and as the 24-hour rolling humidity average steadily increased, Cracks 1, 2, and 3 all reacted with correlating dramatic displacements. Crack 5, however, did not experience as relatively significant a reaction to this series of extreme weather phenomena. Table 5.5 summarizes all rain events that occurred between 15 June 2002 and 31 December 2002. 2003 data are not yet available from the National Weather Service.

Date	Rainfall (in)
7/17/2002	0.52
9/5/2002	0.03
9/6/2002	0.01
9/11/2002	0.27
10/2/2002	0.05
10/26/2002	0.1
10/27/2002	0.17
11/30/2002	0.12
12/16/2002	0.01
12/20/2002	0.03
12/21/2002	0.03

Table 5.5 Summary of rainfall events during monitoring period in 2002. 2003 data not yet available. (National Weather Service)

Figure 5.3 combines several long-term and continuous, triggered time history data collection schemes with Crack 2, to illustrate the dominant effect of weather relative to construction-induced vibration for (a) trackhoe excavation (29 August), (b) trencher excavation (22 November), and (c) small vibratory roller compaction (8 November), and large vibratory roller compaction (18 March). Each event period begins and ends with hourly readings (represented by large solid circles). With respect to the trackhoe plot (a), the largest crack displacement within this time period was 63 micro-inches. The difference between the initial crack width and its width one hour later from temperature change, however, was slightly under 2500 micro-inches. This change is equivalent to an accumulating 60 micro-inch increase in crack width *every two minutes*. More importantly, however, this comparison shows external crack displacement induced by weather phenomena to be well over a factor of ten greater than that of the largest crack displacement induced by the trackhoe at an overall peak particle velocity of 0.08 ips.

Figure 5.4 shows the time of day during which the activity in Figure 5.3 were collected. Trackhoe activity (a) was recorded around 8:30 AM, during which the time rate of change in temperature and humidity are near their peak. Trencher data were recorded later in the morning at 11:00 AM and roller data about 12:30 PM when the rate of change was much smaller as the insolation begins to decline. Weather effects typically reverse themselves for the day between the hours of 1 and 3 PM. These changes show the high sensitivity of the cracks on the stucco exterior. The pair of plots in Figures 5.3 and 5.4 show that even though the hourly rate of change in the weather effect is relatively small at that time, vibratory activity of both the trencher and small roller produce far smaller crack displacement than the changes in temperature and humidity. Furthermore, subsequent changes in weather response that same day can be large.

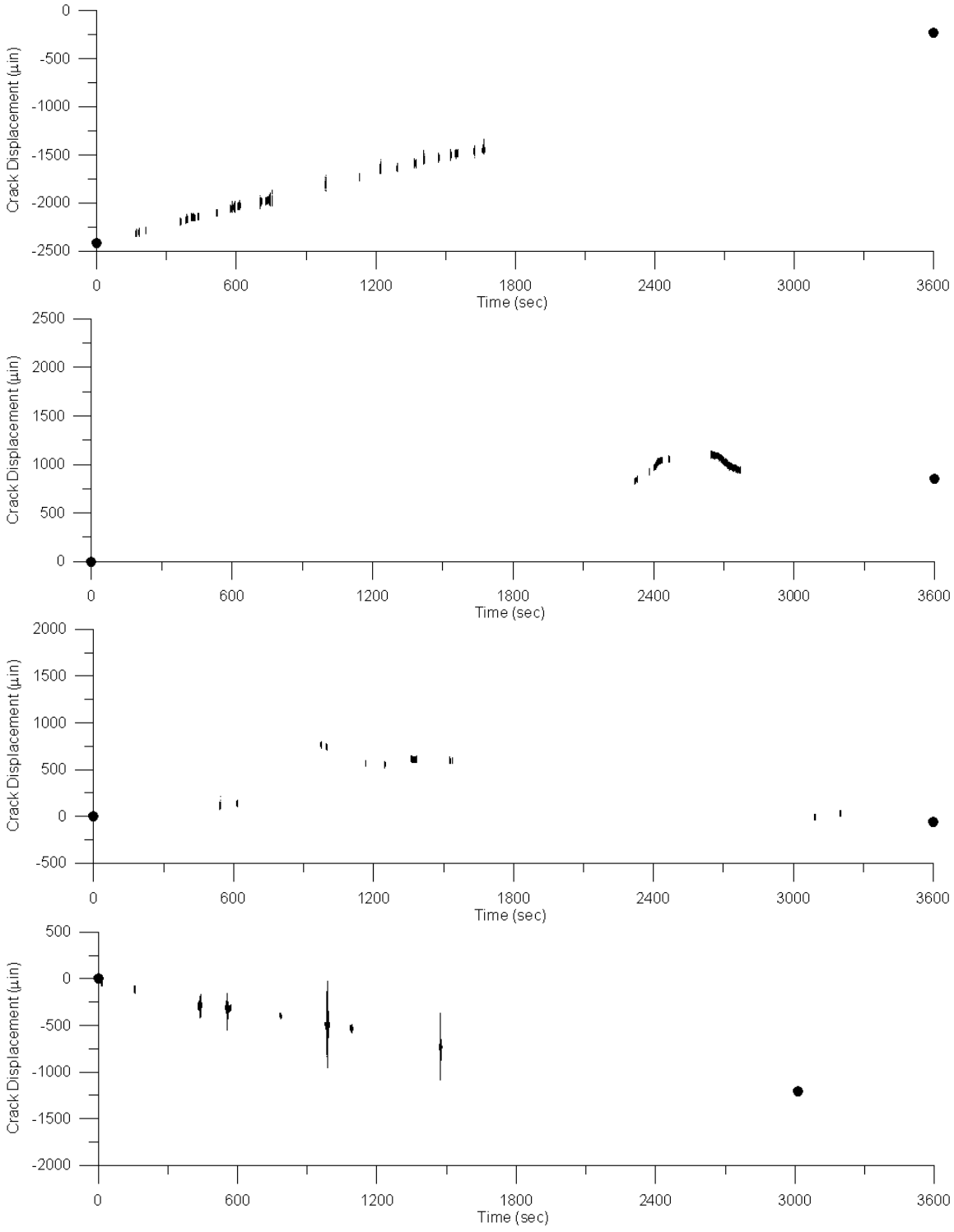

Figure 5.3 Combined Crack 2 time histories and long-term data triggers showing dominant effect of weather versus vibration induced crack displacements over a one-hour period for trackhoe (top), trencher (middle-top), small vibratory roller (middle-bottom), and large vibratory roller (bottom)

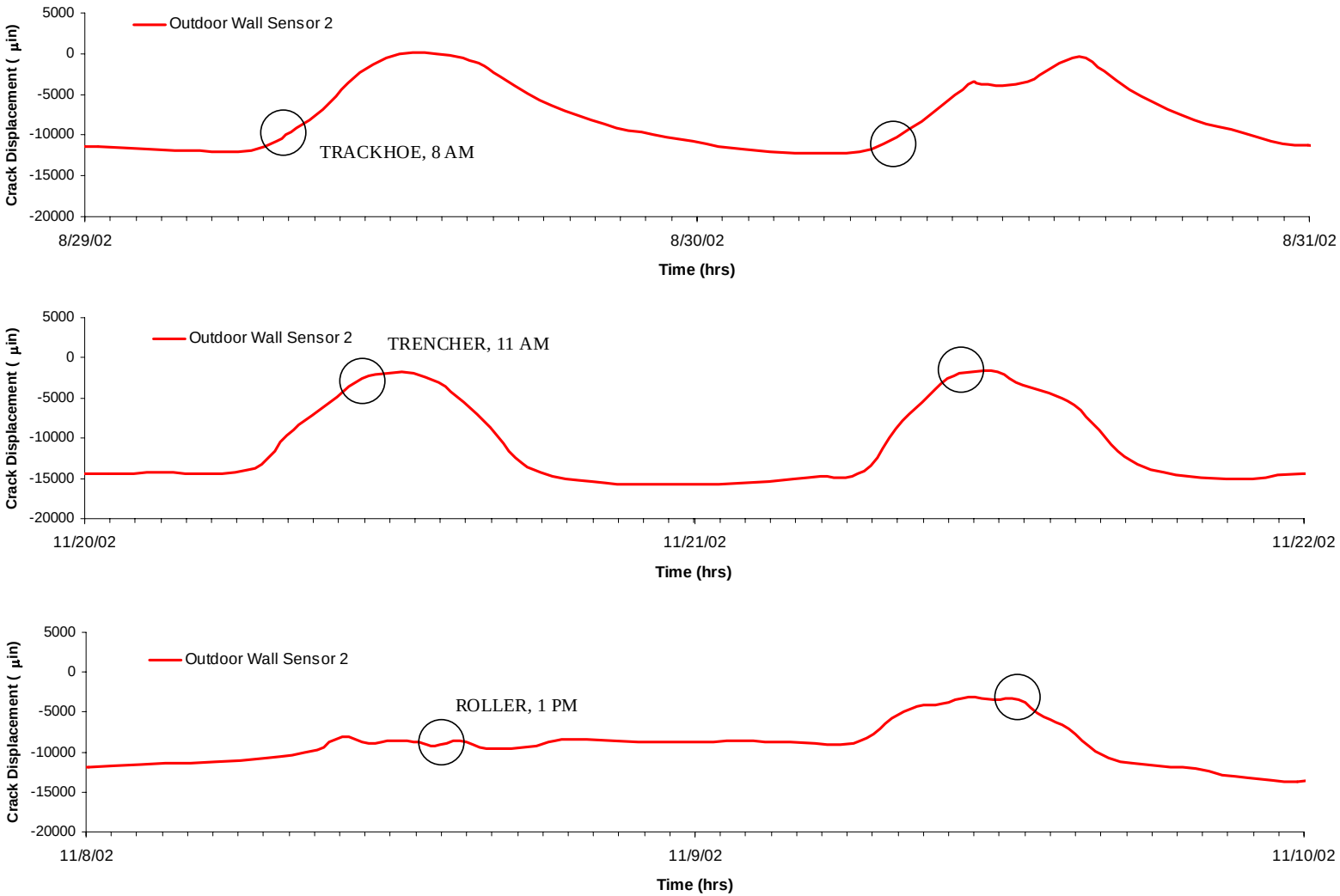

Figure 5.4 Long-term Crack 2 data showing variability in acquisition periods for trackhoe excavation, trencher excavation, and small roller vibratory compaction

To measure the regularity of crack displacement, changes in the width of Cracks 2 and 5 were recorded at a rate of 1 Hz, or 1 data point per second, without vibratory excitation. Figure 5.5 presents this data during the same one hour time period as the plots shown in Figure 5.3, under this modified triggering scheme. Two long-term data points are shown at times 0 and 3600 seconds, and the data between variations in crack response. While this and previous studies have shown that recording long-term and threshold triggered vibratory response does an effective job of conveying the dominant effect that weather phenomena have on cracks, these plots display the not insignificant non-vibratory response that may occur between hourly data points. For example, at approximately the 900-second mark of the small roller data in Figure 5.5, there is a significant deviation from the gradual change in displacement of Crack 2. Looking back to Figure 5.3 which presented all recorded transient events exceeding 0.04 ips during this hour of activity, however, shows that whatever phenomenon caused this deviation was not associated with any instantaneous ground motion large enough to trigger the individual event time history recording system. Even when the largest measured ground excitation events are large enough to appear in this data mode, such as those circled on the small and large vibratory roller plots in Figure 5.5, they are still vastly overwhelmed by the effect of non-vibratory response.

Cracks do not open and close continuously, but rather intermittently over time in a stick-slip fashion. Figure 5.6 (a) shows five seconds of external Crack 5 data recorded at a rate of 10 samples per second (10 Hz), at approximately 8:30 AM on a day when no construction activity significant enough to trigger time history data recording took place in the vicinity of the house. This stick-slip phenomenon may influence the interpretation of vibratory response if it occurs during a transient event. As shown in Figure 5.6 (b), there may be the appearance of “permanent” crack displacement in a recorded time history, or rapid and unexplained crack displacement in continuous data such as that presented earlier for Crack 2 response to the small roller in Figure 5.5. At first one might interpret Figure 5.6 to show that significant crack displacement seen at approximately the 1.2-second mark appears to have been the result of construction machinery induced ground motions. However, it would have occurred without activity in the vicinity of the house at the time of recording. This “stick-slip” effect may create a serious

misconception about the nature of vibration crack response unless it is compared to the long-term response, which shows the true environmentally induced response.

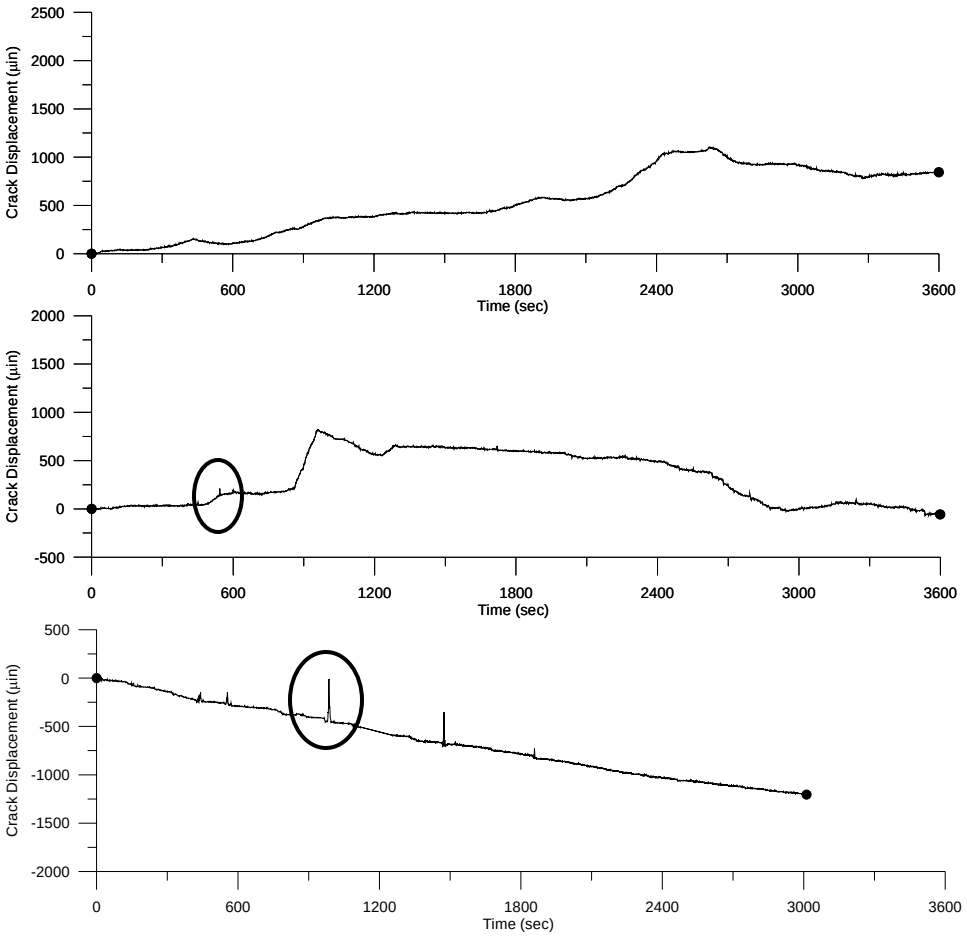

Figure 5.5 Combined long-term and one-hertz continuous data triggering non-vibratory Crack 2 response over the same one-hour time periods as Figure 5.3, for trencher (top), small vibratory roller (middle), and large vibratory roller (bottom). Example vibratory roller events recorded within this time period are circled.

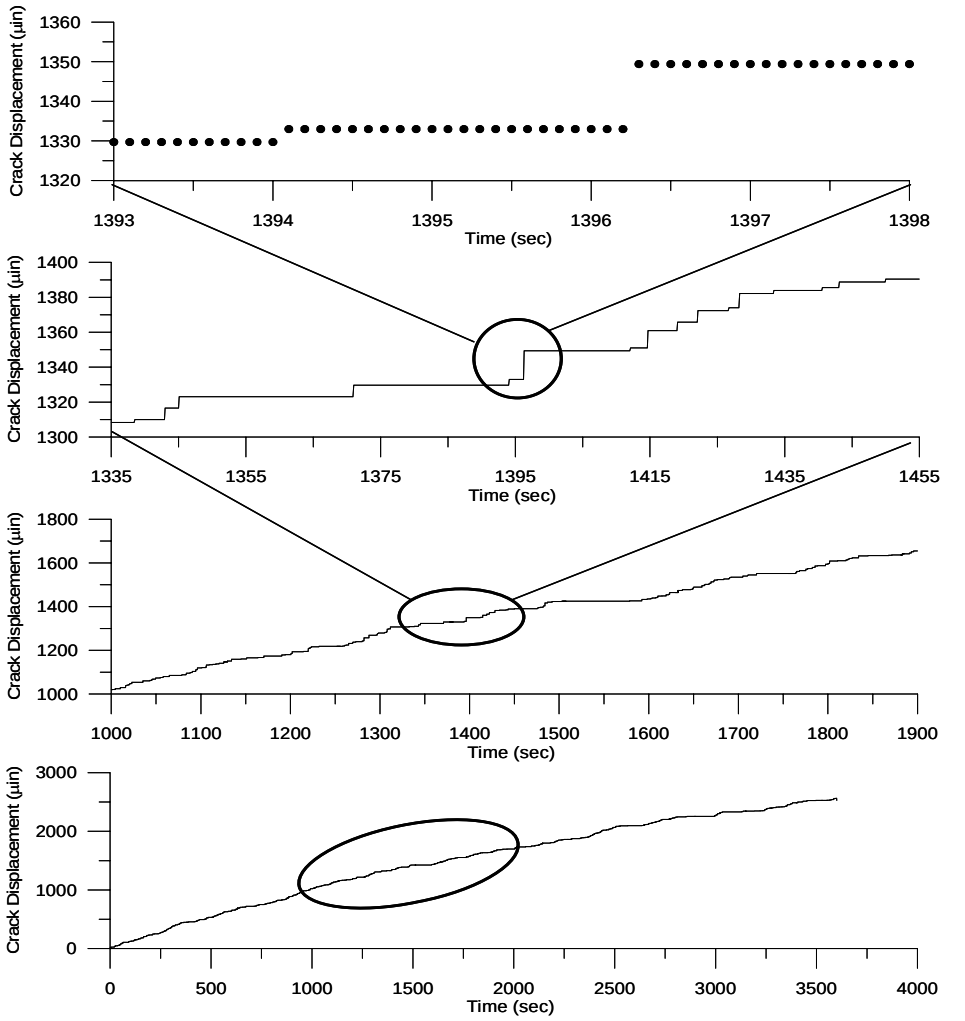

(a)

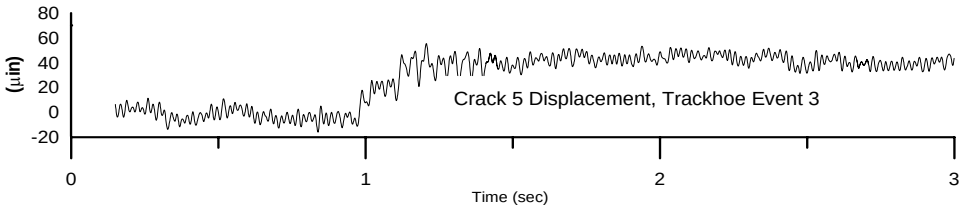

(b)

Figure 5.6 Representation of proposed stick-slip crack displacement effect on external Crack 5 (a) from long-term data taken during a time period without construction activity and (b) trackhoe excavation Event 3 time history on 29 August 2002

Individual Event Triggering and Transient Response

Construction vibration induced ground motion and the resulting crack response were obtained whenever peak particle velocities exceeded 0.04 ips. They were produced by the various construction activities outlined in Chapter 4 during the widening and reconstruction of Ann Road. These activities have been divided into three primary categories, and again into individual, specific activities and events. The four principal categories are:

- General construction and miscellaneous response
- Trackhoe trenching activities involved with the installation of a 12-ft x10-ft reinforced concrete storm culvert,
- Trencher activities involved with the installation of an 8-inch PVC sanitary line,
- Vibratory compaction from trench backfill and sub-grade activities

A 10 micro-inch high-frequency electrical noise produced by the unusually large volume of machine and radio wave traffic in the vicinity of the data acquisition system and an occasionally low vibratory crack response presented a significant challenge in the discrimination of small measured crack response to construction vibrations by machines at typical distances. As a result a *Butterworth* low pass data-filter was employed to eliminate all crack displacement time history components with frequencies greater than 60 Hz. The filtering scheme was not necessary for ground motions. Filtering only improved the discern ability of transient response for external Cracks 2 and 5 and internal Crack 3 for trackhoe and trencher excavation activities; the vast majority of responses in internal Crack 1 were still too small to identify above the remaining noise produced at nearly the same frequency. Figure 5.7 is an example of an unfiltered time history for External Crack 5 responding to small vibratory roller excitation at approximately 46 feet, with its corresponding filtered time history plotted below. The crack displacement can be easily deciphered in this time history, but the figure clearly demonstrates the significant loss in amplitude associated with these necessary filtering activities. This particular event will be explored in detail later in the chapter, but for future reference, any post-filter crack displacement less than 10 micro-inches will be henceforth be considered merely a product of filtered noise, and negligible.

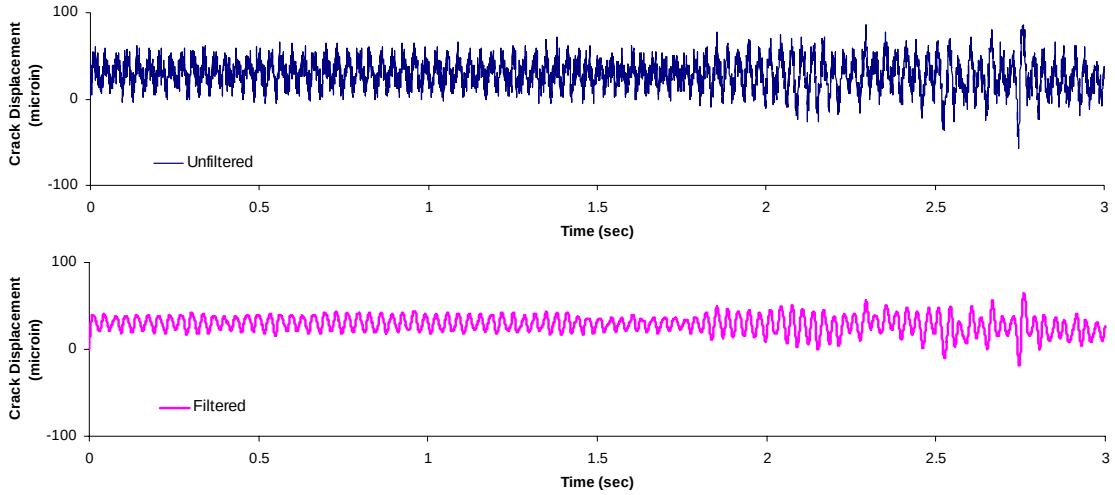

Figure 5.7 Three seconds Unfiltered (top) versus filtered (bottom) Crack 2 displacement data for 3 seconds and peak of vibratory roller compaction event #3 on 8 November 2002

Miscellaneous Activities

In the introduction to this chapter it was noted that one of the inherent challenges to monitoring construction vibrations versus blasting vibrations is the relatively continuous nature of construction activity necessitating unusual triggering schemes. The number, size and specifics of all machinery active in one location on a standard construction site is far too random to identify all sources without continuous on-site inspection. During the monitoring of construction on Ann Road, several construction machines were active near the test house that randomly triggered the system, but did not create ground motions or crack responses significant enough to present in detail. Graders, front-end loaders, and forklifts are examples of these machines.

During the excavation activities to be discussed later, a large number of spurious events shown in Figure 5.8 occurred. All had the same signature pattern: small/large/small amplitudes at approximately half-second intervals. The top four time histories are crack displacement time histories of cracks 1, 2, 3, and 5, which display no response. The bottom three represent longitudinal, transverse, and vertical ground velocity time histories of this event. The significant portion of this ground motion lasts a mere two tenths of a second and results in essentially no crack displacement from any of

the sensors. The exact cause of these frequent events is not entirely known, but could possibly be personnel walking over the geophone.

The greatest challenge these spurious events pose for vibration monitoring is their occurrence during the same event history as other monitored activities. This dual arrival makes it difficult to decipher what degree of ground motion and structural response are results of the desired activity, rather than these miscellaneous activities. Separation of these two activities requires the examination of dominant frequencies within the time histories and will be examined further later in this chapter.

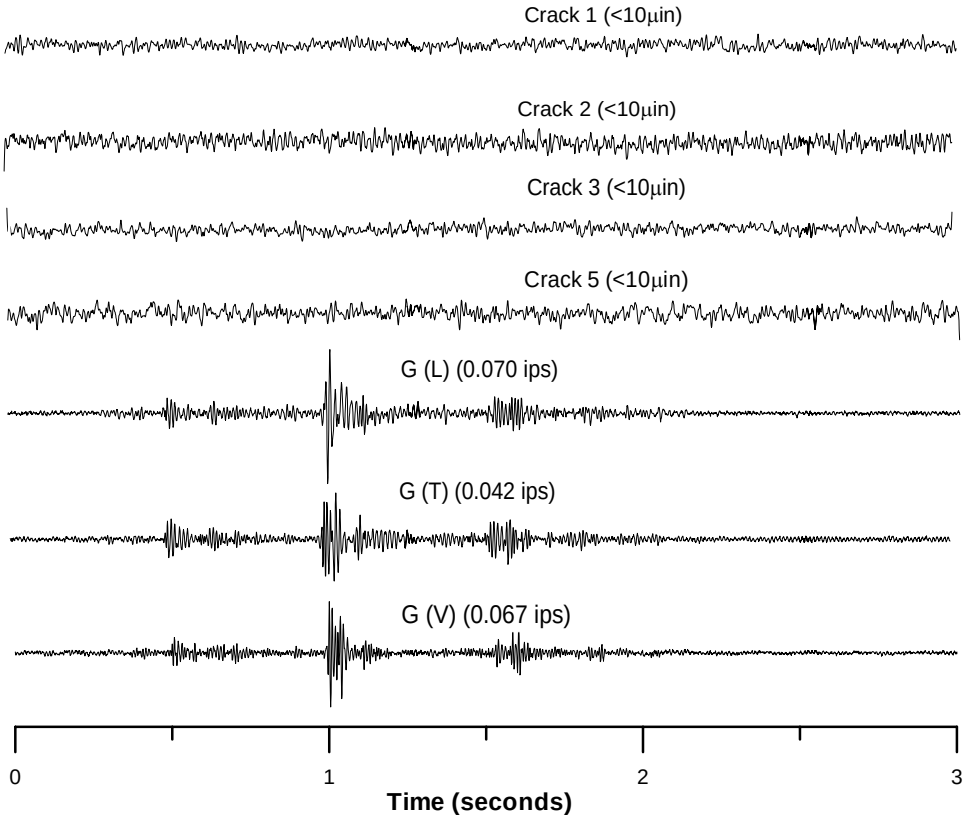

Figure 5.8 Time histories of Crack 1, Crack 2, Crack 3 and Crack 5 from miscellaneous trigger event in August 2002 compared to longitudinal, transverse and vertical ground excitation

Trenching Activities

Figure 5.9 shows time histories of excitation ground motions and the associated internal and external crack response produced by excavation of a 12 foot wide trench with an Hitachi 1200 EX Super track-hoe (shown in Figure 4.4 (a)) at approximately 8:30 AM on August 29th, 2002. The centerline of the trench is oriented parallel to and is approximately 46 feet in front of the house. The top four graphs in Figures 5.9 show crack displacement time histories of cracks 1, 2, 3, and 5. The bottom three time histories show longitudinal, transverse, and vertical ground velocity time histories. This particular excitation produced a peak particle velocity of 0.08 ips in the vertical direction. Crack 2, the external south wall crack nearest the excavation, experienced the greatest displacement of 63 micro-inches zero-to-peak while Crack 5 experienced 26 micro-inches zero-to-peak. Internal Cracks 1 and 3 showed little or no discernable response after filtering of general instrument and electrical noise is performed. The attenuation relationship presented in Figure 4.9 shows this peak particle velocity matches that expected from the trackhoe.

The natural frequency of the wall is calculated employing the Frequency Fourier Transform (FFT) response spectra method described in Chapter 2. Crack 2, the outside south wall sensor, was selected because it is closest to the construction activities and the most responsive, and as a result has the highest signal to noise ratio. Figure 5.10 shows the longitudinal FFT spectra for the Crack (b), the longitudinal component of ground displacement (c), and the ratio (a), which show a dominant frequency of 18 to 22 Hz for this wall.

The SDOF response spectrum for Event 2 on 29 August is presented as Figure 5.11. A damping coefficient of 5% was assumed for all spectra based on average values from previous studies. The approximate dominant frequency of the Las Vegas wall is 20 Hz, therefore the estimated displacement of the structure relative to the ground motion produced by this event was 1510 μin in the longitudinal direction. Single degree of freedom analyses were performed on all longitudinal, transverse and vertical ground motions produced by the excavation activities. These spectra are used to predict cracking potential in structures subjected to excitation ground motions and are described in detail in Chapter 2.

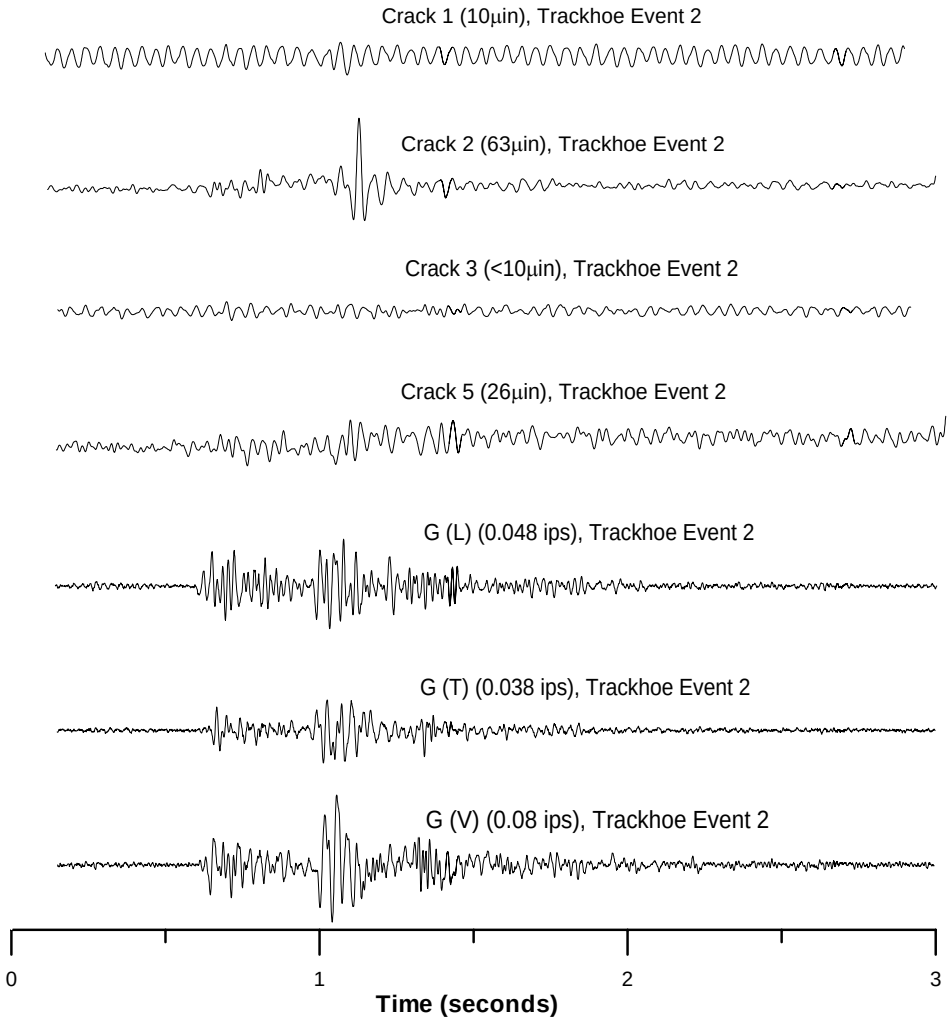

Figure 5.9 Time histories of Crack 1, Crack 2, Crack 3 and Crack 5 from trackhoe excavation event 2 on 29 August 2002 compared to longitudinal, transverse and vertical ground excitation

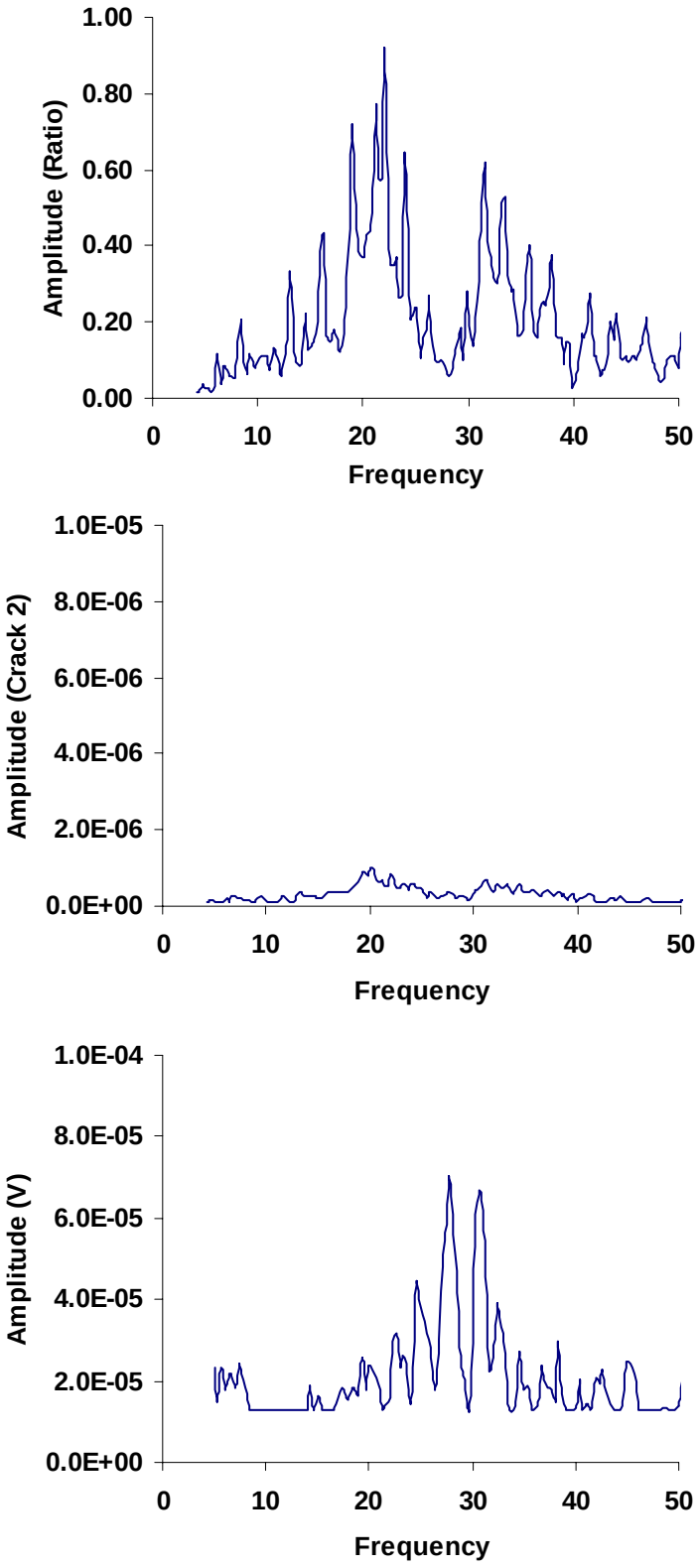

Figure 5.10 Frequency Fourier Transform histogram of Crack 2 divided by vertical ground displacement ratio (top), measured Crack 2 displacement (middle), and calculated vertical ground displacement (bottom) for trackhoe event #2 on 29 August 2002

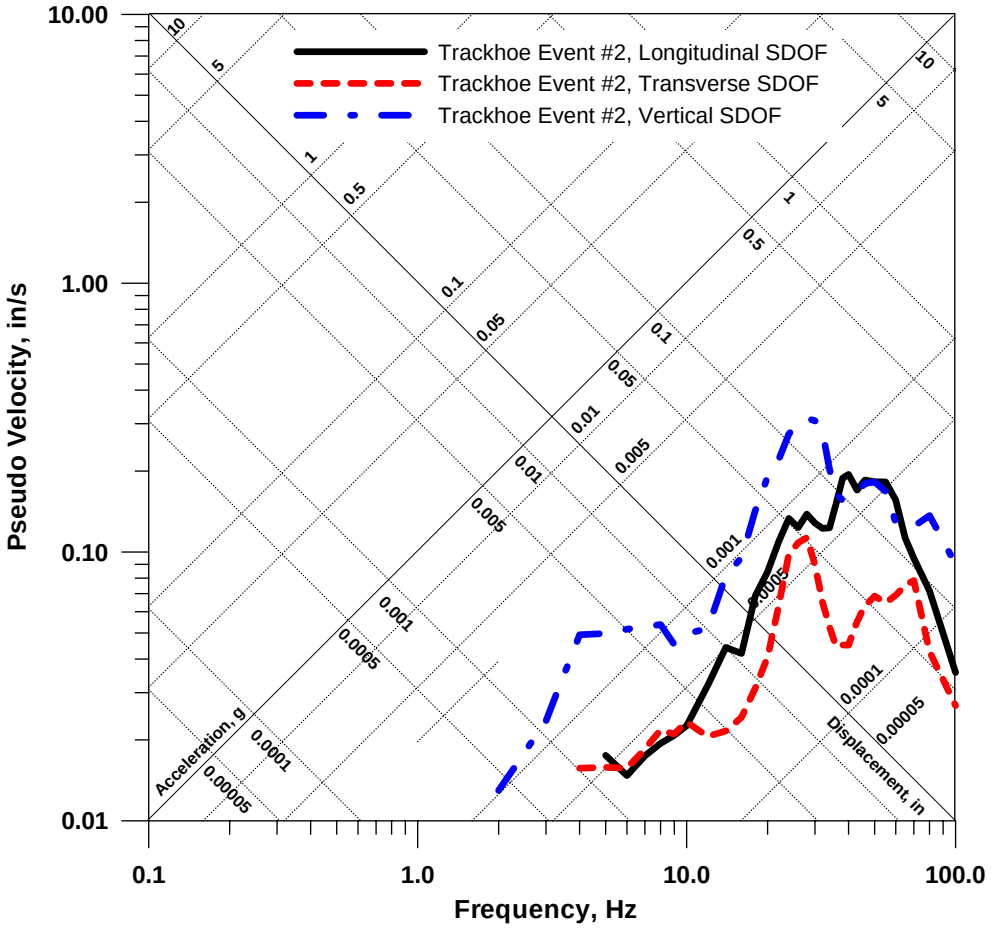

Figure 5.11 Longitudinal, transverse, and vertical single degree of freedom response spectra for trackhoe event #2 on 29 August 2002, showing relative displacement of a 20 Hz structure

Figure 5.12 shows time histories of excitation ground motions and the associated internal and external crack response associated with the excavation of a trench for an 8" PVC sanitary sewer line with the Tesmec TRS-1175 trencher shown in Figure 4.4 (b) at approximately 11:00 AM on November 21st, 2002. The centerline of this trench lies parallel to and approximately 32 feet in front of the house. The top four graphs in Figures 5.12 show crack displacement time histories of cracks 1, 2, 3, and 5. The bottom three time histories show longitudinal, transverse, and vertical ground velocity time histories. These trenching activities constituted the first "continuous" activity in the vicinity of the structure and did not produce particularly large ground motions. Figure 5.12 shows the greatest overall peak particle velocity resulting from the trencher activity of 0.069 ips. From the attenuation study presented in Chapter 4, trencher peak particle

velocities from 30 to 35 feet away should average between 0.01 and 0.03 ips, with occasional spikes similar to those seen throughout the velocity time histories in Figure 5.12. It is theorized that these spikes are a result of the trencher cutting its way through a deposit of caliche, which produces greater vibration. All of the time histories recorded for the trencher are continuous, but very choppy and unharmonious, which is to be expected from chain trenching excavations (Dowding, 1996). Crack displacements were smaller than those of the trackhoe and rollers. A maximum of 17μin was measured from Crack 2, 12μin from Crack 3 and 23μin from Crack 5. This relatively small response is expected due to the relatively small ground motions.

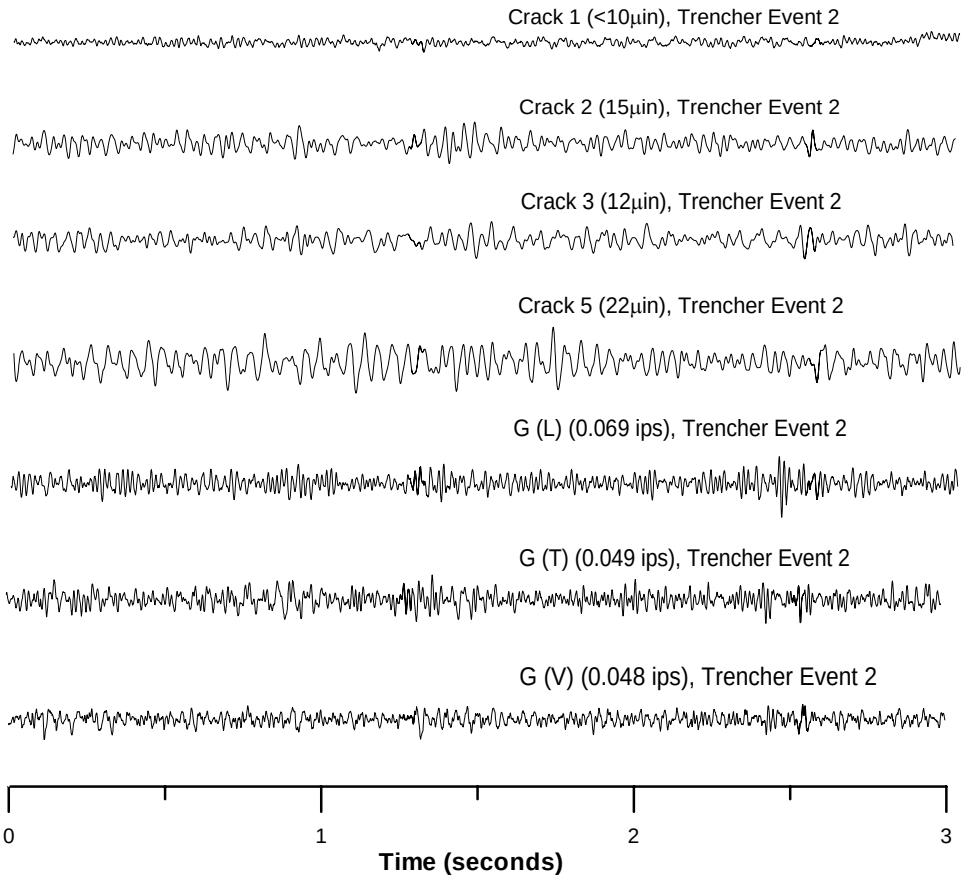

Figure 5.12 Time histories of Crack 1, Crack 2, Crack 3 and Crack 5 from trencher excavation event 2 on 21 November 2002 compared to longitudinal, transverse and vertical ground excitation

Vibratory Compaction

A variety of data were collected for vibratory roller activities in the vicinity of the test house. As reported in Chapter 4, two different rollers were employed for this project; a small roller to compact granular backfill in the culvert trench excavated by the trackhoe, and a larger roller employed to compact granular roadway sub-grade prior to application of the asphalt surface. Both rollers provided continuous time histories that last significantly longer than blasting or trackhoe activities, and are much more harmonic and smooth compared to the chain-excavation of the trencher. Therefore, roller events are not assumed to last 3 seconds, as are the trackhoe and trencher events, but extend as long as the peak particle velocity in any direction exceeds the "significant peak" threshold of 0.04 ips for the small roller and 0.08 ips for the large roller.

Figure 5.13 (a) presents response of internal Cracks 1 and 3, external Cracks 2 and 5 and excitation ground motion velocity time histories produced by vibratory compaction of the granular backfill within the 12-foot wide culvert trench. Compaction was performed with the Dynapac single-drum vibratory roller shown in Figure 4.5 (a). This activity took place during the early afternoon on November 8th, 2002. The top four time histories represent crack displacement time histories for the four cracks, and the bottom three show the corresponding excitation ground velocities. This event produced a peak particle velocity of 0.147 inches per second (vertical) and resulted in a peak overall crack displacement of 46μin from external Crack 2. External Crack 5 sustained a displacement of 34μin, Crack 3 displacement of 16μin, and Crack 1 experienced a stick-slip displacement of 30μin, described earlier.

Many of the time histories measured during vibratory compaction monitoring show unusual changes and overlaps in particle frequencies when examined closely. The three seconds of all Event 3 time histories in Figure 5.13 (a) with the largest peak particle velocities and crack displacements are shown in Figure 5.13 (b). They show a distinct time variation in frequency and amplitude that may have resulted from approaching or run-up. At the 1.5-second mark, the time histories change from a relatively harmonious 0.025 to 0.05 ips longitudinal amplitude, 32 Hz signal to a 0.15 ips amplitude with overlying 32 and 48 Hz frequencies. During this time interval, displacements of external Cracks 2 and 5 also increase significantly from a relatively harmonic 10μin peak-to-peak,

to their maxima of 46μin and 34μin, respectively. At approximately the 7.5–second mark, or 1.5 seconds before the end of the time history, the amplitudes decline, the 48 Hz frequency drops out and the time history returns to its original state. The importance and origin of the run-up phenomena is discussed in Dowding (1996).

Figure 5.14 shows the fourier frequency spectra of Crack 2, longitudinal integrated ground velocity (displacement) and Crack 2 divided by long displacement for this event, and Figure 5.15 is the longitudinal, transverse and vertical SDOF spectra for this event. From the ground displacement FFT spectrum, it is obvious that, along with the dominant vibratory roller frequency of 32 Hz, there is also a significant frequency at 48 Hz. From the Crack 2 spectrum, however, there is no response from the crack at 40 Hz. The ratio spectrum of Figure 5.14, Crack 2 divided by the ground motion, confirms that at 48 Hz the spectrum is below the base line, meaning that the ground motion contains these dominant frequencies, but the crack is not responding.

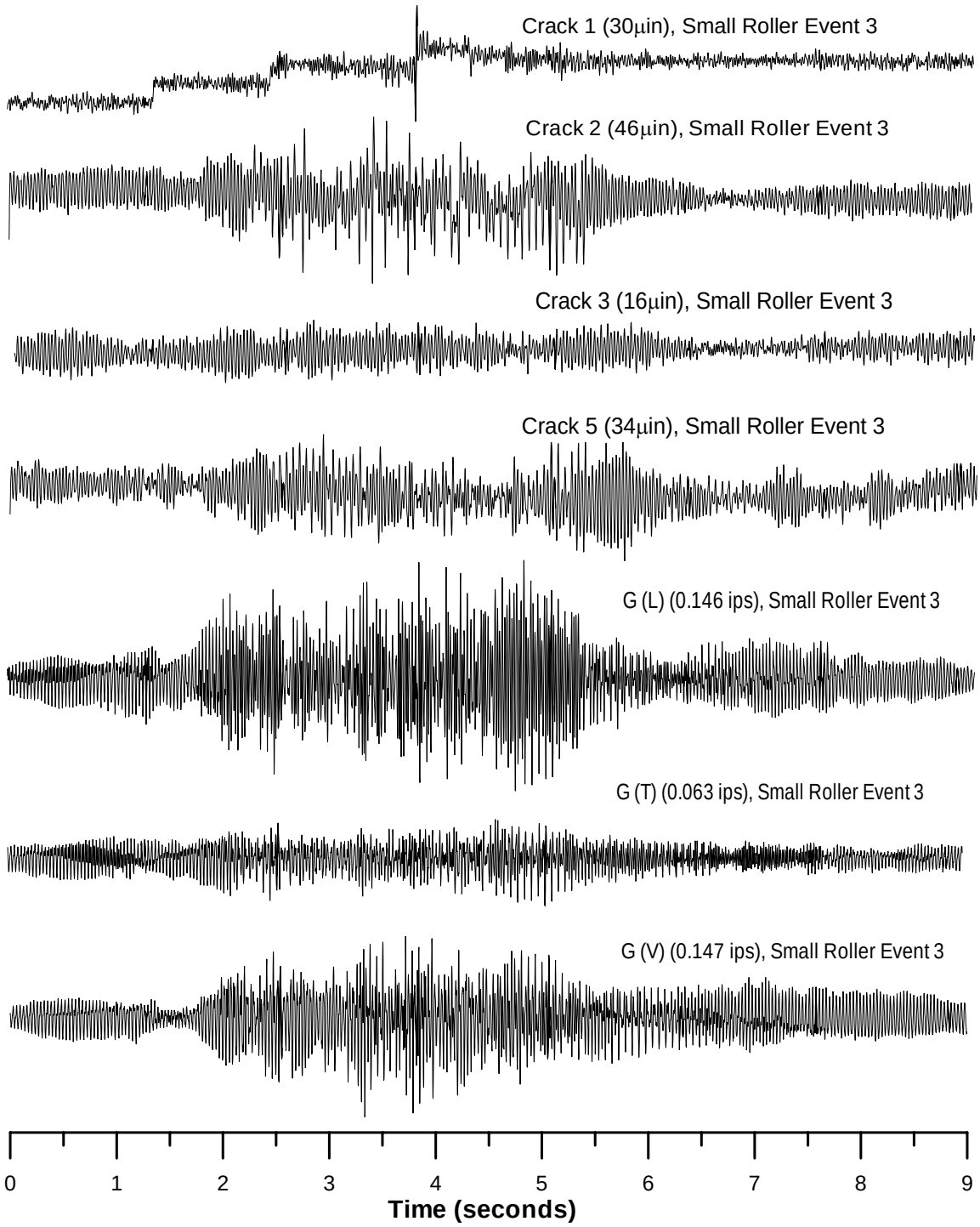

Figure 5.13 (a) Time histories of Crack 1, Crack 2, Crack 3 and Crack 5 from granular trench backfill small single-drum roller compaction Event #3 on 8 November 2002 compared to longitudinal, transverse and vertical ground excitation ground motion

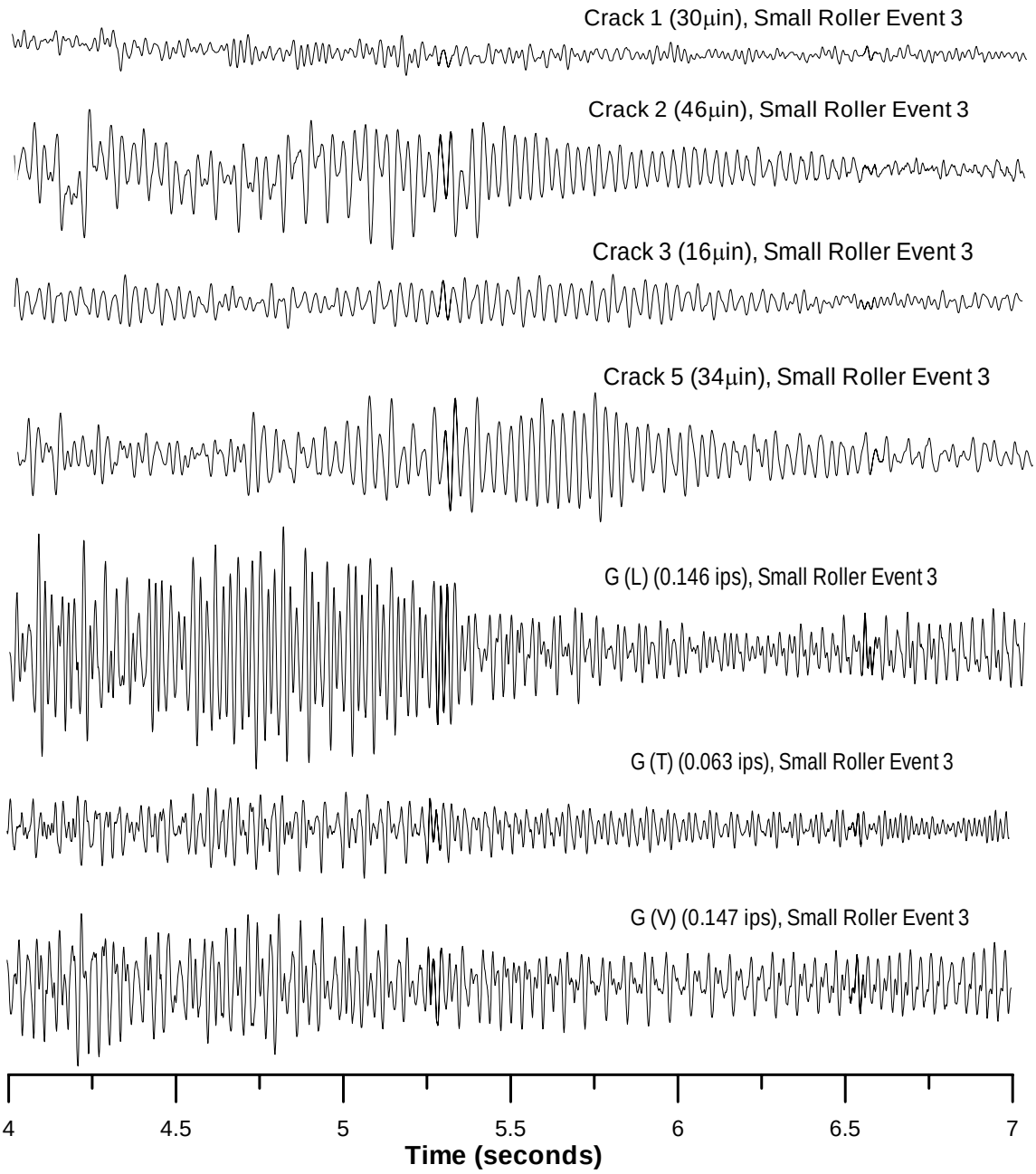

Figure 5.13 (b) 3-second magnification of granular trench backfill small single-drum vibratory roller event 3 time history showing Crack 1, Crack 2, Crack 3, Crack 5, and longitudinal, transverse and vertical ground motion waveforms

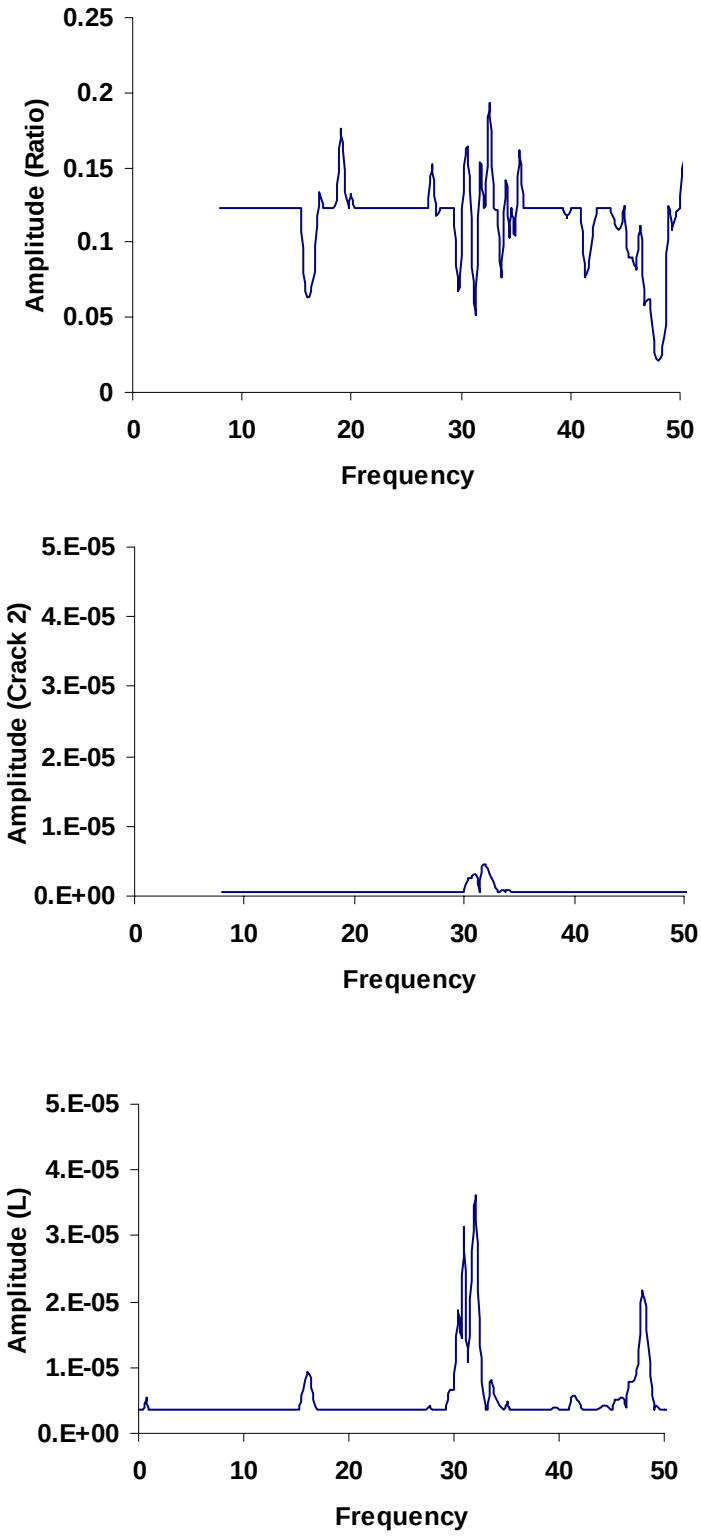

Figure 5.14 Frequency Fourier Transform histogram of Crack 2 displacement divided by longitudinal ground displacement ratio (top), measured Crack 2 displacement (middle), and calculated longitudinal ground displacement (bottom) for small vibratory roller event #3 on 8 November 2002

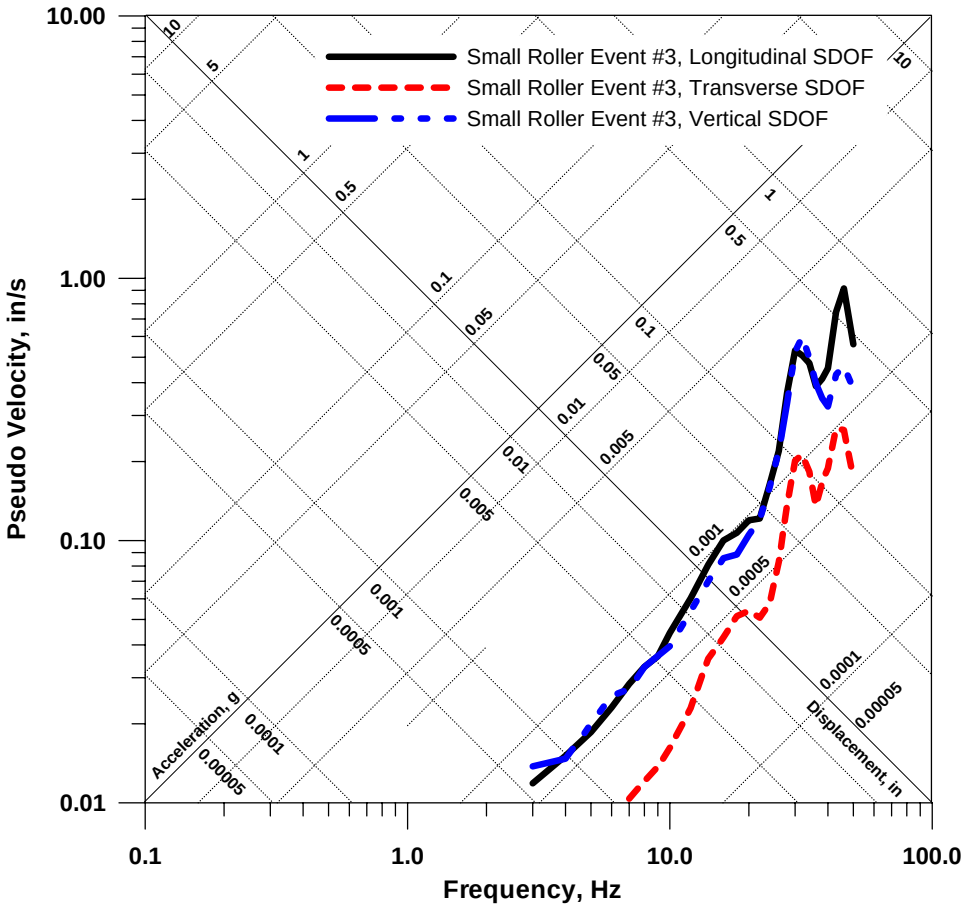

Figure 5.15 Longitudinal, transverse, and vertical single degree of freedom response spectra for small roller event #3 on 8 November 2002

Figure 5.16 presents response of internal Cracks 1 and 3 displacement, external Cracks 2 and 5 displacement and excitation ground motion time histories for the vibratory compaction of stone sub-grade in front of the house. Compaction of the sub-grade was conducted with the Ingersall-Rand (IR) Pro-Pack series SD115 soil compactor shown in Figure 4.5 (b). The top four time histories represent crack displacement time histories for the four cracks, and the bottom three show the corresponding excitation ground velocities. A 3-second waveform magnification of Crack 1, Crack 2, Crack 3, Crack 5 and tri-axial ground motion with the highest peak particle velocities presented in Figure 5.16 (a) are shown in Figure 5.16 (b). This event, and all sub-grade compaction monitoring, occurred the afternoon of 18 March 2003.

The events recorded from the IR soil compactor were conducted at distances of 8, 31, and 55 feet parallel to the house, and varied in exposure time. The peak particle

velocity for event 3 was 0.237 ips in the vertical direction, while the events varied in PPV from 0.039 to 0.456 ips. The largest PPV occurred in the longitudinal or vertical directions, and the lowest in the transverse direction. Crack displacements varied greatly, with Crack 2 responding the most. Crack 2 displacement for event 3 in Figure 5.16 (a) was 110μin, Crack 3 displacement was 40μin, and Crack 5 displacement 32μin. Crack 2 displacement for all the events varied from 25μin to 450μin. The largest response was produced by activity within 10 feet of the house and was the largest response produced by any construction activity.

These events consist of time histories recorded at two different frequencies (23.5 Hz and 32 Hz) and two "nominal amplitude", or centrifugal force levels. The frequency of vibration is controlled by a dial located next to the operator, and varies from approximately 18 to 32 Hz. The nominal amplitude adjustment is made via a switch, also located next to the operator, and has only two settings. Adjusting this setting will change the amount of energy released into the ground, and therefore allow the contractor to control the level of vibration and peak particle velocities in the vicinity of the house. Figure 5.17 shows the SDOF response spectra for this event. From the time history and response spectra the same 48 Hz overlying high-frequency pulse can be seen during the higher amplitude ground motions that was first presented under the small roller. When the ground motions are reduced, the high-frequency pulse again disappears. These frequency effects, and the large roller FFT, will be presented in further detail at the end of the chapter.

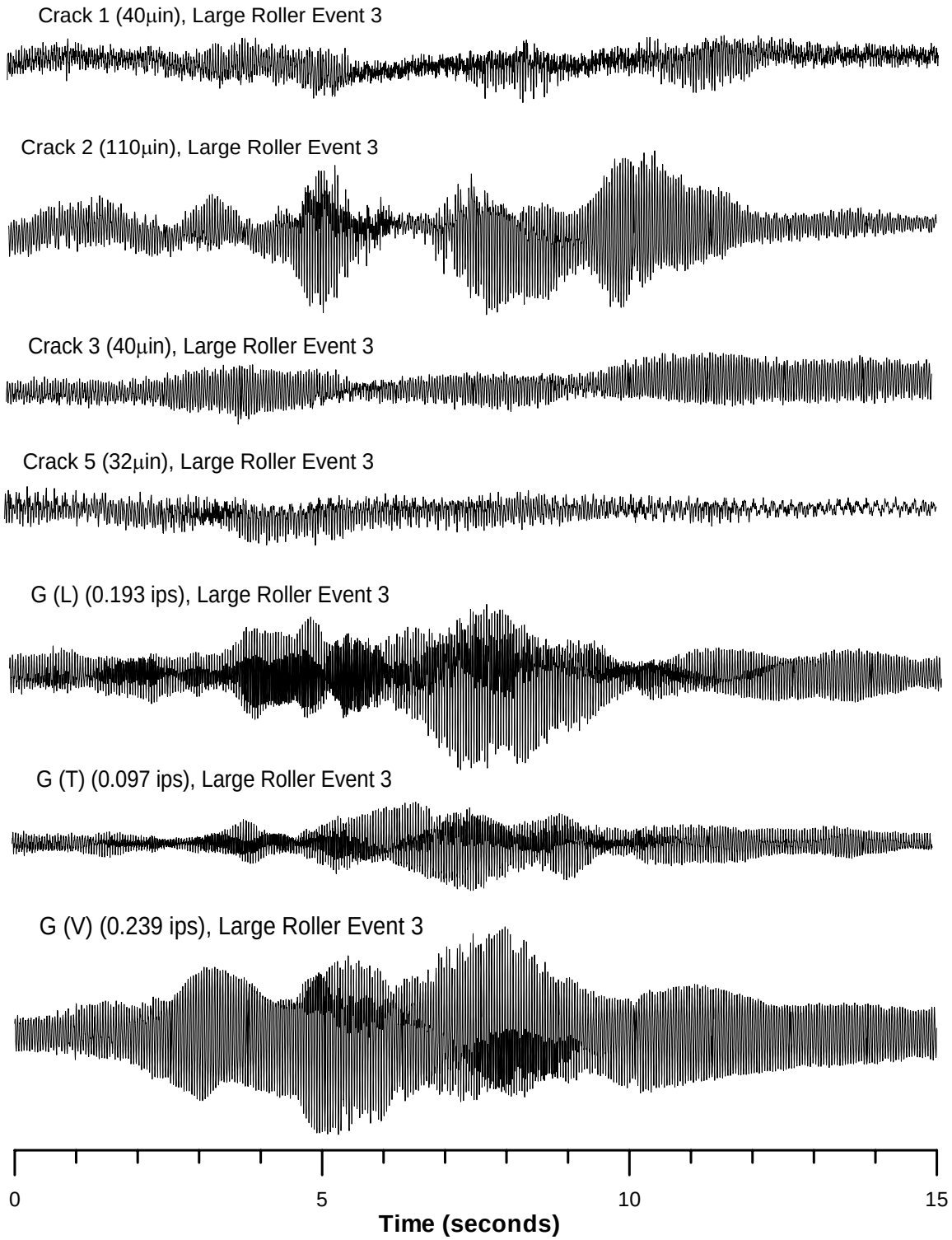

Figure 5.16 (a) Time histories of Crack 1, Crack 2, Crack 3 and Crack 5 from granular sub-grade large single-drum roller compaction Event #3 on 18 March 2003 compared to longitudinal, transverse and vertical ground excitation

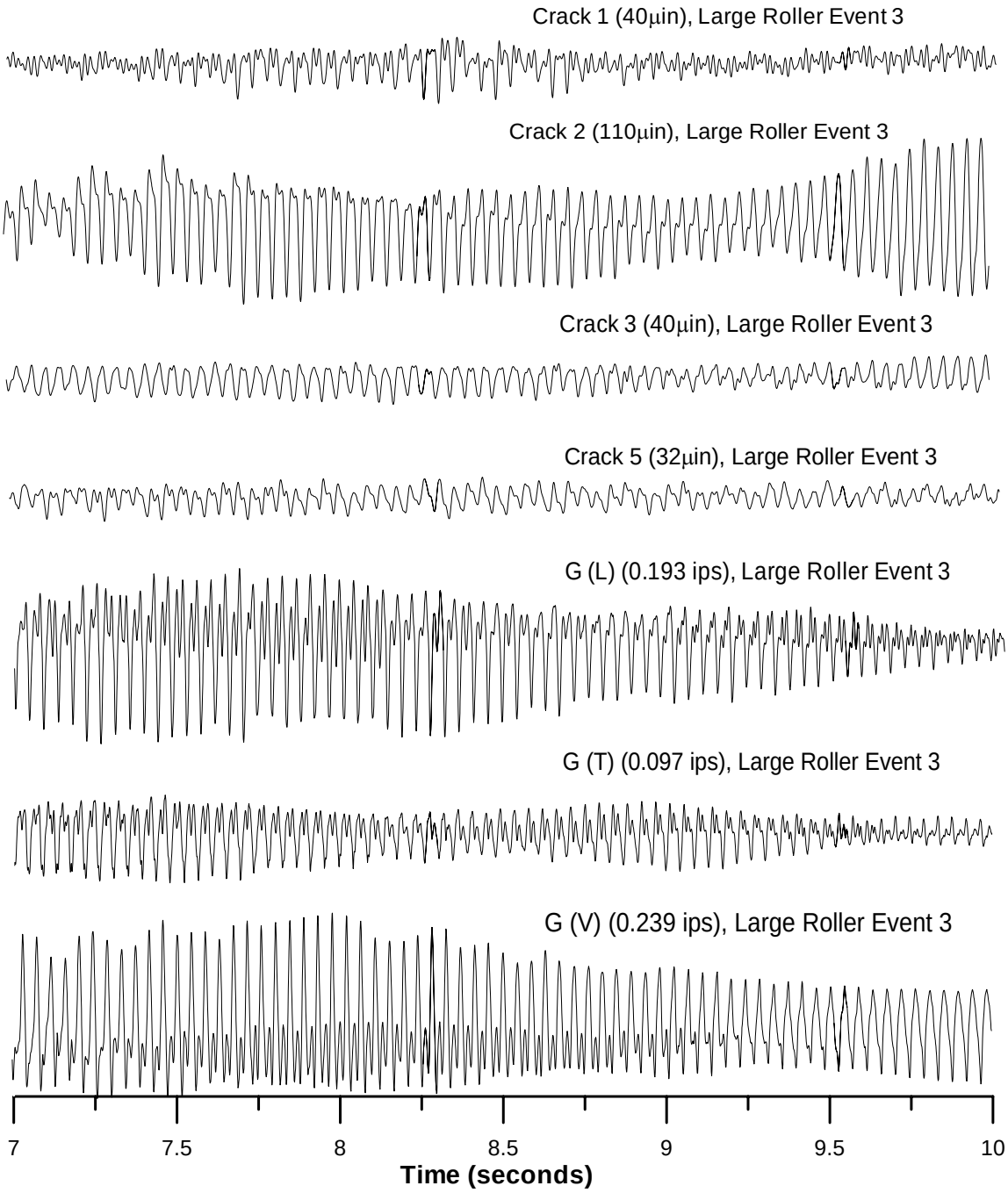

Figure 5.16 (b) 3-second magnification of granular sub-grade large vibratory single-drum roller compaction event 3 time histories showing Crack 1, Crack 2, Crack 3, Crack 5, longitudinal, transverse and vertical ground motion waveforms

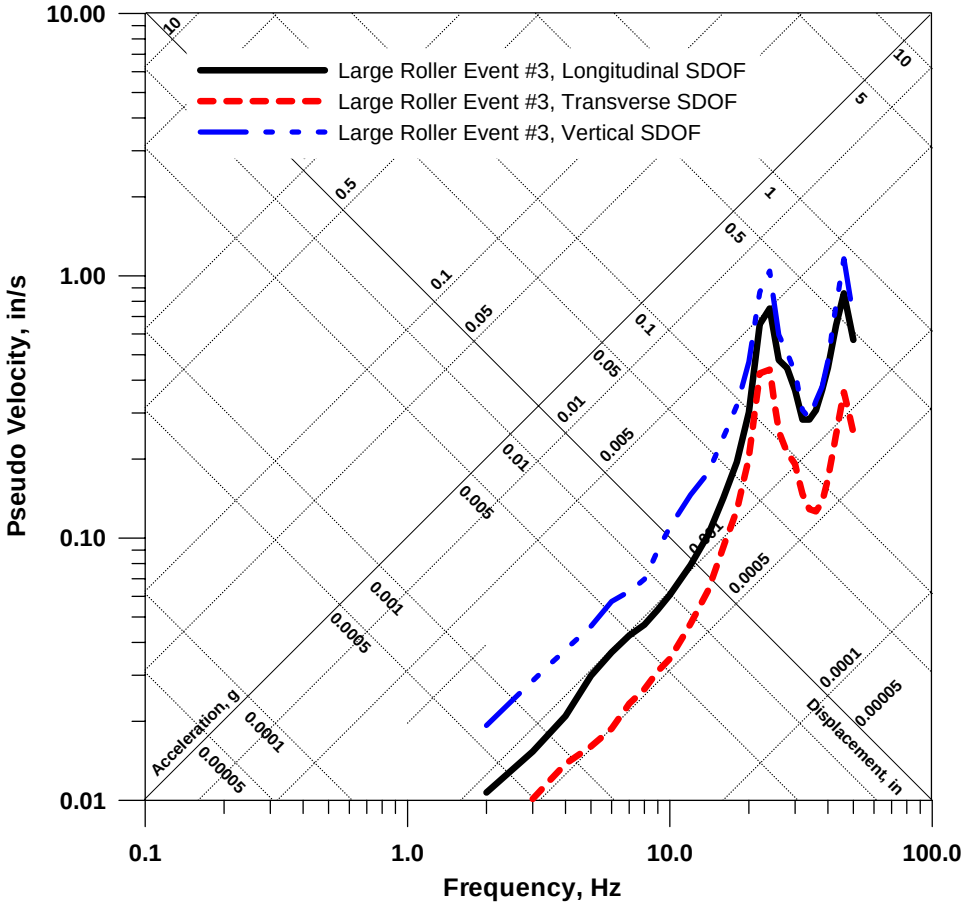

Figure 5.17 Longitudinal, transverse, and vertical single degree of freedom response spectra for large roller event #3 on 18 March 2003

Comparisons of Traditional Motion Controls with Measured Crack Displacements

Since measurement of crack displacement is a new approach to assessing the effect of construction vibrations, it is important to understand how the traditional controls of ground and structural motions correlate to crack displacement. To investigate the correlation, maximum measured response of Cracks 2, 3, and 5 produced by trackhoe, trencher and vibratory roller construction vibrations are compared in Figures 5.18, 5.19, and 5.20 to traditional ground motion controls of peak particle velocity, ground displacements via integrated velocity, and computed structure/wall displacement. Figure 5.18 shows trackhoe activity, 5.19 shows trencher activity, and 5.20 shows vibratory roller compaction from both machines. Displacement calculations for integration of velocities and single degree of freedom follow the methods outlined in Chapter 2. Crack 1 did not show enough consistent response outside the static noise level (≈10μin) after filtration to warrant correlation consideration. The geodynamic controls considered for correlation are those also traditionally employed in blasting studies.

As described in Chapter 2, analyzing SDOF response spectra of blast and construction induced ground excitations relative displacements of structures can be estimated at various dominant frequencies. Two approaches to comparing SDOF relative displacements to measured crack displacements are employed. The first approach is to find the relative displacement associated with the dominant frequency of the structure or wall, in this case approximately 20 Hz. Due to the fact that the dominant frequency is not universally 20 Hz, but tends to float about that value, the second approach is to take an average SDOF relative displacement between 18 and 22 Hz.

Correlation of crack response with ground motion is a function of crack location, planar direction and the machine creating the vibration. External Crack 2 and internal Crack 3 lie in the plane of longitudinal motion and External Crack 5 lies in the plane of transverse motion. Crack 2 was the most responsive to the trackhoe and vibratory roller motion, while Crack 5 was the most responsive to the trencher. Crack 3 was consistently the least responsive of all Cracks subject to correlation. Table 5.6 summarizes all correlation and regression coefficient data for peak particle velocity, integrated ground displacement and single degree of freedom correlations to Cracks 2, 3, and 5.

Trackhoe Correlations Crack #		R^2 by Peak Particle Velocity (in/sec)	R^2 by Relative Displacement of Structure Method		
			Integration of Velocities G_{max}	SDOF Method f_n = 20 Hz	SDOF Method f_n = 18-22 Hz
Crack 2	(L)	0.000	0.221	0.233	0.323
	(T)	0.033	0.233	0.497	0.698
	(V)	0.827	0.698	0.532	0.590
Crack 3	(L)	0.624	0.072	0.124	0.163
	(T)	0.005	0.124	0.247	0.257
	(V)	0.287	0.257	0.126	0.096
Crack 5	(L)	0.071	0.068	0.451	0.511
	(T)	0.078	0.451	0.834	0.793
	(V)	0.663	0.793	0.575	0.552

Trencher Correlations Crack #		R^2 by Peak Particle Velocity (in/sec)	R^2 by Relative Displacement of Structure Method		
			Integration of Velocities G_{max}	SDOF Method f_n = 20 Hz	SDOF Method f_n = 18-22 Hz
Crack 2	(L)	0.947	Negative	0.942	0.000
	(T)	Negative	0.964	0.063	0.090
	(V)	0.519	0.605	0.605	Negative
Crack 3	(L)	0.947	Negative	0.942	0.000
	(T)	Negative	0.964	0.063	0.090
	(V)	0.519	0.605	0.605	Negative
Crack 5	(L)	0.990	Negative	0.703	Negative
	(T)	Negative	0.980	0.000	0.000
	(V)	0.206	0.885	0.885	Negative

Roller Correlations Crack #		R^2 by Peak Particle Velocity (in/sec)	R^2 by Relative Displacement of Structure Method		
			Integration of Velocities G_{max}	SDOF Method f_n = 20 Hz	SDOF Method f_n = 18-22 Hz
Crack 2	(L)	0.920	0.960	0.820	0.720
	(T)	0.680	0.560	0.180	0.140
	(V)	0.910	0.770	0.770	0.310
Crack 3	(L)	0.940	0.960	0.930	0.880
	(T)	0.830	0.750	0.370	0.320
	(V)	0.970	0.890	0.890	0.480
Crack 5	(L)	0.920	0.950	0.720	0.610
	(T)	0.620	0.470	0.110	0.080
	(V)	0.870	0.690	0.690	0.210

Table 5.6 Summary of R^2 linear regression correlation coefficients of measured Crack 2, 3, and 5 displacement with directional peak particle velocity and computed relative displacement methods for all trackhoe, trencher and vibratory roller events

Figure 5.18 (a), (b), (c), and (d) show the trencher producing such small ground motions that correlations are nearly impossible with regard to the traditional controls. This lack of relationship is most likely the result of very low response from all the cracks. Response was generally so low as to be indistinguishable from the electronic noise. Displacements of Crack 3 are never significantly above the 10min noise level.

Correlations of Crack 2, 3, and 5 response to longitudinal, transverse, and vertical peak particle velocities, ground displacements, and SDOF relative displacements from trackhoe activities are presented as Figure 5.19 (a), (b), (c), and (d), but are not particularly strong. With the exception of Crack 3, all the best correlations (with respect to correlation coefficient, R^2 values) lie in the vertical direction. This unusual lack of correlation does not conform to results from typical blasting studies. Traditionally, crack response to blasting vibrations correlate best to ground and structural motions in the plane in which they lie. This does not necessarily imply that they respond with the largest crack displacements to these motions, but that there is typically a noticeable correlation between the two. This lack of correlation may also be the result of the low response, as was the case discussed above with the trencher.

Correlations of crack response to peak particle velocities, ground displacements and single degree of freedom calculations produced by trench backfill and roadway sub-grade vibratory roller compaction are presented in Figure 5.20 (a), (b), (c), and (d). Crack response was large enough to produce a wide range of response to variable excitation and thus meaningful correlations. All cracks responded best to peak particle velocities and displacements in the longitudinal direction, Crack 2 responded best to SDOF response in the transverse direction, and Cracks 3 and 5 best SDOF in the long direction. Vibratory compaction produced the largest overall and widest range of peak particle velocities, plus the most harmonious frequencies. The attenuation study presented in Chapter 4 reveals that peak particle velocities between 0.1 and 0.2 are expected when the small roller is operated at its 32 HZ low frequency at a distance of 40 feet.

Several of the time histories from the large roller compaction represent a “worst-case” scenario. For four of the events, the roller passed within 10 feet of the house, an atypically small separation between the roller and the house. These events made it

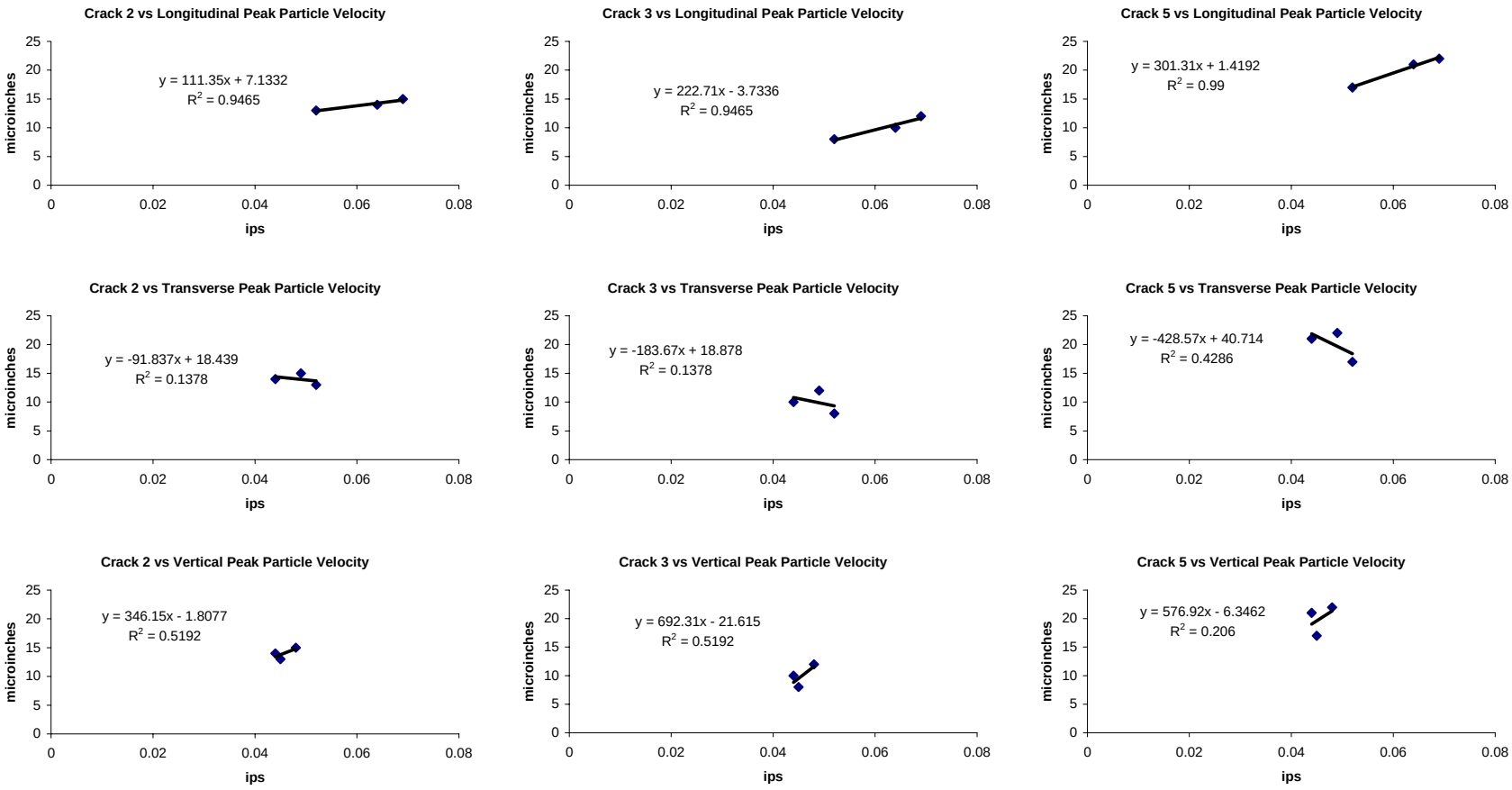

Figure 5.18 (a) Microinch crack 2, 3, and 5 displacement versus directional peak particle velocity correlations for trencher excavation events

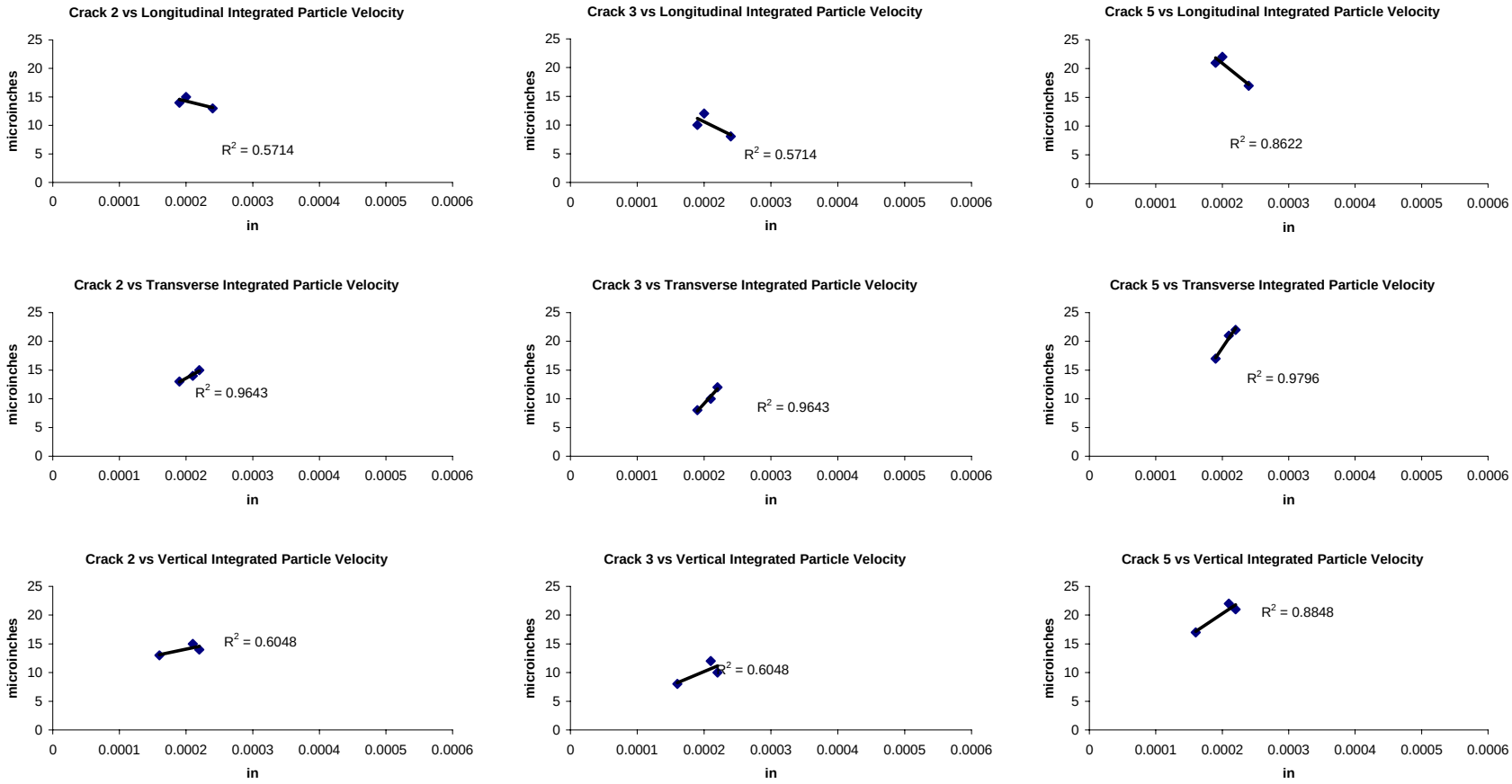

Figure 5.18 (b) Microinch crack 2, 3, and 5 displacement versus directional integrated particle velocity correlations for trencher excavation events

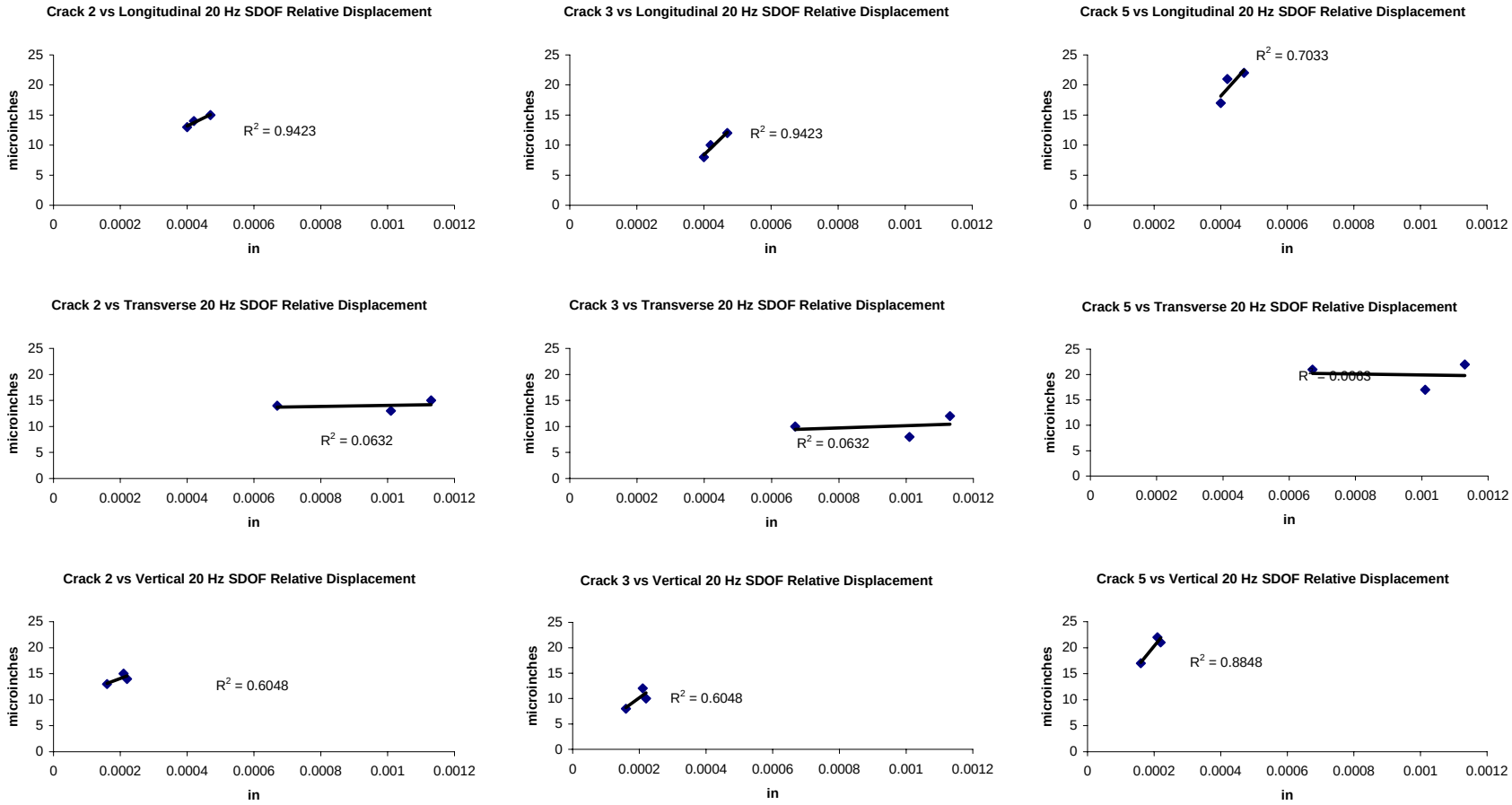

Figure 5.18 (c) Microinch crack 2, 3, and 5 displacement versus directional 20 Hz SDOF relative displacement correlations for trencher excavation events

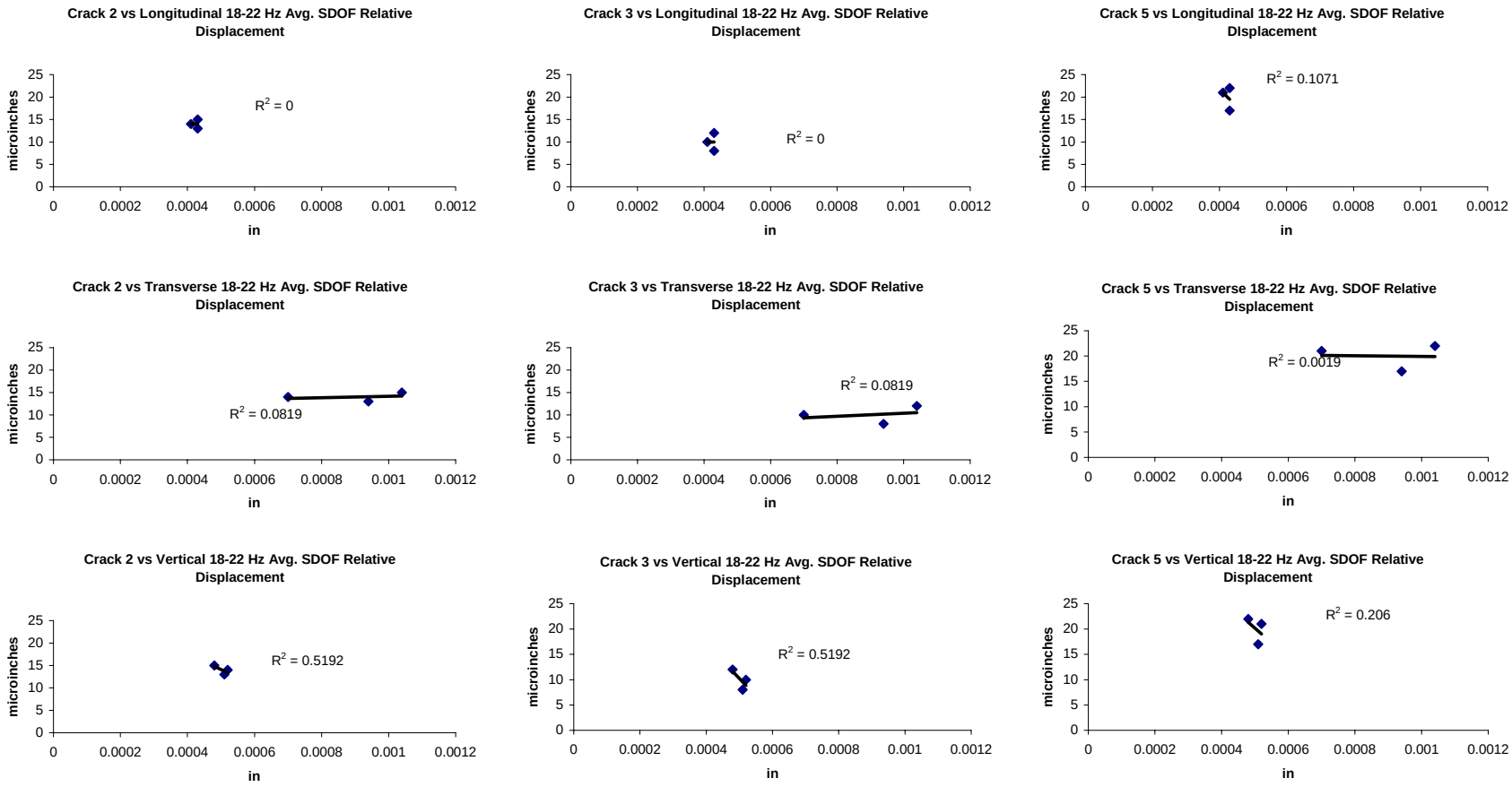

Figure 5.18 (d) Microinch crack 2, 3, and 5 displacement versus directional 18-22 Hz average SDOF relative displacement correlations for trencher excavation events

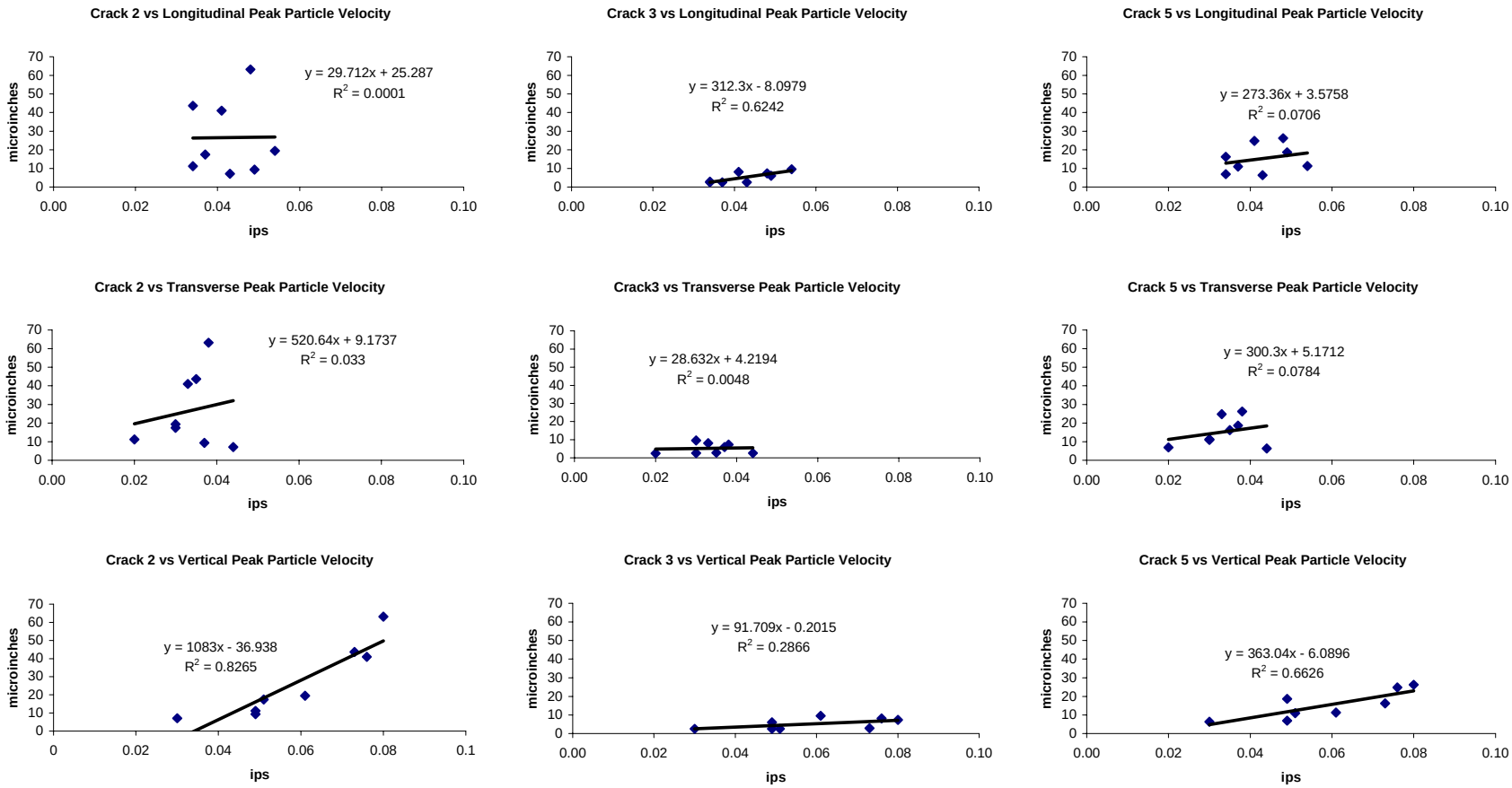

Figure 5.19 (a) Microinch crack 2, 3, and 5 displacement versus directional peak particle velocity correlations for trackhoe excavation events

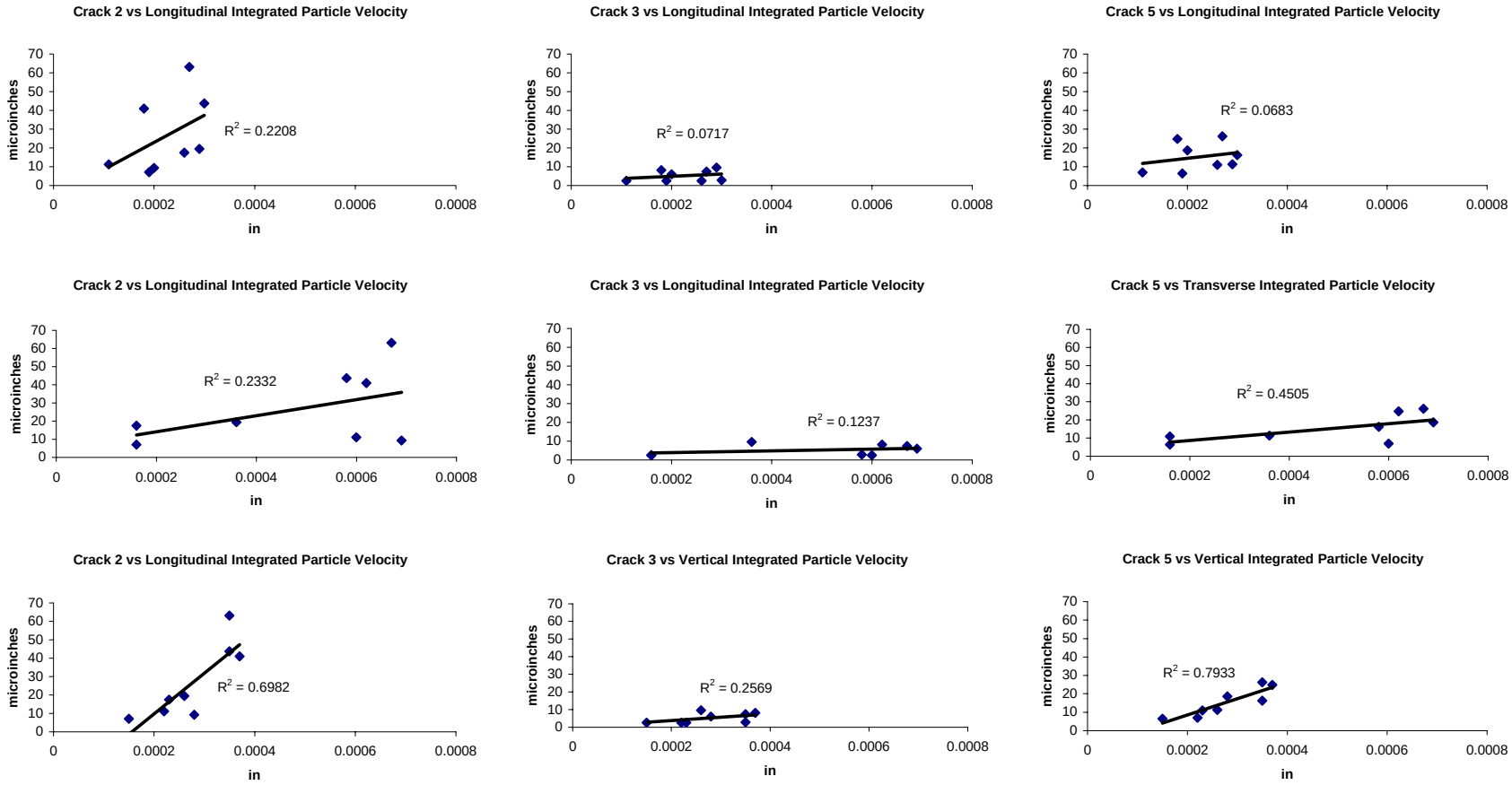

Figure 5.19 (b) Microinch crack 2, 3, and 5 displacement versus directional integrated particle velocity correlations for trackhoe excavation events

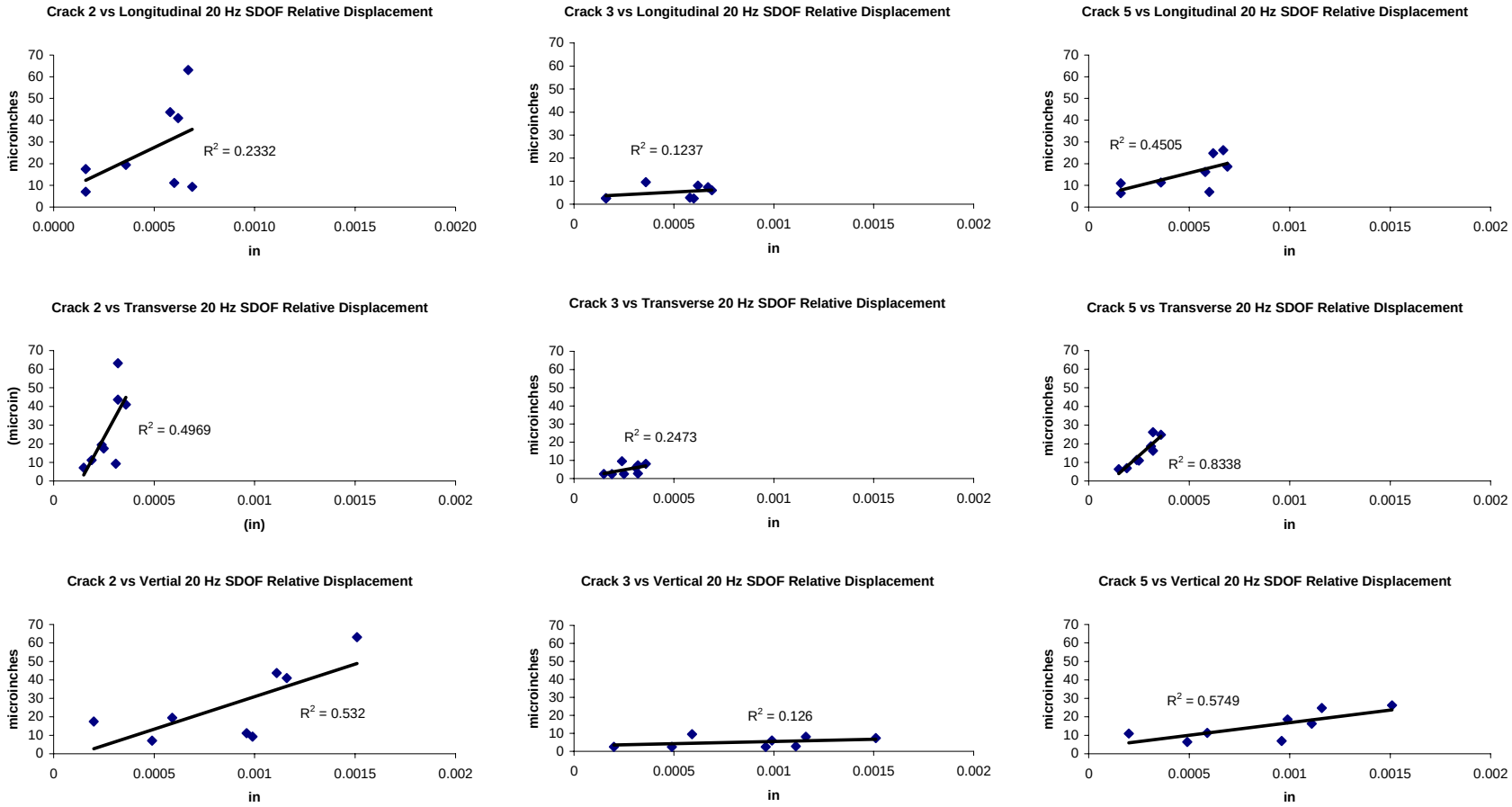

Figure 5.19 (c) Microinch crack 2, 3, and 5 displacement versus directional 20 Hz SDOF realtive displacement correlations for trackhoe excavation events

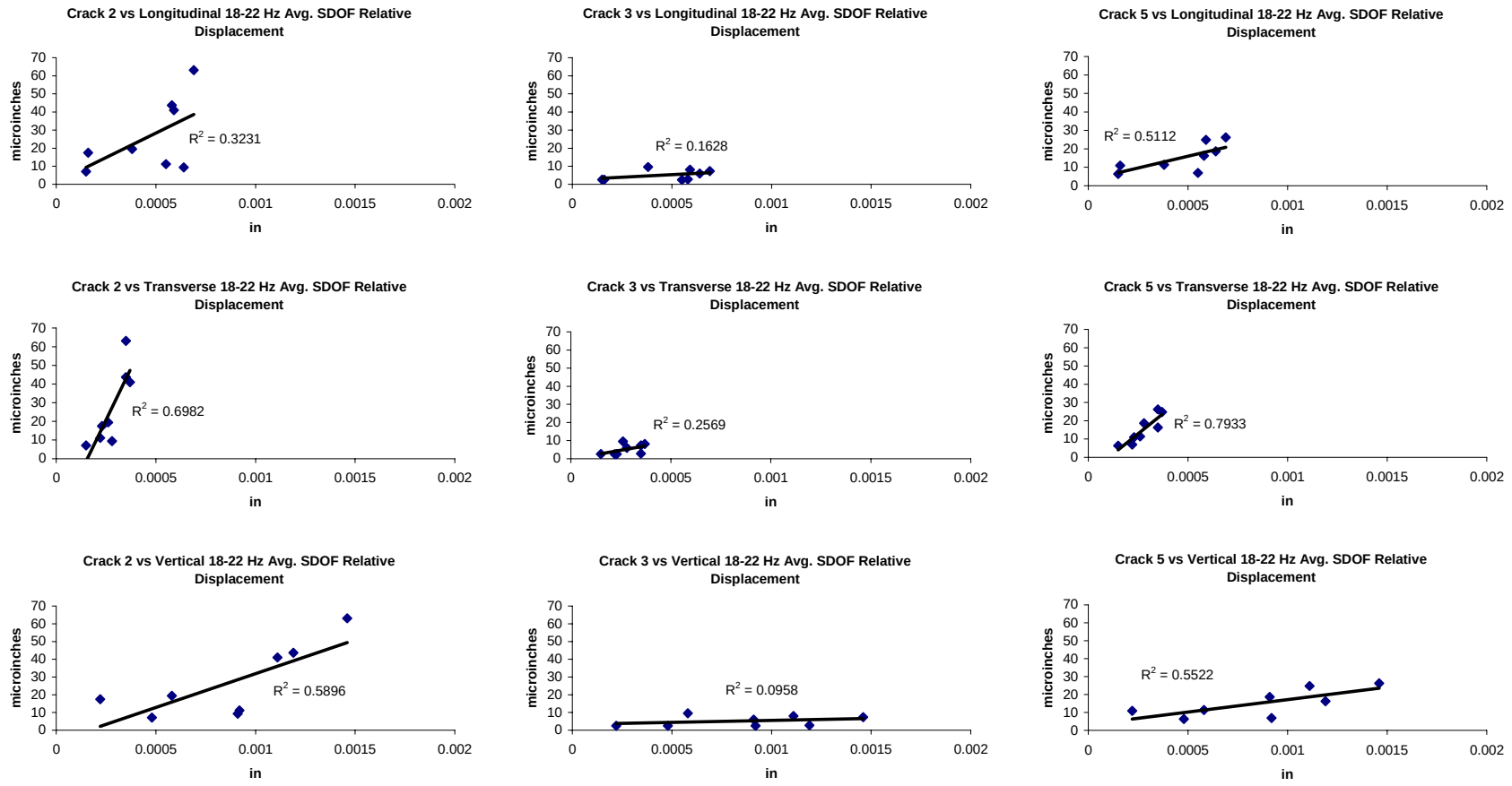

Figure 5.19 (d) Microinch crack 2, 3, and 5 displacement versus directional 18-22 Hz average SDOF relative displacement correlations for trackhoe excavation events

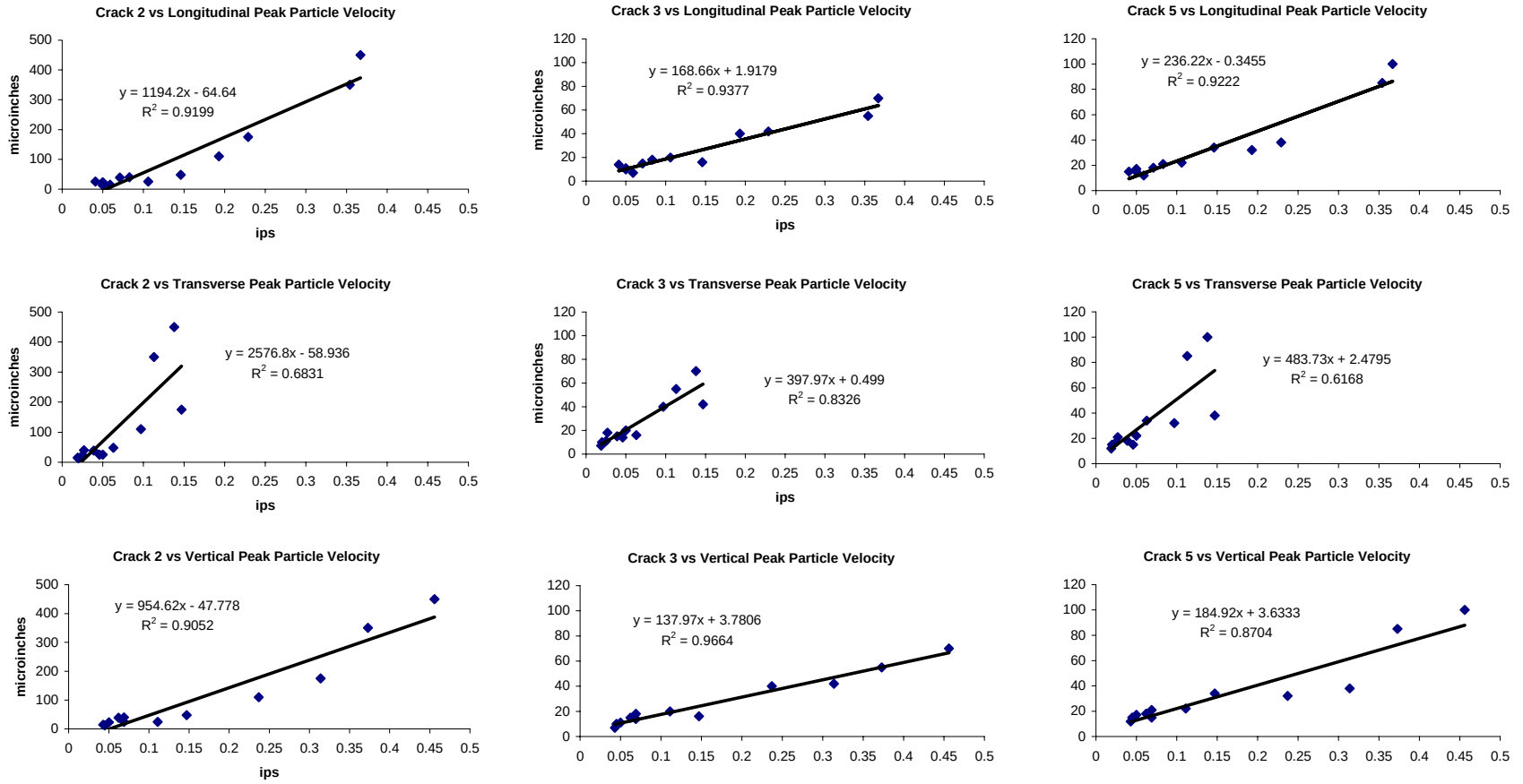

Figure 5.20 (a) Microinch crack 2, 3, and 5 displacement versus directional peak particle velocity correlations for vibratory roller compaction events

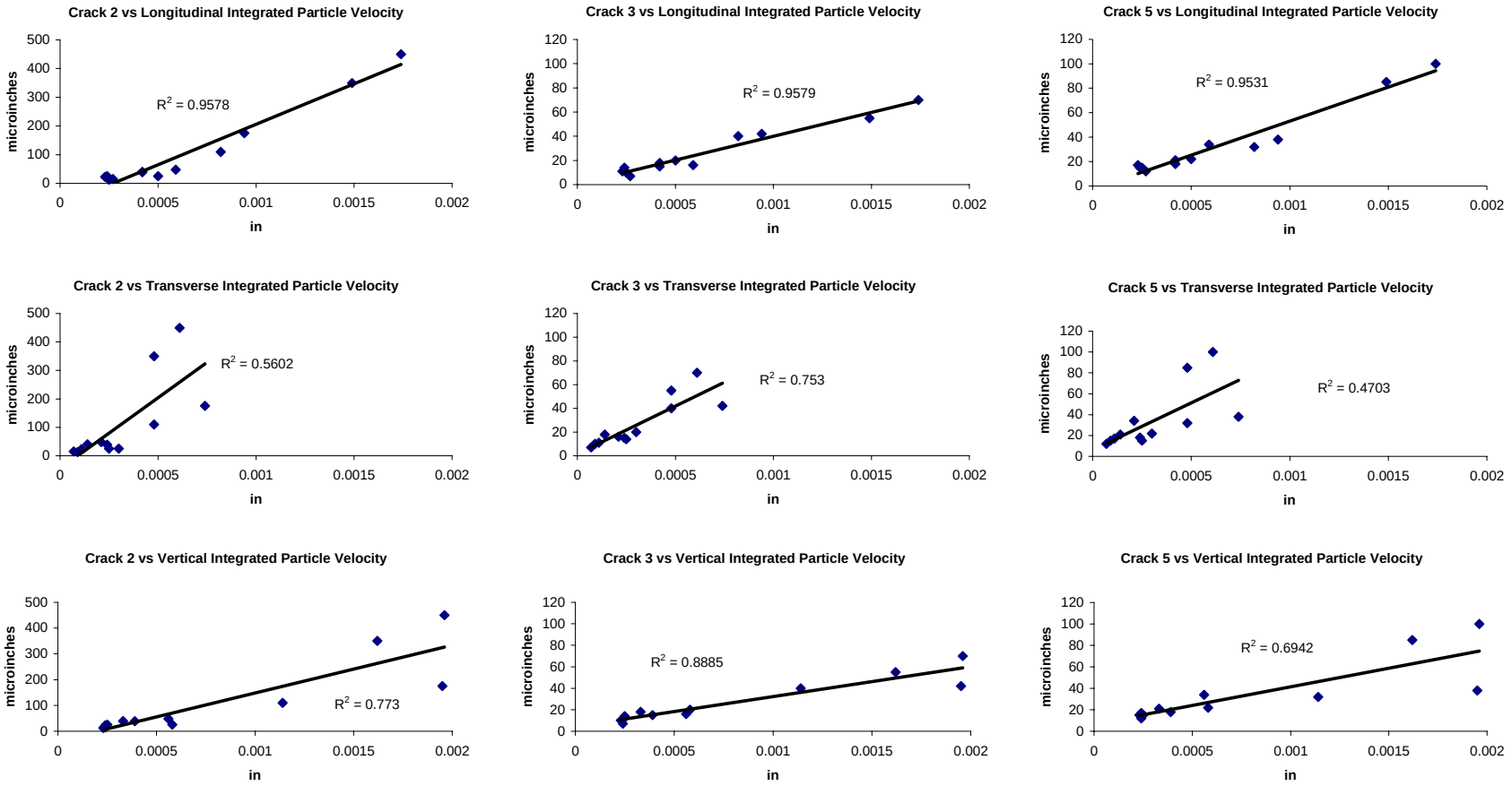

Figure 5.20 (b) Microinch crack 2, 3, and 5 displacement versus directional integrated particle velocity correlations for vibratory roller compaction events

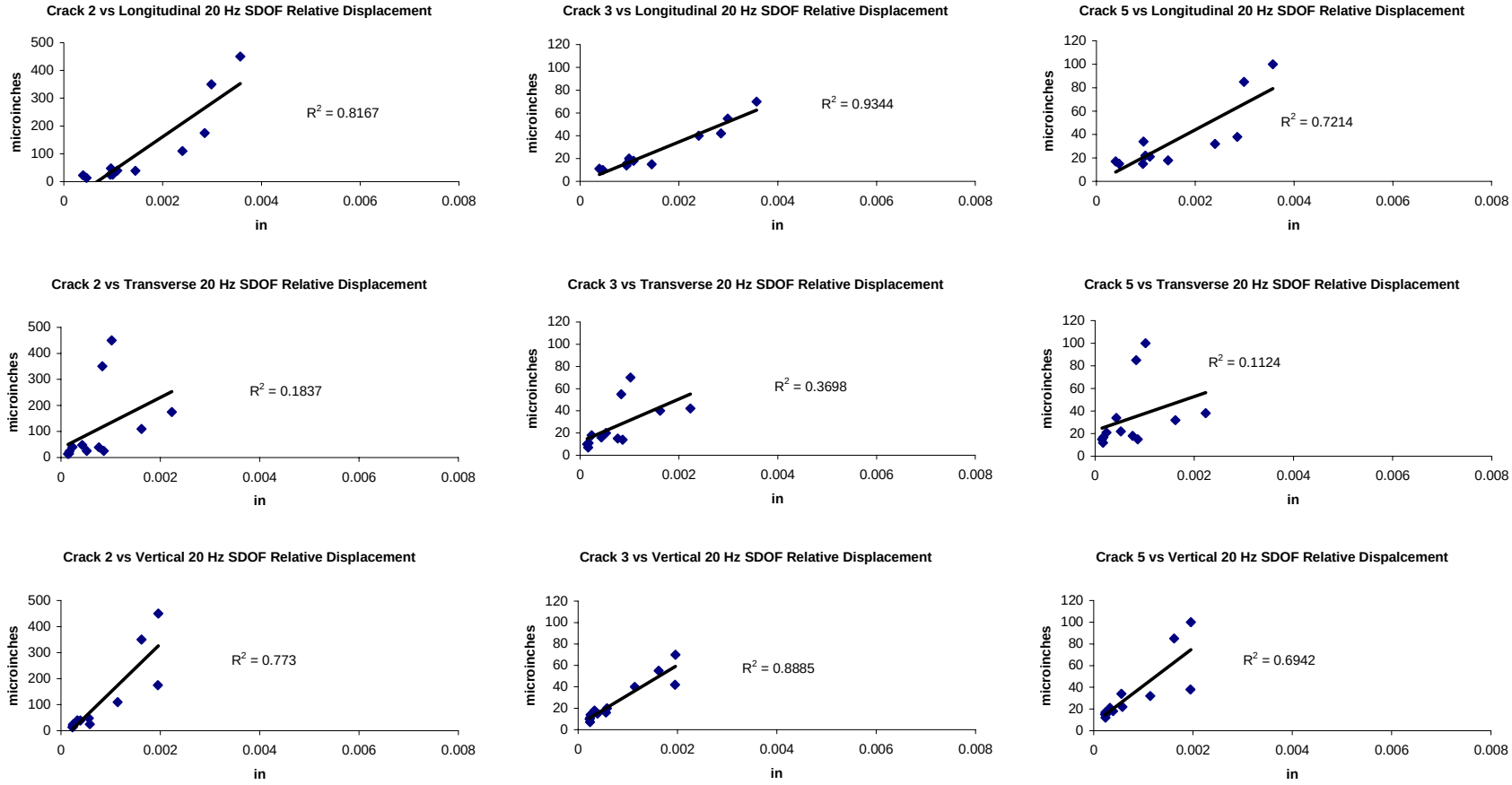

Figure 5.20 (c) Microinch crack 2, 3, and 5 displacement versus directional 20 Hz SDOF relative displacement correlations for vibratory roller compaction events

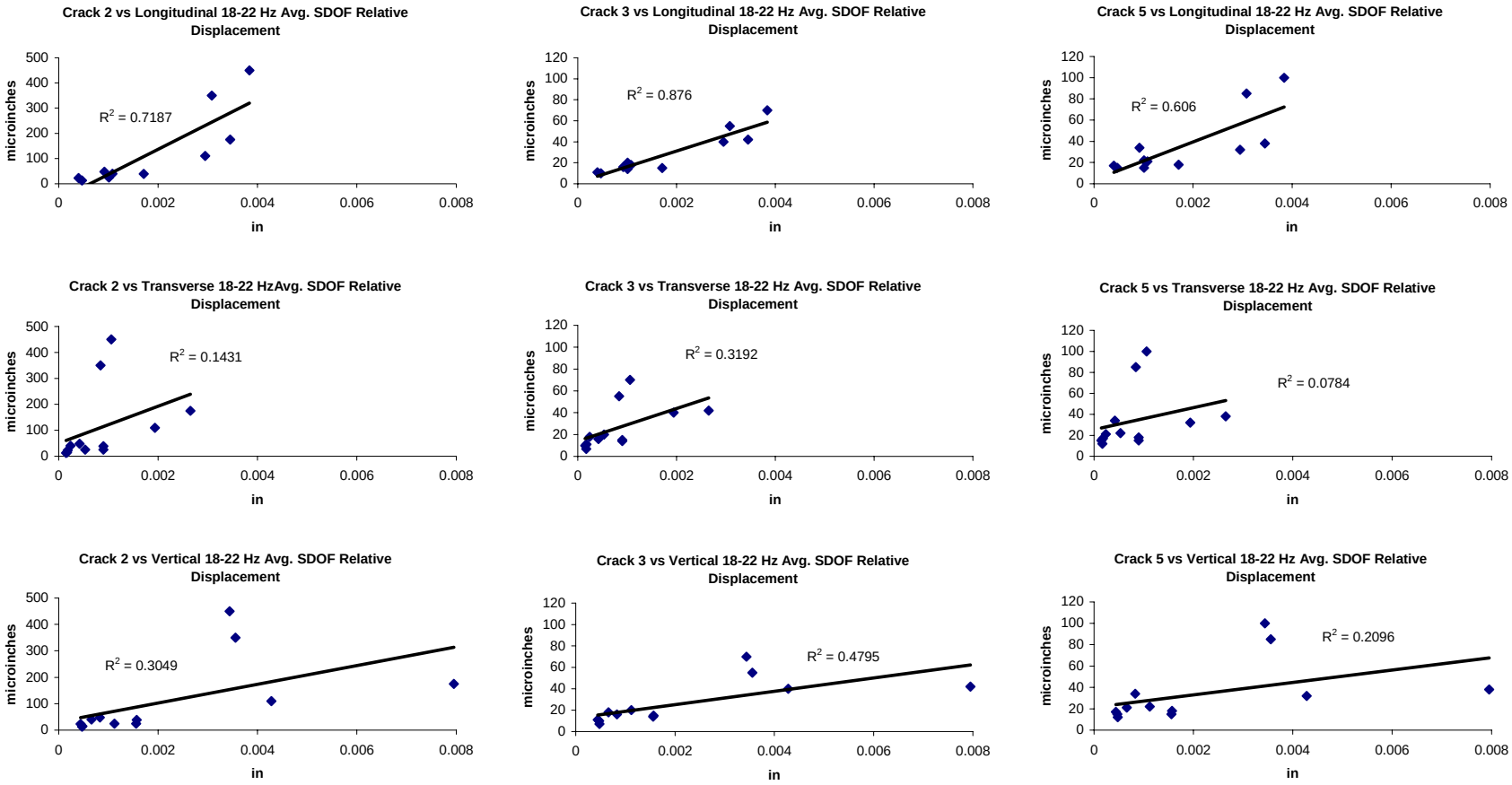

Figure 5.20 (d) Microinch crack 2, 3, and 5 displacement versus directional 18-22 Hz average SDOF relative displacement correlations for vibratory roller compaction events

possible to examine and correlate a broad and complete range of peak particle velocities, much like traditional blasting studies. These correlations over a wide range of excitation provide the best insight into the construction vibration sensitivity of the cracks.

An important issue presented by vibratory compaction is the effect of excitation frequency on crack displacement, an issue discussed in Chapter 3 for blasting. 15-25 Hz is a common natural frequency for a structure wall, but only the large roller produced frequencies within this normal range. Events 1 through 4 were conducted at a frequency of approximately 23 Hz, while events 5 through 8 were at 32Hz. Regardless of the frequency associated with these eight roller events, Crack 2 response correlates best with peak particle velocity, seen in Figure 5.20 (a), regardless of excitation frequency.

Figure 5.21 shows longitudinal ground displacement, Crack 2 displacement, and Crack 2 divided by longitudinal ground displacement FFT spectra for large roller events 3 and 6, both recorded at the same distance (≈8ft). Despite the fact the wall should have only one response frequency, it responds most at the active vibration frequency whether it is 23 or 32 Hz. It is possible that there are two modes of response, one near 20 Hz and the other near 30 Hz. This possibility is supported by review of the FFT response associated with trackhoe event 2 in Figure 5.10, which shows amplified wall response at both 20 and 30 Hz.

To be discussed in Chapter 6, the local nature of close proximity construction vibrations may promote the component excitation and response over whole structure excitation and response. This local nature of excitation may contribute to the observation of possible dual roller response modes, such as those described above. Figure 5.22 (a) compares the single degree of freedom response spectra for large roller events 2 and 7 (low amplitude excitation), while Figure 5.22 (b) compares events 3 and 6 (high amplitude excitation).

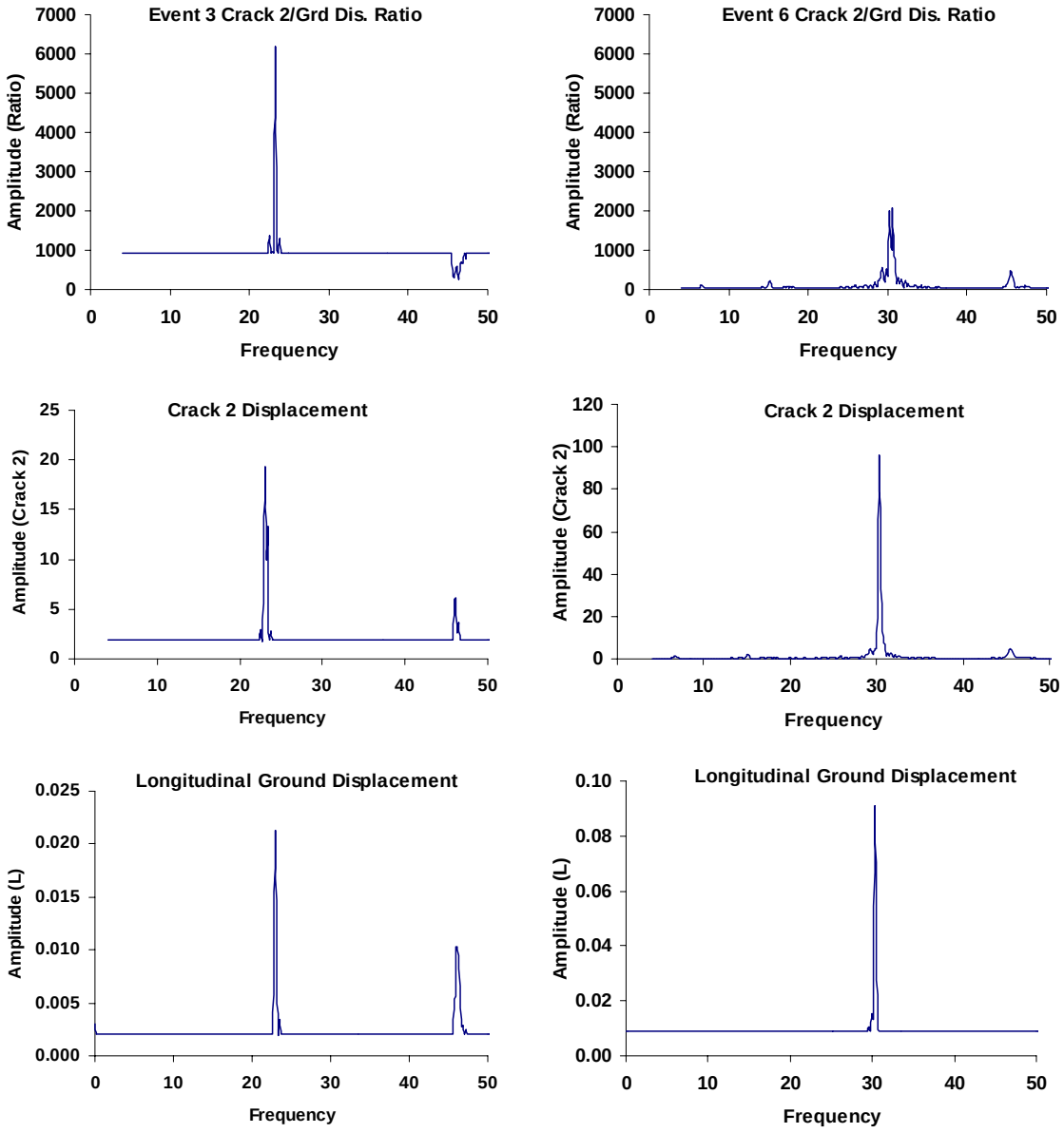

Figure 5.21 Frequency Fourier Transform histogram of Crack 2 displacement divided by longitudinal ground displacement ratio (top), measured Crack 2 displacement (middle), and calculated longitudinal ground displacement (bottom) for large vibratory roller events #3 (left) and #6 (right) on 8 November 2002

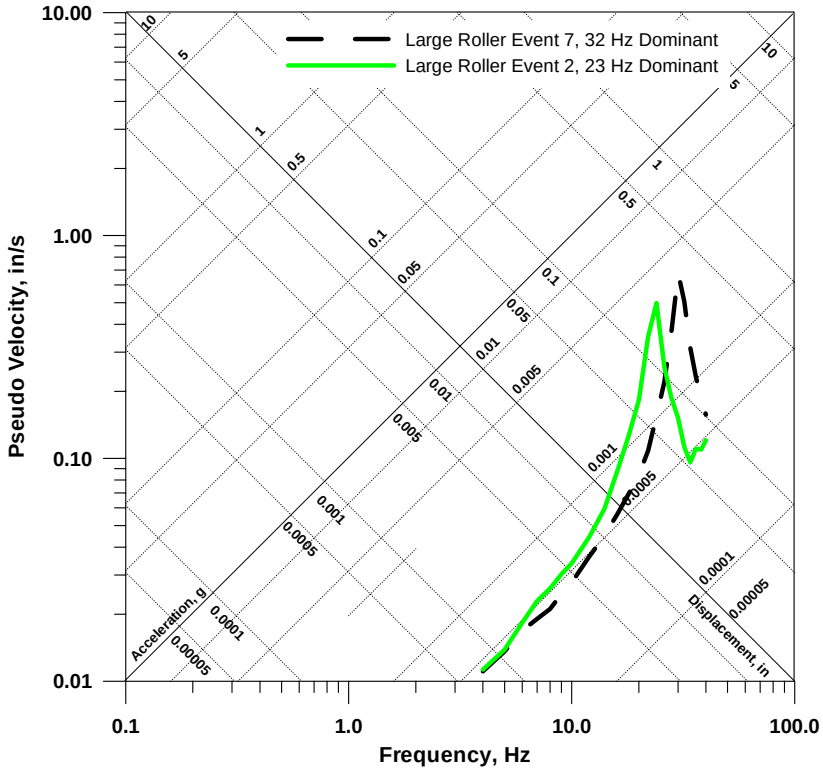

Figure 5.22 (a) Longitudinal single degree of freedom response spectra for large roller events #2 and #7 (low amplitude)

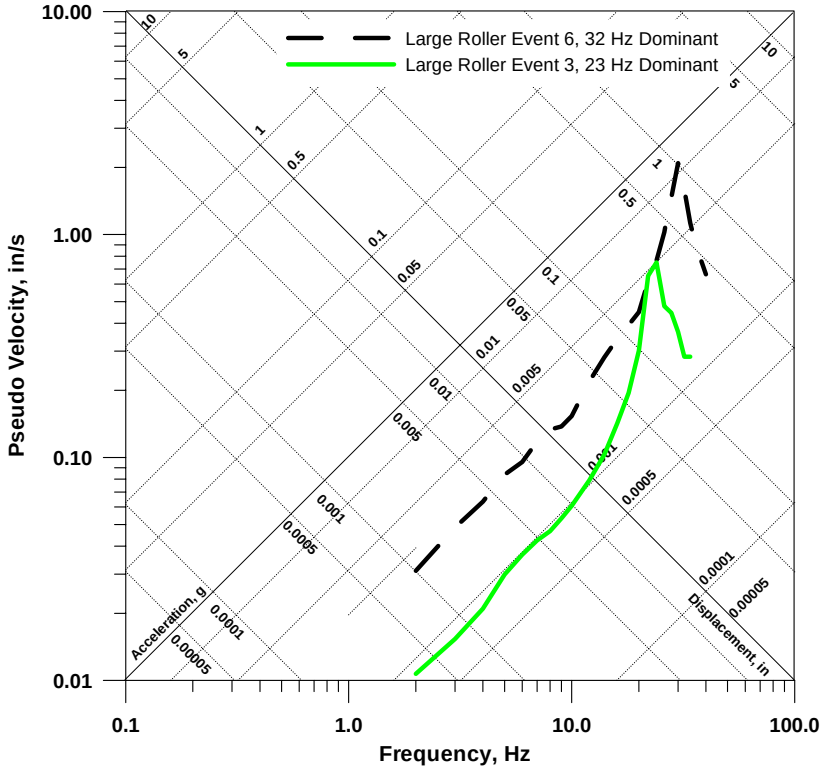

Figure 5.22 (b) Longitudinal single degree of freedom response spectra for large roller events #3 and #6 (high amplitude)

Chapter 6

Comparison of Crack Displacements Resulting from On-Site Blasting Vibrations and On-Site Construction Vibrations

Introduction

This chapter compares the effects of blasting in the Connecticut aggregate quarry in Chapters 2 and 3 with the construction activities in North Las Vegas, Nevada from Chapters 4 and 5. Comparisons are made with descriptors that are employed across disciplinary boundaries to define the effects of excitation ground motions near structures and homes. These descriptors are based upon the concepts of geo and structural dynamics as applied to situations involving blasting, construction or earthquake induced ground motions in order to predict structural response.

The descriptors of ground excitation waveforms that have been shown to have a significant impact on overlying structures are amplitude, number of principal pulses, frequency (or period) and wavelength. Non-waveform specific, but equally important factors, are absolute distance from the energy source and dynamic properties of the structure itself, such as damping and natural frequency (Dowding, 1996). Each of these properties and factors is associated with a particular analysis tool which will be employed for the purposes of comparison. The effect of time histories is compared by examining the peak amplitude (particle velocity), the number of "significant peaks", and the length of the "significant waveform" within the time history. Frequency effects are shown

through calculation of single degree of freedom (SDOF) response spectra, and wavelengths are calculated from peak waveform frequencies and a general knowledge of the surrounding soil/rock medium. Plane-wave theory is employed to show non-uniform arrival at structures and explore the effects of absolute distance. Finally, structural "sensitivity" will be established by determining a relationship between crack displacements and weather-induced displacements.

Time Histories

Five different construction activities will be evaluated: quarry blasting, trackhoe and trencher excavation, and two types of vibratory compaction. The differences between excitation vibrations caused by blasting and construction, as well as those between the construction equipment itself are all significant. The time histories chosen for analysis are those that produced substantial, if not the highest, ground motions. Time histories (introduced in previous chapters) to be discussed are:

- Blast Event 15, PPV=0.345 ips
- Trackhoe Event #2, PPV=0.08 ips
- Trencher Event #2, PPV=0.069 ips
- Small Roller Event #3, PPV=0.147 ips
- Large Roller Event #3, PPV=0.237 ips

Table 6.1 summarizes all the information pertinent to these events and the analysis to follow. Figure 6.1 compares time histories of crack displacement for Connecticut Cracks 1 and 3 and Crack 2 in Las Vegas resulting from blasting and the four construction induced vibrations respectively. Figures 6.2, 6.3, and 6.4 compare the longitudinal, transverse, and vertical components of ground motion. Crack 2 response was chosen for comparison, as it is consistently the most responsive of all the Las Vegas cracks.

Principal characteristics of the construction time histories shown in Figures 6.2-4 are summarized in Table 6.1. These are peak particle velocity, number of significant peaks, length of significant excitation, dominant frequency and wavelength. "Significant peak" is defined as any zero-to-peak value in a velocity time history that exceeds 75% of the peak particle velocity. "Significant excitation" is defined as the time during which velocity peaks exceed 50% of the control, or peak particle velocity (Dowding, 1996).

Furthermore, pulses and waveforms are only quantified by the positive or negative, zero-to-peak side of the time history that contains the overall peak. For instance, blast 15 had 7 significant pulses and a 0.62 second excitation. Trackhoe event 2 had 2 significant pulses with a significant excitation of 0.14 seconds. Trencher event 2 produced only 1 significant peak, with a very short 0.08 second excitation. The two roller events caused the most sustained vibration. Small roller event 3 contained 10 significant pulses with a 2.7 second excitation, and large roller event 3 contained 35 significant pulses over 4.3 seconds of excitation.

While the parameters in Table 6.1 provide a means of quantitatively describing what is visually evident in Figures 6.2-6.4, they ultimately cannot be quantitatively combined to easily predict differences in response. The response spectrum can integrate all of these parameters because it employs the full waveform of the excitation. Thus the next two sections focus on a method to normalize the excitation, employment of the single degree of freedom response spectrum, and calculations and visualizations of wavelength to help demonstrate the differences in the structural response produced by these different forms of excitation.

Event	Peak Particle Velocity (ips)	75% Peak (ips)	# of Significant Peaks	50% Peak (ips)	Length of Significant Excitation (sec)	Peak SDOF Frequency (Hz)	Dominant FFT Frequency (Hz)	Wavelength (ft)	Crack Displacement '(#, Location)' (μin)
Blast 15	0.345	0.259	7	0.173	0.65	20	23	435	90 (3, Conn)
Trackhoe #2	0.080	0.060	2	0.040	0.14	25	22	182	63 (2, LV)
Trencher #2	0.069	0.052	1	0.035	0.08	70	54	74	15 (2, LV)
Small Roller #3	0.147	0.110	10	0.074	2.7	30	32	125	48 (2, LV)
Large Roller #3	0.237	0.178	23	0.119	4.50	24	24	167	110 (2, LV)

Table 6.1 Summary of information pertaining to time histories and waveforms, frequency response, and crack displacements

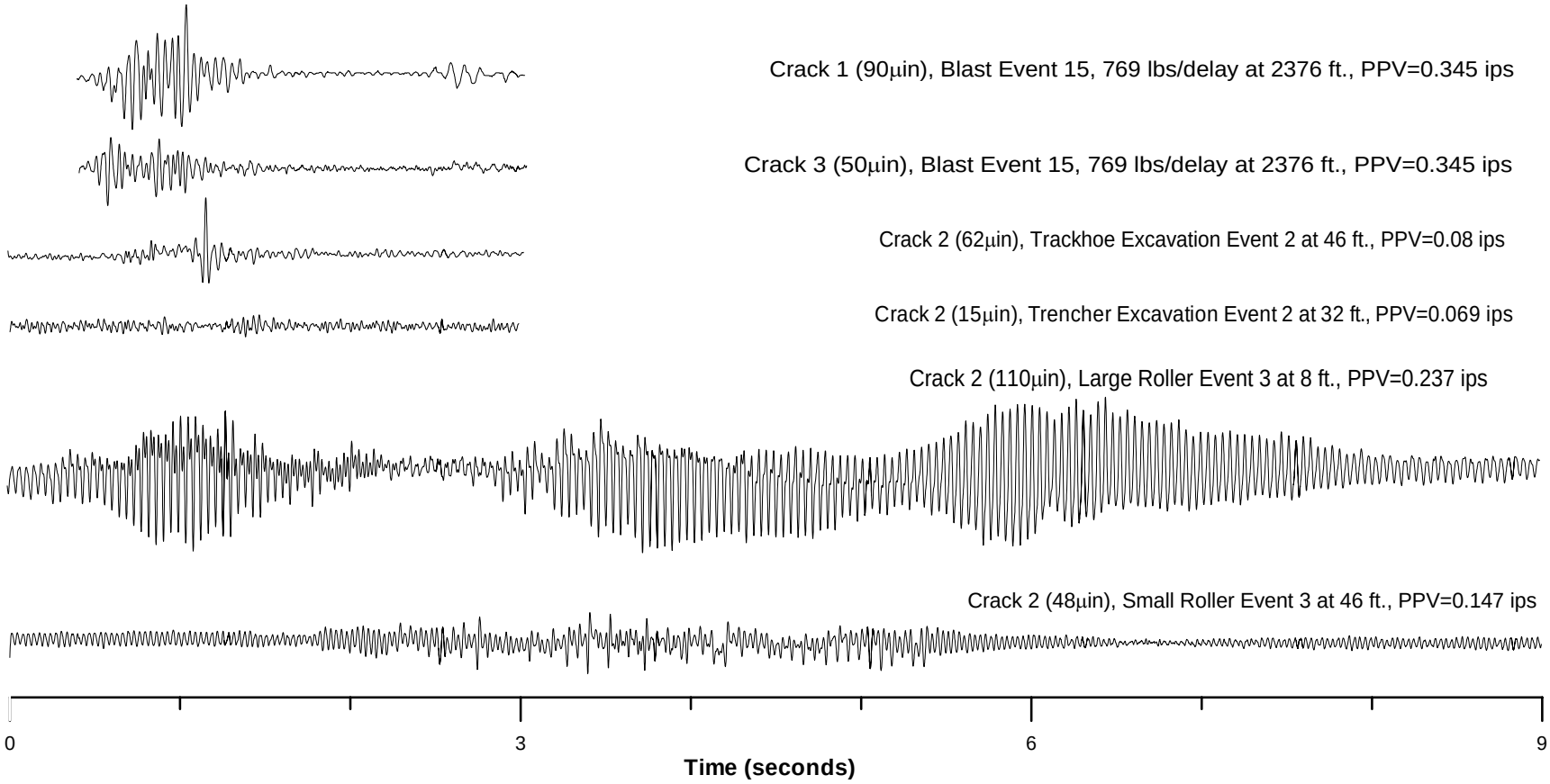

Figure 6.1 (a) Global time histories of Connecticut Crack 1 and 3 displacements from blast event 15 and Las Vegas Crack 2 displacement from trackhoe event 2, trencher event 2, small vibratory roller event 3 and large vibratory roller event 3

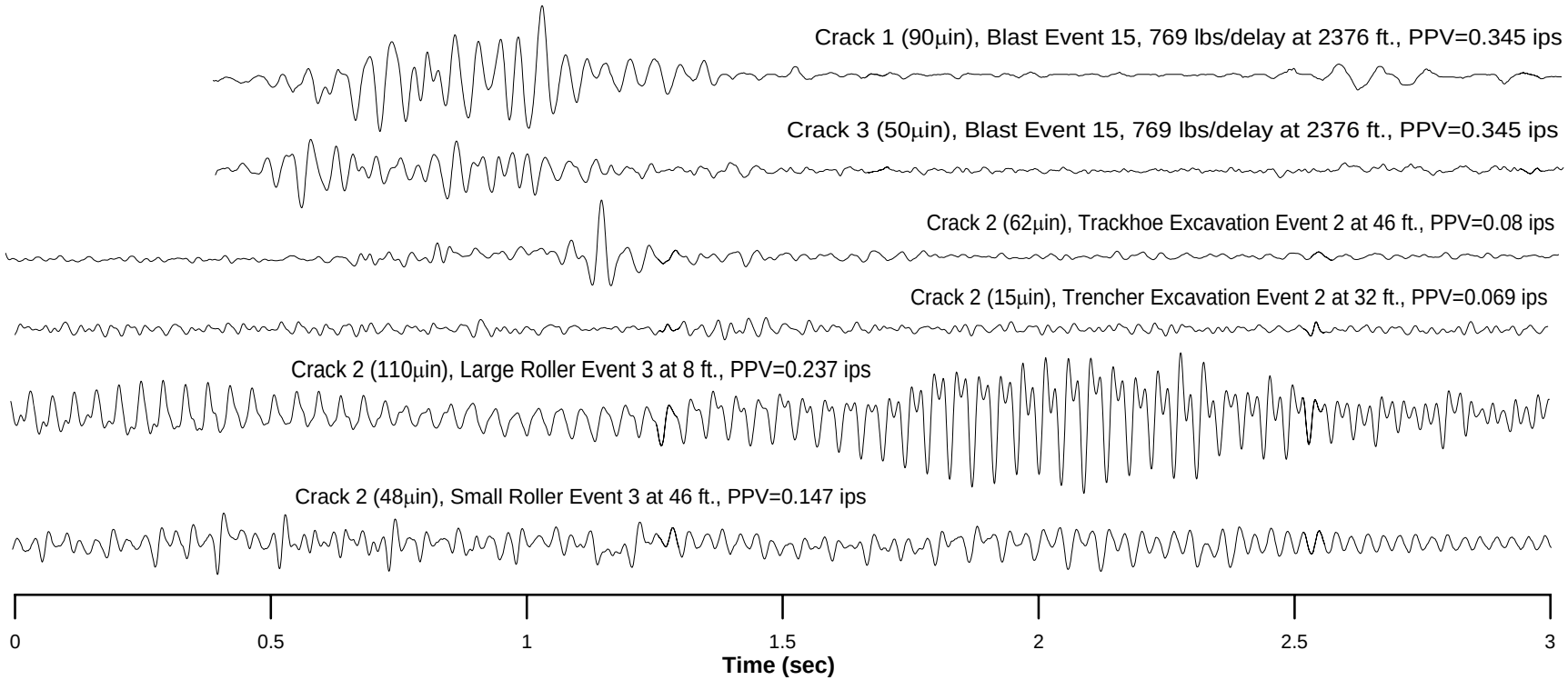

Figure 6.1 (b) 3-second time history magnification of Connecticut Crack 1 and 3 displacements from blast event 15 and Las Vegas Crack 2 displacement from trackhoe event 2, trencher event 2, small vibratory roller event 3 and large vibratory roller event 3, showing detail of waveforms

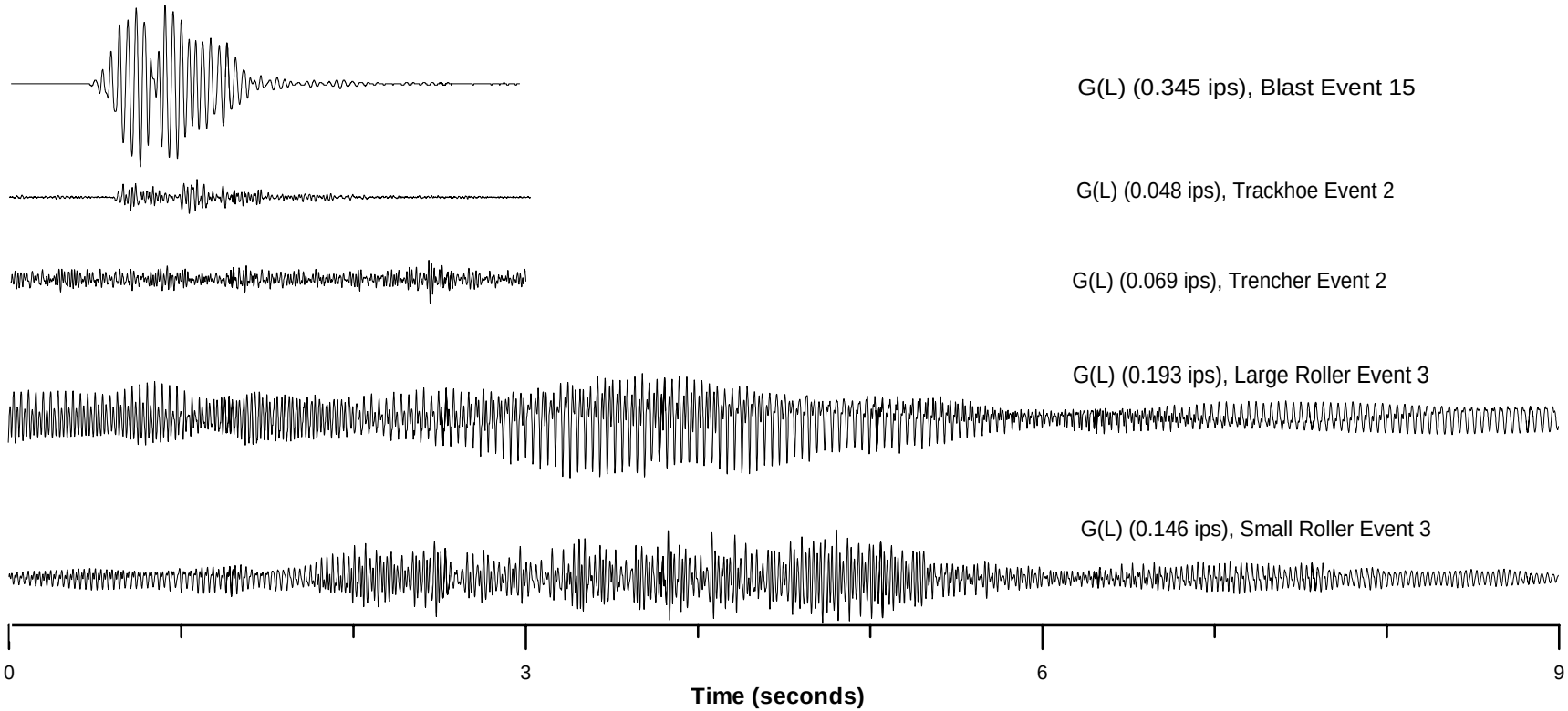

Figure 6.2 (a) Global time histories of longitudinal particle velocity from blast event 15 in Connecticut, and trackhoe event 2, trencher event 2, small vibratory roller event 3 and large vibratory roller event 3 in Las Vegas

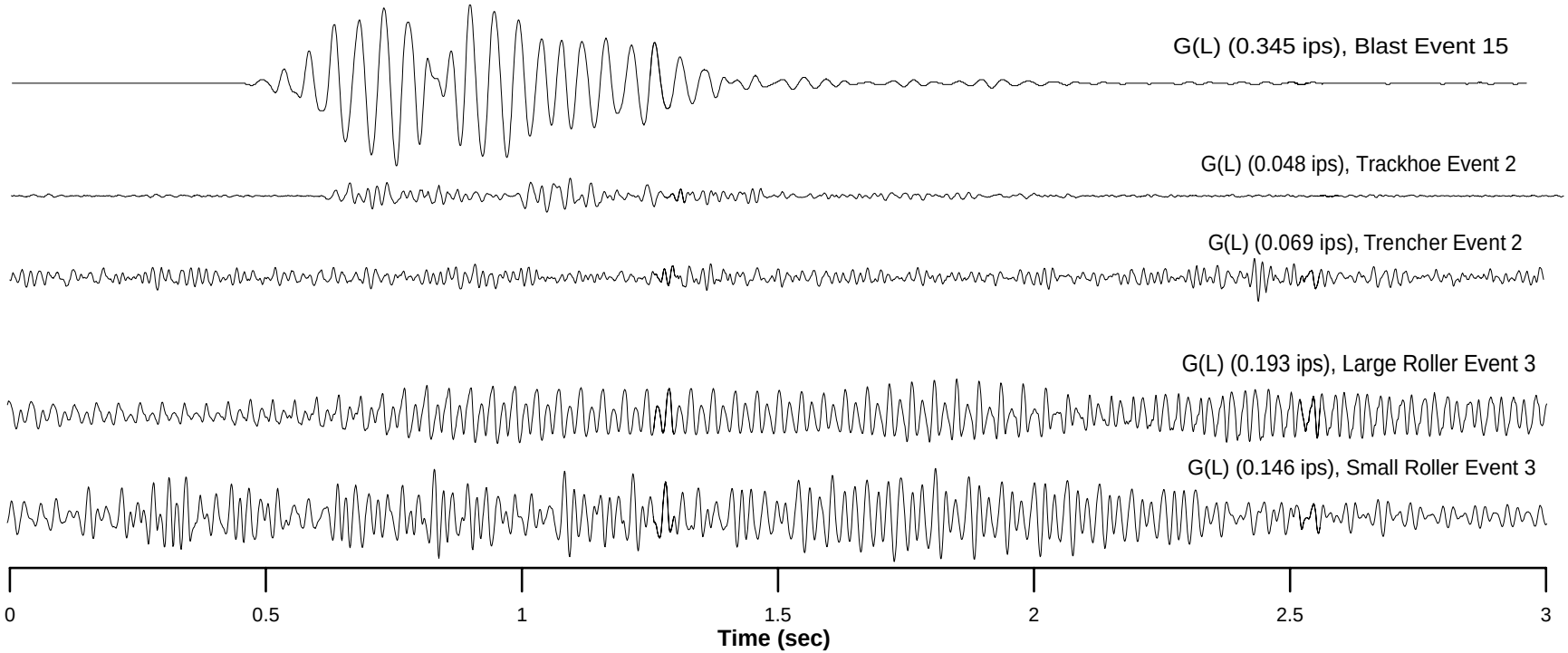

Figure 6.2 (b) 3-second time history magnification of longitudinal particle velocity from blast event 15 in Connecticut, and trackhoe event 2, trencher event 2, small vibratory roller event 3 and large vibratory roller event 3 in Las Vegas, showing detail of waveforms

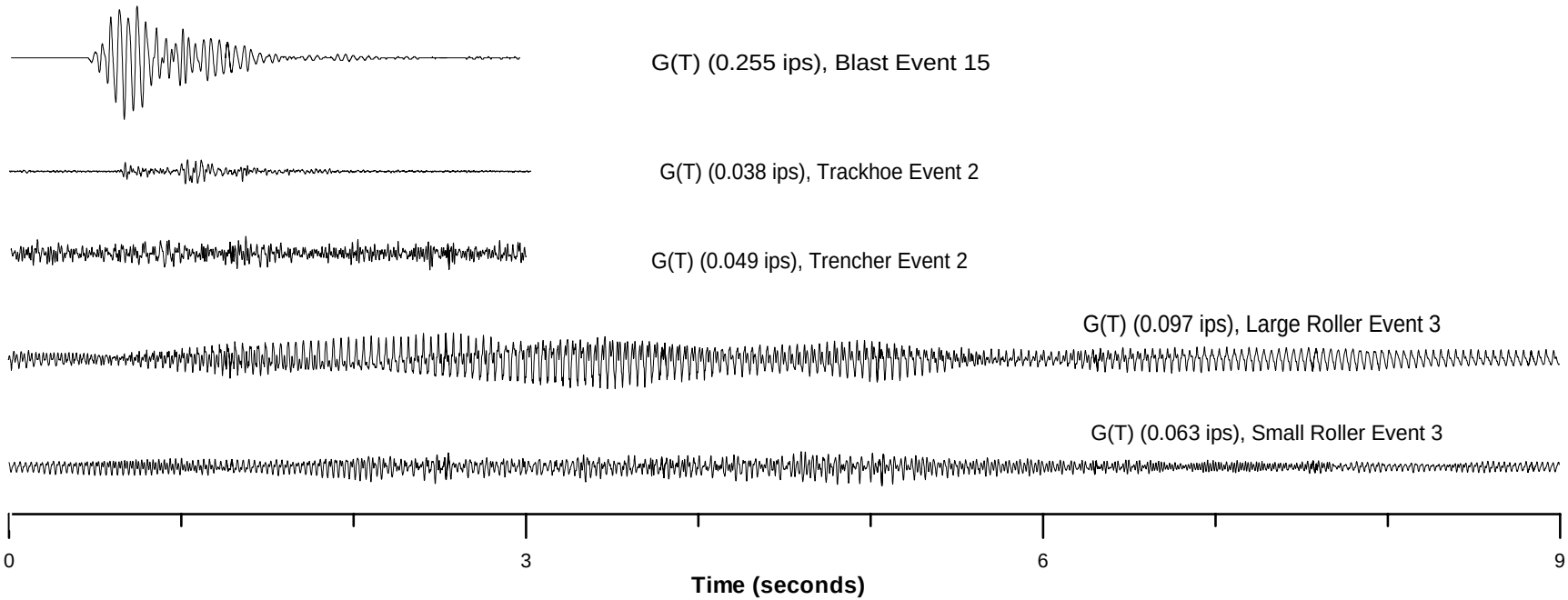

Figure 6.3 Time histories of transverse particle velocity from blast event 15 in Connecticut, and trackhoe event 2, trencher event 2, small vibratory roller event 3 and large vibratory roller event 3 in Las Vegas

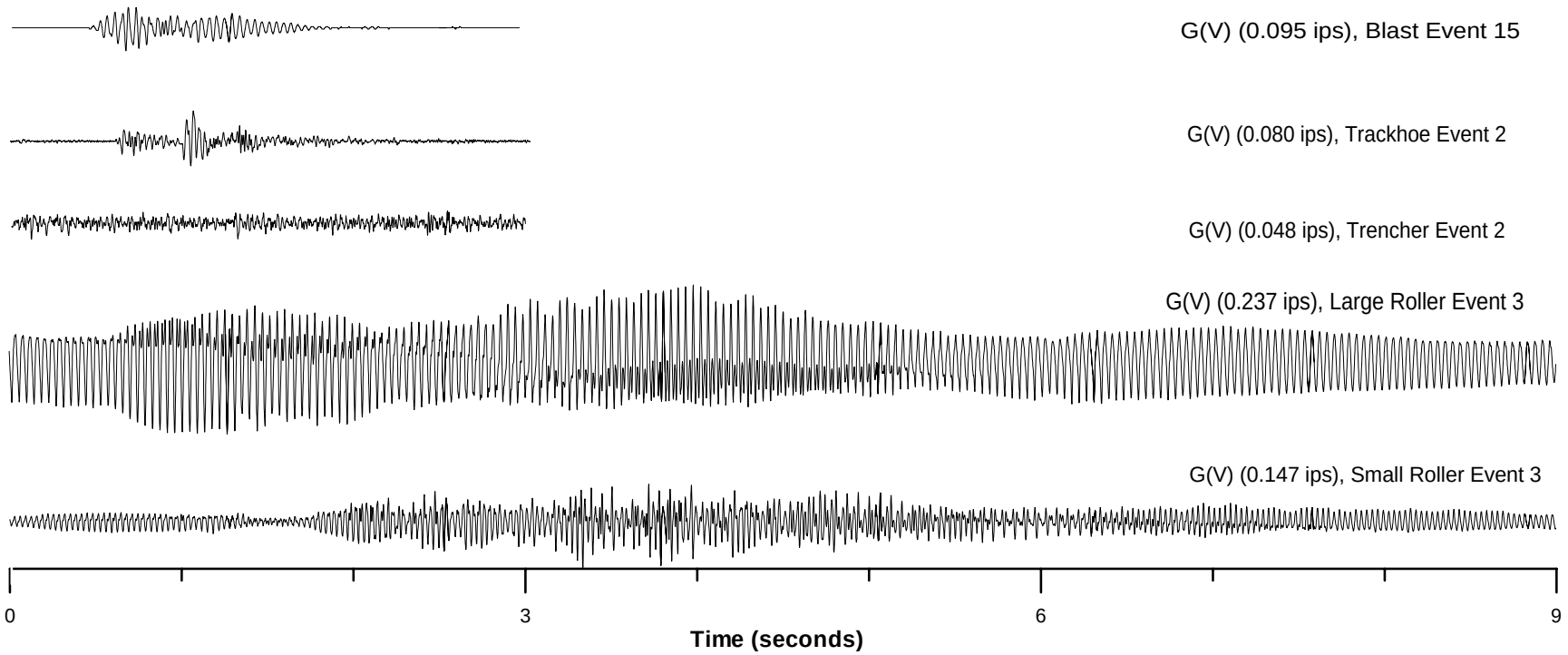

Figure 6.4 Time histories of vertical particle velocity from blast event 15 in Connecticut, and trackhoe event 2, trencher event 2, small vibratory roller event 3 and large vibratory roller event 3 in Las Vegas

Single Degree of Freedom Response Spectra

Since response spectrum techniques encompass the full waveform, they can be employed to visualize expected differences in response from the widely varying excitation and displacements. The critical response factor in predicting and quantifying the cracking potential of construction vibrations is discussed in terms of differential movements that occur between structural components. The importance and influence of ground vibration and natural structural frequencies on these differential movements has been studied and well documented. Construction and blasting vibrations achieve maximum amplitude response with dominant frequencies above the natural frequency of the responding superstructure and near and above that of the walls.

Events studied in Chapters 2 and 5 occurred at varying distances from their respective structures, thus some means of normalization is needed. Comparing the crack response to machinery excitation 40 feet away to that from the large roller 8 feet away presents misleading information.

A two-step normalization process was followed. First, all construction equipment vibration was normalized by considering only events that occurred at a typical distance of 30 feet (≈10m). Normalization to a 30 ft stand-off distance eliminates the difficulty of comparing varying peak particle velocities from different equipment produced as a function of differences in stand-off distance. This normalization produces similar peak particle velocities (0.1 to 0.12 ips) at 30 ft in the trackhoe and vibratory rollers, while the trencher produces far smaller peak particle velocities (0.03 ips). Comparison of construction vibrations with those produced by blasting through the normalization process is more challenging. Blasting occurred at distances in excess of 2000 ft, so it was decided as the second step in the normalization process to employ only blast events that produced peak particle velocities (0.14 and 0.13 ips) similar to those produced by the trackhoe and rollers at 30 ft. Figure 6.5 presents the single degree of freedom response spectra for all 30 ft. normalized construction events, plus the two blasting events producing similar peak particle velocities. These spectra will be discussed in the following section.

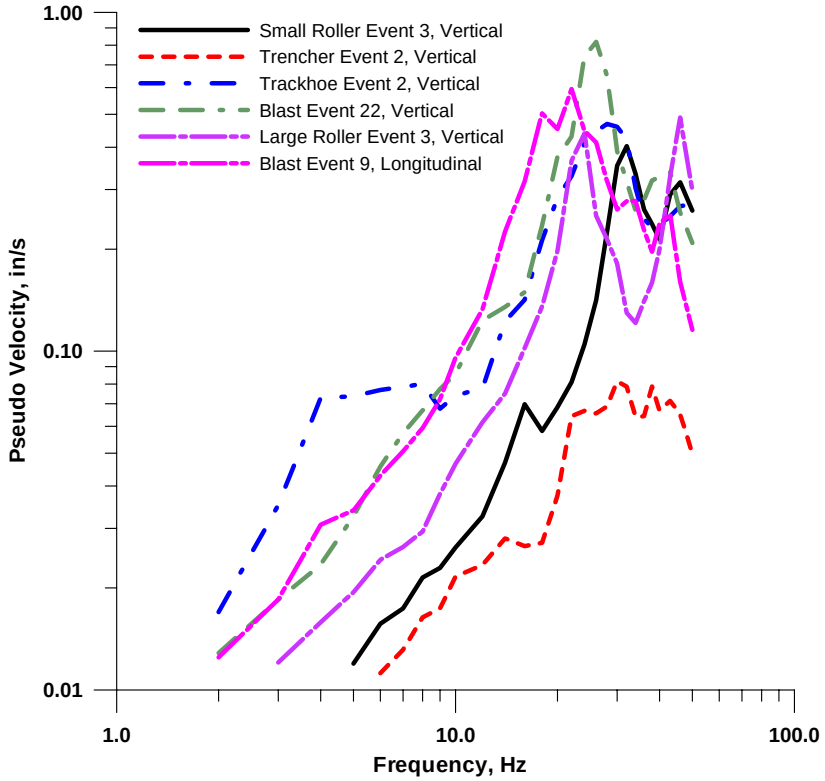

Figure 6.5 Vertical single degree of freedom response spectrum for blast event 22 in Connecticut (PPV=0.13 ips) and trackhoe event 2, trencher event 2, small roller event 3 and large roller event 3 in Las Vegas (PPV normalized to 30 feet), and Longitudinal SDOF spectrum for blast event 9 in Connecticut (PPV=0.14)

Homogenous Excitation

The wavelength and proximity of the excitation source control the degree to which the structure is excited homogenously or uniformly. Comparison of blast and construction vibration effects provides an opportunity to illustrate the effects of uniform versus localized excitation. Vibration wavelengths are a function of excitation frequency and propagation velocity as shown by Equation 5.1

$$\lambda = c * (1/f)$$

where λ is wavelength, c is propagation velocity and f is frequency. In addition, vibrations from construction normally involve soils, whose relatively high compliance compared to rock leads to shorter wavelengths. The following discussion illustrates the importance of these concepts.

Two types of structural motion, or displacement, are responsible for micro-inch crack displacements: homogenous superstructure displacement and individual wall component displacement. Superstructure displacements traditionally occur at frequencies between 5 and 12 Hz, while individual walls respond at 12 to 20 Hz. Wavelengths have significant influence over the degree of homogenous superstructure versus individual wall component displacement occurring as a result of construction or blasting vibrations, making them an important comparison. For rock blasting at the Connecticut site, the propagation velocity is approximately 10,000 ft/sec. Vibration frequencies maximize between 20 and 30 Hz. The wavelength for blast event 15 is approximately 400-450 ft. In Las Vegas soils, the propagation velocity is significantly lower, about 4000 ft/sec. Vibration frequencies for the construction equipment at the Las Vegas site were approximately 28 Hz for the trackhoe, 35 Hz for the trencher, 32 Hz for the small roller, and 23 Hz for the large roller (in Event 3). These wavelengths vary between 100-200 ft.

Figure 6.6 compares vibration wavelengths to scale with the long axis of the Connecticut and Las Vegas houses. Wavelengths are 7 to 8 times longer than the long axis of the house for rock motions in Connecticut, thus the vibrations generate homogenous superstructure motion at anywhere from 5 to 12 Hz. At the Las Vegas site, the approximate wavelengths of the construction vibrations are only 2 times longer than the long axis of the house, and produce individual wall component displacement at higher (18-22 Hz) frequencies. From the single degree of freedom spectra presented earlier in Figure 6.5, it is obvious that these natural frequency response variations produce significantly differing relative displacement structural response.

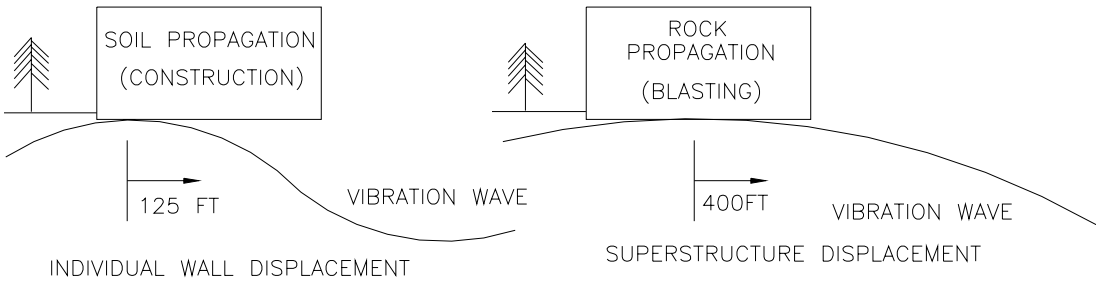

Figure 6.6 Visual comparison of wavelengths (λ) producing individual wall component displacement with soil propagation (λ=125 ft) and homogenous superstructure displacement with rock propagation (λ=400 ft)

Absolute distance from the energy source producing blasting or construction vibrations also affects the uniformity or homogeneity of the excitation. Figure 6.7 shows both the Connecticut house, at approximately 2500 ft. from the source of blasting at the quarry, and the Las Vegas house, between 10 and 50 ft. from the activities of the construction equipment. As the energy propagates outward from the source (all assumed to create a circular wavefront in plan view), the radius of curvature of the front increases with distance and the particle motions within the rock and soil become increasingly parallel. When this particle motion becomes parallel, the wave can be approximated as a plane wave. At distances greater than 100 ft. from the source for a 60 ft. wide house, the wavefront is said to behave as a plane, or without curvature (Dowding, 1996). As stated before, the Connecticut structure lies well outside this 100 ft. range, meaning the waves coming from the quarry are most certainly acting as a plane-wave. The Las Vegas structure, however, is closer than 100 ft from the source of construction vibrations. Therefore, different portions of the structure can be expected to react to the same ground motions within a time history at differing times.

Differing times of maximum response illustrate the local nature of excitation with unusually close construction vibration. In addition, these timing differences can make data collection of construction-induced crack displacements with a single geophone a significant challenge. In Connecticut, where the wave moves as a plane, the vibration of the entire superstructure can be assumed to occur at the exact same time (to the millisecond) as the vibration of the geophone. At the Las Vegas site, however, there is a significant time lag between the maximum vibration of the geophone and the maximum response of Crack 5, situated on the western exterior wall approximately 30 feet from the location of the geophone.

Figure 6.8 shows Crack 2 and 5 time histories compared with longitudinal, transverse, and vertical ground velocity time histories (bottom) resulting from large roller event 6. It can be seen that, while the peak displacement of Crack 2 occurs at roughly the same time as the peak ground motions, the peak response of Crack 5 occurs four to five seconds before the peak ground motions at the geophone. Figure 6.9 shows that, if the roller is moving west to east (as it was during this event), that when the peak motions are

occurring at the wall containing Crack 5, they will be significantly attenuated by the time they reach the geophone 30 feet away.

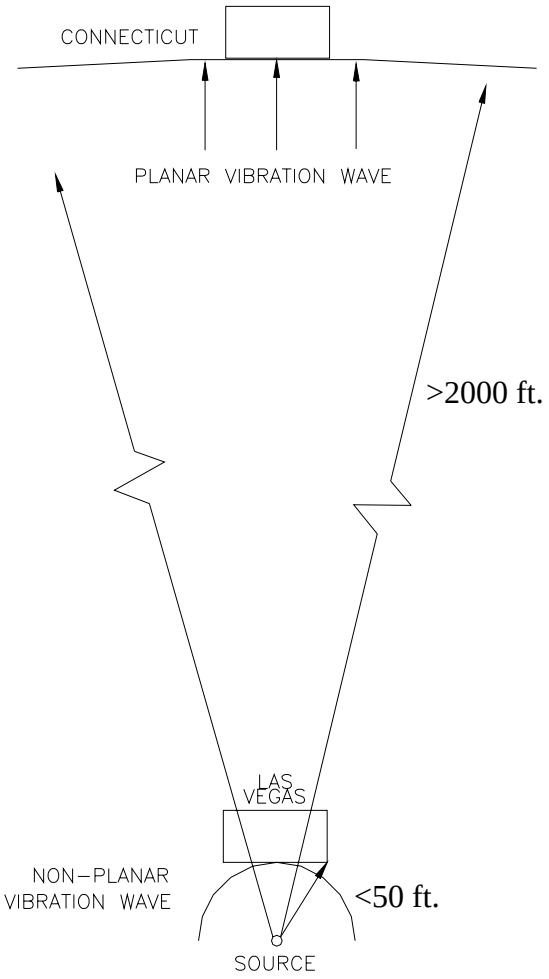

Figure 6.7 Plane wave theory of radial geodynamic wave motion impacting structures in Connecticut and Las Vegas

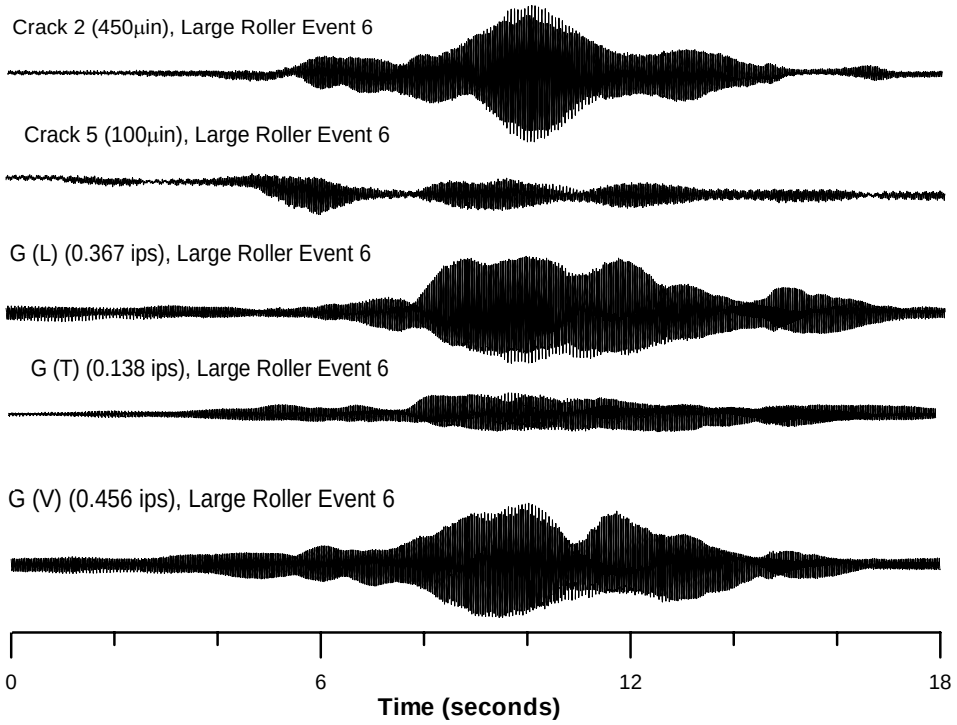

Figure 6.8 Crack 2 and 5 displacement, longitudinal, transverse and vertical time histories of large roller event 6 showing time lag in Crack 5 versus Crack 2 response

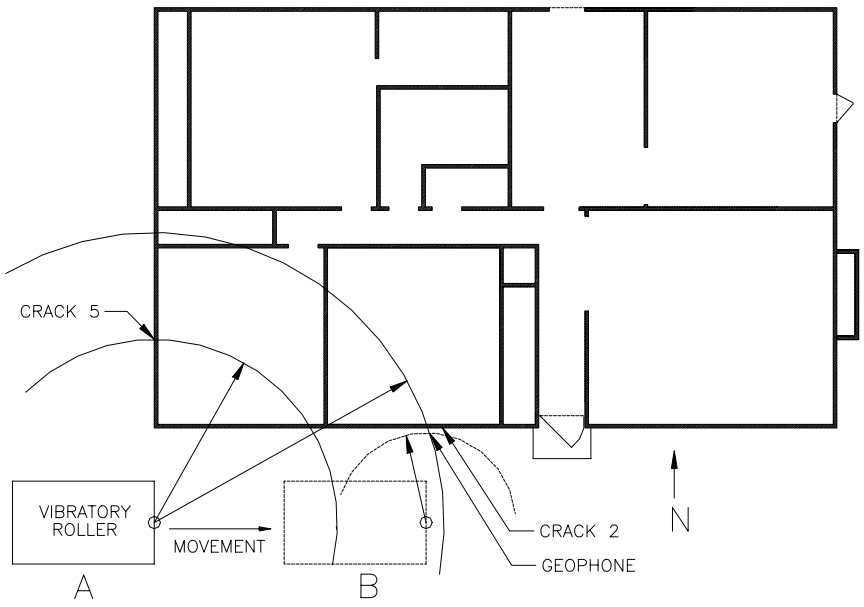

Figure 6.9 Visualization of time lag existing between Crack 5 response and Crack 2 response during large roller event 6, resulting from radial plane wave motion

Crack Sensitivity

The final descriptor that will have a significant effect on crack displacements is the sensitivity of the wall and structure to any effect, be it produced by transient vibration or long-term weather. Response of structural components depends on many different loading effects such as foundation movements, in-home climate control, changes in weather patterns, etc. Sensitivity depends on wall material composition, framing details, support details, etc. To compare sensitivities independent of vibration source, the long-term data from Chapters 2 and 5 are examined to choose extreme weather events resulting in significant humidity changes for the determination of crack response. Sensitivity was calculated as the change in 24-hour rolling average crack displacement (Δ Crack Displacement) divided by the corresponding change in 24-hour rolling average of humidity (Δ Humidity). Each of these ratios was then plotted as Figure 6.10 to determine an average. Not all these points were produced by the same humidity event, as some rain events last longer than others, some produce less rainfall with a greater humidity change, etc. Thus normalizing these factors out is particularly difficult. Table 6.2 lists the events and responses employed to produce these comparisons.

In Figure 6.10 separate crack sensitivity functions are calculated by assuming, in the short-term, zero change in humidity will produce zero crack displacement. Each crack is thus associated with a specific sensitivity. Figure 6.10 (a) shows Connecticut Crack 1 sensitivity is 400μin/%, and Crack 3 is 115μin/%. Figure 6.10 (b) shows Las Vegas Crack 1 sensitivity is 150 μin/%, Las Vegas Crack 3 is 130μin/%, Las Vegas Crack 2 is 165μin/%, and Las Vegas Crack 5 is 150μin/%. As expected, Connecticut Crack 1 is by far the most sensitive to changes in humidity, followed by the external Las Vegas cracks, and finally the Las Vegas ceiling and Las Vegas and Connecticut drywall cracks.

Establishing criteria for vibration induced crack sensitivity and finding a method of correlating sensitivities in Connecticut to those in Las Vegas presents several challenges. It has been established earlier that the structures studied in Connecticut and Las Vegas are constructed of different materials with different support systems. Furthermore, blasting and construction vibrations produce significantly different excitation motions in terms of homogeneity of excitation as well as time history.

Comparing crack displacements resulting from homogenous structural motion of a two-story structure with crack displacements from localized structural motion of a single-story slab-on-grade structure would require a sophisticated and elaborate normalization procedure beyond the scope of this project. To make matters more challenging, as shown above each crack responds with its own sensitivity to environmental and (by implication) vibratory effects. This difference must be normalized as well. Ideally, monitoring blasting and construction vibration-induced crack displacements in the same structure would effectively normalize these factors.

		Humidity	Crack 1	Crack 3	Crack 1	Crack 2	Crack 3	Crack 5
	Date	Change	Change	Change	Change	Change	Change	Change
		(%)	(μin)	(μin)	(μin)	(μin)	(μin)	(μin)
Connecticut								
	6/27/2002	11	5000	1000				
	6/29/2002	13	7500	1500				
	7/26/2002	25	10000	2500				
Las Vegas								
	9/12/2002	18				2900		
	10/28/2002	40				6500		5700
	10/30/2002	30						5000
	11/9/2002	22				4100		2200
	9/10/2002	7.69			1100		950	
	10/31/2002	8.31			1320		1150	
	12/20/2002	2.65			470		365	

Table 6.2 Events and crack responses employed in the calculation of crack sensitivity to environmental (humidity) change

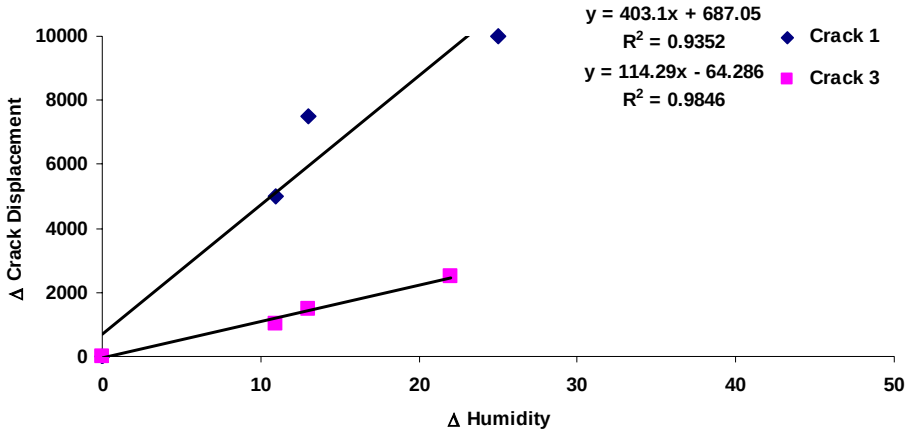

Figure 6.10 (a) Connecticut Cracks 1 and 3 sensitivity to humidity change

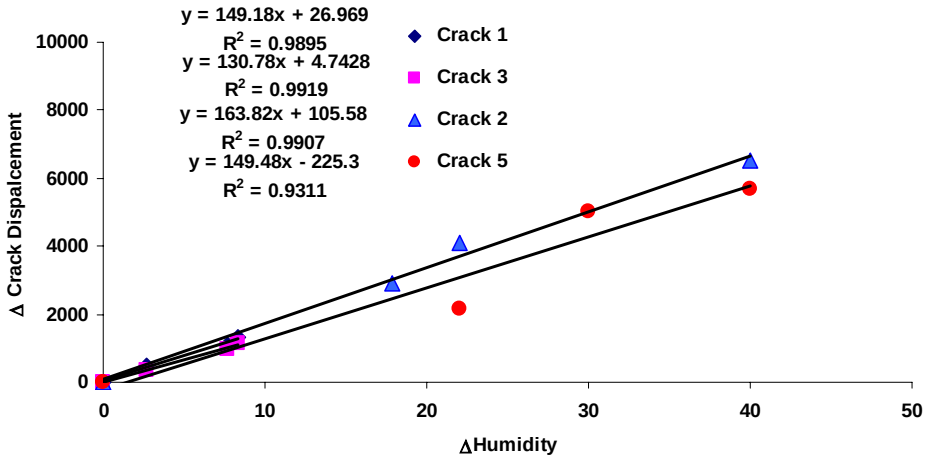

Figure 6.10 (b) Las Vegas Cracks 1, 2, 3, and 5 sensitivity to humidity change

Chapter 7

Conclusions

This thesis summarizes micro-inch crack response to blast-induced ground motions from the Stiles Road Quarry in Southbury, Connecticut, construction-induced ground motions along West Ann Road in Las Vegas, Nevada, and environmental phenomena at both sites. Both of these structures were instrumented and their response studied as part of the development of an Autonomous Crack Measurement (ACM) system sponsored by the Infrastructure Technology Institute at Northwestern University through a block grant from the United States Department of Transportation.

Responses of the Connecticut structure were measured with velocity transducers instrumented in the traditional manner of those in the study sponsored by the United States Department of the Interior Office of Surface Mining (OSM). Ground motions were measured in three orthogonal axes in front of the house. Structural response was measured with three upper structure velocity transducers, three lower structure velocity transducers, two mid-wall velocity transducers, an air pressure transducer, and for the final month of study, a mid-ceiling velocity transducer. One wall and two ceiling cosmetic drywall cracks were fit with eddie current "Kaman" sensors to measure micro-inch displacement response to environmental and blast-induced ground vibrations produced by an aggregate quarry approximately 2500 feet away.

Ground motions at the Las Vegas structure were measured with an in-ground tri-axial geophone customary to all ACM sites. Micro-inch displacements were measured across two interior drywall cracks and two exterior stucco cracks with LVDT displacement gages. No velocity response was measured in this structure. Construction adjacent to the house (all within 50 feet) involved excavation for the installation of a 10'x12' reinforced concrete box culvert by trackhoe, excavation of an 8-inch water service line trench by chain trencher, and vibratory compaction of trench backfill and granular sub-grade for the reconstruction of West Ann Road.

The synthesis of measurements and calculations from the response of the Connecticut site structure led to the following conclusions:

- Long-term environmental and weather crack displacement (temperature and humidity) in this structure is 40 to 90 times greater than the crack displacement caused by either the largest measured blast-induced ground motion (0.345 ips) or airblast (132 dB).
- Crack 1 responded as much, and correlated better to, large air over-pressures (+130 dB) as it did to large ground motions (+0.30 ips). Bedroom wall Crack 3 responded insignificantly to airblasts.
- Response of ceiling Crack 1 correlated best to measurements that involve absolute mid-ceiling displacements.
- Upper and lower structure response must be monitored on single-story walls constructed of the same material. If multi-story walls are instrumented, they must be of the same construction. Failure to isolate differing construction types results in erroneous relative displacement calculations.
- To compare structure and crack response, structural response should be measured along the same wall, or at least in the same portion of the house, as the crack itself.

Examination of the effects of blast design on crack displacements at the Connecticut site led to the following conclusions:

- Frequency of blast-induced ground motions had a significant effect on crack displacements.

- Crack 1 (apartment ceiling) response to unusually high airblast overpressure was as large as that from significant ground motions.
- Total number of holes, delay timing, or total shot time individually had less impact on crack displacement than frequency or the presence of unusually high airblasts.
- Borehole geometry and layout had a relatively minor, albeit existent, effect on crack displacement.

The synthesis of measurements and calculations of response from the Las Vegas, Nevada site structure led to the following conclusions:

- Trackhoe, trencher, and vibratory roller construction in the vicinity of the structure (<50 ft) did not create significant (<0.5 ips) ground motions.
- Long-term environmental and weather-induced crack displacement was 30 to 150 times greater than the crack displacement caused by the largest measured construction-induced ground motion (0.435 ips).
- Cracks in Las Vegas site structure appear to displace in a stick-slip fashion, rather than evenly over time. Further examination of this phenomenon is needed.
- One hour of typical weather-induced Crack 2 displacement was twice as large as that produced by the largest vibratory event (0.435 ips) occurring during the same time period.
- On-site inspection of vibration-inducing construction activities would greatly diminish the difficulty in identifying specific sources of excitation. Unique data acquisition triggers make the monitoring process accurate, albeit difficult.
- Electrical noise, human sources, and other unidentifiable activities may trigger systems while monitoring construction vibrations, and methods of identifying these events are important.
- For excitation frequencies between 20 and 30 Hz, crack displacement correlated best with peak particle velocity.

The comparison of measurements and results from the structures at the Connecticut and Las Vegas sites led to the following conclusions:

- Due to shorter wavelengths, nearby construction vibrations at the Las Vegas site from movable sources produced response more localized in time than were those from longer wavelength, distant blast-induced vibrations at the Connecticut site.
- Localized in time, component responses at the Las Vegas structure may have been accentuated by the small radii of curvature of the excitation vibrations.
- Cracks at the Connecticut and Las Vegas sites reacted to changes in humidity with different sensitivities, which may be the result of differences in construction.

References

Aimone-Martin, C. (2002). Ann Road Expansion Project Attenuation of Ground Velocity Measurements, Report, Aimone-Martin Associates LLC, Socorro, NM.

Aimone-Martin, C., Faroni, K., and Gelormino, T. (2000). Fifteen Years of Blast Vibration Control and Improved Public Relations at Two Traprock Quarries, General Conference Proceedings, International Society of Explosives Engineers, Cleveland, OH.

Dowding, C.H. (1996). Construction Vibrations, Prentice Hall, Upper Saddle River, NJ.

Huang, F. et al. (1994). "NUVIB Vibration Analysis Program User's Manual, Version 1.01." Department of Civil and Environmental Engineering, Northwestern University, Evanston, IL.

McKenna, L.M. (2002). Comparison of Measured Crack Response in Diverse Structures to Dynamic Events and Weather Phenomena, M.S. Thesis, Department of Civil and Environmental Engineering, Northwestern University, Evanston, IL.

Somat Ease version 3.0 (1999). Somat Corporation, Champaign, IL.

Somat TCE eDAQ version 3.5.1 (2001). Somat Corporation, Champaign, IL.

Somat TCS for Windows, version 2.0 (1999). Somat Corporation, Campaign, IL.

White Seismograph Data Analysis, version 5.0.4 (1998). White Industrial Seismology, Inc., Joplin, MO.

Appendix A

Conversion Factors for Connecticut and Las Vegas Instruments

Connecticut

Kaman Gage/Crack 1, Apartment Addition

- mils = (-0.014317)+(2.2085*V)-(0.31059*(B6^2))+(0.29495*(V^3))-(0.080215*(V^4))+(0.0095915*(V^5)); V = SoMat Voltage

Kaman Gage/Crack 2, Living Room Ceiling

- mils = (-0.034437)+(2.2312*V)-(0.47524*(V^2))+(0.40754*(V^3))-(0.10769*(V^4))+(0.011889*(V^5)); V = SoMat Voltage

Kaman Gage/Crack 3, Bedroom Wall

- mils = (-0.018637)+(2.4437*V)-(0.7242*(V^2))+(0.52212*(V^3))-(0.013227*(V^4))+(0.013873*(V^5)); V = SoMat Voltage

Kaman Gage/Crack 4, Null (in Apartment)

- mils = (-0.0019227)+(2.2032*V)-(0.25826*(V^2))+(0.25371*(V^3))-(0.069226*(V^4))+(0.0086497*(V^5)); V = SoMat Voltage

micrometers = mils*25.4

microinches = micrometers*39.37

Las Vegas

LVDT Displacement Gages, All Crack and Null Response

- micrometers = V/7.87; V = eDAQ Voltage
- microinches = micrometers*39.37

Geosonics Inc. Tri-axial 4.5 Hz Geophone

- Longitudinal, Transverse and Vertical Velocity (in/sec) = V/1000/0.8

Appendix B

Specifications for Construction Equipment in Las Vegas

Hitachi 1200 EX Super Trackhoe

- Operating Weight = 108,000 kg
- Body Weight = 77,170 kg
- Normal Bucket Capacity = 3.8 m^3
- Track Width = 710 mm
- Track Length = 6,410

Tesmec TRS 1175XL Chainsaw

- Weight w/ 10-foot Boom and 26-inch Rotary Cutters = 61,235 kg
- Chainsaw Transport Length w/ 10-foot Boom= 12.4 m
- Net Flywheel Horsepower at Full Load RPM = 370

Dynapac CC 522 Single-Drum Roller

- Operating Mass = 26,130 lbs
- Frequency/Amplitude High = 3,000 vpm / 0.028 in.
- Frequency/Amplitude Low = 3,000 vpm / 0.012 in.
- Centrifugal Force High/Low = 28,800 / 14,625 lbs
- Speed = 0 to 7.5 mph
- Drum Width/Diameter = 77 in. (6.4 ft.) / 55 in. (4.6 ft.)

Ingersoll-Rand SD 115F Single-Drum Roller

- Operating Mass = 26,420 lbs
- Frequency = 18.3-31.5 Hz
- Nominal Amplitude = 0.054 / 0.027 in.
- Centrifugal Force High/Low = 55,000 / 27,400 lbs
- Speed = 0 to 7.1 mph
- Drum Width/Diameter = 84 in. (7 ft.) / 59 in. (5 ft.)